7-25-2016 12:00 AM

Short-term Deflections of Reinforced Concrete Beams

Caitlin Mancuso
The University of Western Ontario

Supervisor
Dr. F. M. Bartlett
The University of Western Ontario

Graduate Program in Civil and Environmental Engineering
A thesis submitted in partial fulfillment of the requirements for the degree in Master of Engineering Science

ABSTRACT

Excessive deflection of concrete beams is a recurring serviceability problem. Provisions in current building codes, CSA A23.3-14 and ACI 318-14, account for some but not all of the contributing factors. The effect of loading concrete members at very young ages on the associated deflections remains uncertain.

Concrete stress-strain data reported by others are used to investigate if conventional stress-strain relationships, and empirical equations in A23.3-14 for tensile strength and elastic modulus are accurate for young concretes. Moment-curvature analyses based on conventional simplifying approximations used for flexural analysis are performed. For concretes less than one day old, the conventional relationships and empirical equations yield unconservative results. For older concretes, however, the conventional stress-strain relationships, empirical equations and conventional simplifying assumptions yield accurate results.

Current practice is to compute deflections using either a whole-member analysis with an average effective moment of inertia, or a discretized analysis with unique effective moments of inertia for each discrete element. Branson proposed equations for the effective moment of inertia for use in either analysis. Bischoff proposed an improved equation, for use in whole-member analysis only. The current research quantifies suitable modifications to the Bischoff Equation for use in discretized analysis: the exponent applied to the cracking-to-applied moment ratio term should be increased from 2 to 3.

Test-to-predicted ratios for 65 beams investigated by others are used to quantify the accuracy of the various alternative deflection calculation procedures and to identify key parameters for

accurate computation of deflections. The Bischoff Equation with the cracking moment computed using full modulus of rupture yields the best results. When the recommended reduced modulus is used, the difference between results using the Branson and Bischoff Equations is indistinguishable.

Keywords: Early-Age Concrete*;* Moment-Curvature Analysis; Instantaneous Deflections; Reinforced Concrete; Effective Moment of Inertia; Branson's Equation; Bischoff's Equation.

ACKNOWLEDGMENTS

I would like to express my deepest gratitude to my supervisor, Dr. F. M. Bartlett. He has been a wonderful mentor and completing this thesis would not have been possible without his guidance and support. Dr. Bartlett's passion and dedication to the field of engineering is inspiring, and if I am able to emulate a fraction of that I know I will have a fulfilling career.

Thank you to all the faculty and staff at Western University for making my undergraduate and graduate studies a truly great experience. I am grateful for all of the friendships I have made throughout this journey.

The financial support provided from the Natural Sciences and Engineering Research Council (NSERC), in the form of a Canada Graduate Scholarship (CGS-M), from the Province of Ontario and the Faculty of Engineering at Western University, in the form of a the Queen Elizabeth II Graduate Scholarship in Science and Technology (QEII-GSST) is gratefully acknowledged.

Informal contributions, interest and suggestions from Kevin MacLean, Dr. Tibor Kokai and their colleagues from the Toronto office of Read Jones Christoffersen are also gratefully acknowledged.

Last, but most certainly not least, I would like to thank my family. Mom and Dad, without your love, support and patience throughout this process I would not have been able to do this. Thank you for being my biggest cheerleaders.

TABLE OF CONTENTS

LIST OF FIGURES

LIST OF TABLES

LIST OF APPENDICES

NOMENCLATURE

$A_{\%}$	the probability that the actual deflection will be within a range of the predicted value
A_s	area of tensile flexural reinforcement
b	width of concrete compression zone
b_{fl}	flange width of a T-beam
b_w	web width of a T-beam
c	distance from extreme compression fibre to neutral axis
c/d	maximum neutral axis depth limit for flexural members
C_c	compressive force magnitude
d	distance from extreme compression fibre to centroid of tension reinforcement
E_c	elastic modulus of concrete
E_cI_{cr}	flexural rigidity of concrete
E_s	elastic modulus of steel
f_0	compressive strength of concrete
f'_c	specified compressive strength of concrete
f_c	concrete compressive stress at extreme fibre
f_{ct}	split cylinder strength (mean value = $\overline{f}_{ct}$)
f_r	modulus of rupture of concrete (mean value = $\overline{f}_r$)
f_y	specified yield strength of steel
h	overall thickness or height of member
I_{cr}	moment of inertia of cracked section transformed to concrete
I_e	effective moment of inertia
I_g	moment of inertia of gross section
k_1	ratio of the average concrete compressive stress to the maximum stress
k_2	ratio of the distance between the extreme compression fibre and the resultant of the compressive force to the depth of the neutral axis
k_3	ratio of the distance between the extreme compression fibre and the resultant compressive force for the trapezoidal portion of the Modified Hognestad stress-strain curve to the depth of the neutral axis
kd	depth from the extreme compression fibre to the neutral axis, elastic-cracked analysis
L	span length
m	exponent applied to the M_{cr}/M_a term in effective moment of inertia equation
M_0	nominal applied bending moment
M_a	applied bending moment (in positive moment region, M^+, in negative moment region, M^-)
M_{cr}	cracking moment
M_f	moment due to factored loads
M_{f6}	ultimate flexural resisting moment, according to the Appendix of ACI 318-56
M_n	nominal moment capacity
M_r	factored flexural resistance
M_s	moment due to service loads
M_y	yield moment
n	modular ratio (E_s/E_c)

P	concentrated point load
P_L	probability that a test-to-predicted ratio will fall below a range
P_U	probability that a test-to-predicted ratio will fall above a range
s	sample standard deviation
T_s	tensile force magnitude
w	applied uniformly distributed load
w_f	factored applied uniformly distributed load
w_L/w_D	live-to-dead load ratio
y_t	distance from centroidal axis of section to the extreme fibre in tension
x	the ratio of the extreme compression fibre strain to the strain at peak stress
$\overline{x}$	sample mean
Z	unit value of the standard normal distribution

Greek Symbols

γ_c	density of concrete
Δ_{mid}	midspan deflection of a member
ε	concrete compressive strain
ε_0	concrete compressive strain at peak stress
ε_s	tensile strain in flexural reinforcement
ε_{ult}	ultimate extreme fibre concrete compression strain
ε_y	yield strain of steel
κ	weighting coefficient
ρ	flexural reinforcement ratio (in positive moment region, ρ^+, in negative moment region, ρ^-)
σ_c	concrete compressive stress
σ_s	steel tensile stress
Ψ	curvature of a flexural member
Ψ_{max}	maximum curvature of a flexural member
ϕ_i	section curvature

CHAPTER 1: INTRODUCTION

1.1 BACKGROUND

Excessive deflection of concrete floor slabs is a recurring serviceability problem (Gilbert 2012, Stivaros 2012). Others have investigated contributing factors including: construction methods and associated loading (Kaminetzky & Stivaros 1994), cracking due to restrained shrinkage, creep and flexure (Bischoff 2007, Scanlon & Bischoff 2008), and early-age concrete properties (ACI 435 1995, Khan 1995). Provisions in current building codes, CSA A23.3-14 in Canada (CSA 2014) and ACI 318-14 in the United States (ACI 2014), account for some but not all of these effects. The effect of loading concrete members at very young ages (3 days is not uncommon given current construction practices) on the associated deflections remains unknown. Construction loads may subject young concrete to large bending moments causing flexural cracking. Accurate predictions of the modulus of rupture, the elastic modulus and the cracked moment of inertia, are necessary because computed deflections are sensitive to these properties.

1.1.1 Conventional Material Property Quantification for Concrete

Conventional stress-strain relationships, such as those proposed by Todeschini et al. (1964) and Hognestad (1951), and empirical relationships for predicting concrete material properties, such as the elastic modulus and the modulus of rupture, have been developed for mature concrete using the 28-day specified concrete compressive strength. The behaviour of very young concretes, however, may differ markedly from more mature

concretes (MacGregor & Bartlett 2000). There is a need, therefore, to quantify the difference in compressive stress-strain response and verify that conventional idealizations and simplifications conventionally assumed for flexural analysis can accurately predict the flexural behaviour of young-age concrete.

Common practice is to use stress-strain idealizations derived from mature concrete, i.e., the Todeschini and Modified Hognestad relationships, to determine the compressive response of concrete in compression. It is unclear however if the simplifying approximations conventionally adopted in flexure theory, such as the compressive stress block idealization at the ultimate limit state, are valid for young concretes.

The ascending portion of the moment-curvature response is of particular interest for deflection calculations, and is often approximated by the cracked flexural rigidity, $E_c I_{cr}$, of the member. It is therefore necessary to predict accurately the elastic modulus, E_c, and cracked moment of inertia, I_{cr}, and so determine if this conventional simplifying approximation still holds for young concretes.

1.1.2 Effective Moment of Inertia for Computation of Instantaneous Deflections

In a reinforced concrete member, flexural cracking occurs along the span where the applied moment exceeds the cracking moment. At these discrete locations the cracked moment of inertia applies. Between cracks, the moment of inertia approaches the gross moment of inertia: this is widely known as the tension stiffening effect (e.g., MacGregor & Bartlett 2000). The effective moment of inertia is, therefore, intended to provide a transition between the upper and lower bounds of the gross and cracked moments of

inertia. The two most familiar equations for calculating the effective moment of inertia were developed by Branson (1965) and Bischoff (2005). Current practice is to compute deflections idealizing the member as either a single element, where an average effective moment of inertia is assigned to the entire member, or a number of discrete elements, where the member is idealized as discrete elements, each with unique effective moments of inertia.

Branson originally proposed two equations for effective moment of inertia, a 3rd-power equation for use in single-element idealization and a 4th-power equation for use in discretized-element idealization. These two equations are based, however, on an incorrect mechanical model that idealizes the stiffnesses of the cracked and uncracked regions as springs in parallel, when they should be in series (Bischoff 2007). Therefore, Branson's method overestimates the tension stiffening effect and is unconservative, especially for lightly reinforced members (CAC 2016). Bischoff has proposed a single equation, based on the correct mechanical model, for use in the single-element idealization only. It is necessary to determine a modification to allow use of the Bischoff Equation to compute the deflection of a discretized member.

The process of member discretization requires consideration of element length and mesh size. A finer element mesh will increase the accuracy of the results, but requires a greater computational demand. It is therefore necessary, particularly for design office use, to optimize the mesh size so that both satisfactory accuracy and computational demands for analysis are achieved.

With any method of analysis, the accuracy of the deflection calculation depends upon the accuracy of the analysis including the quantification of the input parameters (ACI 435 1995). It is impossible to eliminate inaccuracy caused by the uncertainty of the input parameters because the interaction between factors affecting concrete deflections is highly complex. The accuracy of the analysis can however be quantified, and it is necessary to do so for the various alternative deflection calculation procedures.

Flexural members are subjected to tensile stresses due primarily to restraint of concrete shrinkage. When using the Branson Equation, A23.3-14 (CSA 2014) requires that the cracking moment, M_{cr}, be calculated using a reduced modulus of rupture, $0.5f_r$, for beams, one-way and two-way slabs. When using the Bischoff Equation, Scanlon and Bischoff (2008) recommend that M_{cr} be calculated using $0.67f_r$. Therefore, these recommended modulus of rupture reductions must be considered when quantifying the various procedures. There are therefore eight alternative deflection calculation procedures, shown in Table 1-1, involving: the Branson or Bischoff Equations, the single-element or discretized-element idealizations, and the full or reduced moduli of rupture.

Table 1-1: Alternative Deflection Calculation Procedures

Equation	Branson		Bischoff	
Idealization	Single-Element m =3	Discretized-Element m =4	Single-Element m =2	Discretized-Element m =?
Modulus of Rupture	Not Considering Restraint of Shrinkage Full f_r		Not Considering Restraint of Shrinkage Full f_r	
	Considering Restraint of Shrinkage $0.5f_r$		Considering Restraint of Shrinkage $0.67f_r$	

1.2 OBJECTIVES

The primary objective of the research reported in this thesis is to provide guidance for the accurate computation of deflections, including identification of the key influencing factors and recommendations concerning young-age concrete. The specific objectives of this research are as follows:

1. To determine if conventional stress-strain idealizations and empirical equations to quantify material properties can reasonably model stress-strain data and material properties determined experimentally for young concretes (e.g., Khan 1995, Jin et al. 2005).
2. To verify the accuracy of the Branson 4^{th}-power equation and to determine a similar modification to the Bischoff Equation for use in a discretized analysis.
3. To quantify the accuracies of deflections computed using the various alternative deflection calculation procedures using experimentally observed values and to also identify factors necessary to compute deflections accurately.

1.3 OUTLINE OF THESIS

Chapter 2 presents an investigation into the early-age material properties of concrete used to compute instantaneous deflections. Concrete compression stress-strain data reported by others (Khan 1995, Jin et al. 2005) are compared to the Todeschini (1964) and Modified Hognestad (1951) stress-strain relationships. Empirical equations presented in CSA A23.3-14 (CSA 2014) for tensile strength and stiffness properties (i.e., f_r and E_c) are compared to those determined experimentally for young concretes. Moment-curvature

analyses based on conventional simplifying approximations, the reported concrete stress-strain data, and the Todeschini and Modified Hognestad relationships are performed to quantify the accuracy of these methods for young-age concretes.

Chapter 3 presents the Branson and Bischoff Equations for the effective moment of inertia and typical single-element and discretized-element idealizations for deflection calculations. Test cases of flexural members with various end fixities, reinforcement ratios, and live-to-dead load ratios are explored to quantify suitable modifications to the Bischoff Equation for use in discretized-element idealizations. A mesh sensitivity analysis is performed to determine the largest practical mesh size for design office use.

Chapter 4 presents an investigation of the accuracy of the various alternative deflection calculation procedures by comparing predicted deflections to observed values for simply supported and continuous test beams reported by others. Deflections are computed based on the material properties, section geometry and other relevant data reported and test-to-predicted ratios are calculated. Factors that have a major impact the accuracy of computed deflections are also investigated. The database of members investigated covers a wide range of reinforcement ratios, span-to-depth ratios, and section geometries, subjected to varying curing conditions and applied loadings.

Finally, Chapter 5 presents the summary, conclusions and recommendations for future research.

CHAPTER 2: EARLY-AGE CONCRETE

2.1 IMPORTANCE OF EARLY-AGE MATERIAL PROPERTIES FOR DEFLECTIONS

The commentary to ACI 318-14 (2014) cautions, "At early ages, a structure may be adequate to support the applied loads but may deflect sufficiently to cause permanent damage." Concrete strength and stiffness properties are important for deflection calculations and at very young ages are influenced by the following factors related to construction (Kaminetzky & Stivaros 1994):

- *The chosen construction techniques* – curing and finishing methods impact the concrete material properties at a given age.
- *The general construction schedule* – accelerated construction schedules mean that concrete slabs may not have reached appreciable strength when significant construction loads are applied (ACI Committee 347 2005).

Large bending moments applied to young concrete cause flexural cracking. Accurate prediction of the modulus of rupture at young ages is, therefore, important for flexural members. Deflection calculations are particularly sensitive to the computed member stiffness, so it is also necessary to quantify accurately the elastic modulus, E_c, and the cracked moment of inertia, I_{cr}.

ACI 318-14 (2014) specifies that construction loads shall not exceed "the combination of superimposed dead load plus specified live load shall be supported…unless analysis indicates adequate strength to support such additional load", while CSA A23.3-14 has no

such specification. ACI Committee 347 (2005) provides slightly more guidance and recommends formwork be designed for a minimum design value for combined dead and live loads of 100lb/ft^2 (4.8kPa).

Construction loads may be beyond the control of the designer, but the removal of formwork for multistory construction should be a part of a planned procedure considering the concrete strength and age at transfer (ACI 2014). Typical floor construction cycles, i.e., from the casting of a concrete slab to the removal of shores and casting of the subsequent slab above, range from 3.5 to 7 days (Monette & Garnder 2015). A prudent contractor would likely not remove the formwork if the concrete is less than 3 days old. Grundy and Kabaila (1963) have demonstrated that, using conventional shoring systems, a slab can experience construction loading as great as 2.25 times its self-weight at 14 days after casting.

2.1.1 Characteristics of Early-Age Concrete

The behaviour of concrete at very young ages may differ markedly from that of mature concrete (MacGregor & Bartlett 2000). Conventional stress-strain relationships used for moment-curvature analysis have been developed based on mature concrete. However, experimental stress-strain data suggest that the shape of the stress-strain curve for very young concrete can be different (e.g., Khan 1995, Jin et al. 2005). It is therefore necessary to define the age at which the conventional simplifications and idealizations do not apply, as this has not been previously verified.

Concrete strength and other material properties, such as the elastic modulus, E_c, and the modulus of rupture, f_r, increase with age. Two empirical relationships are given in CSA A23.3-14 (CSA 2014) to quantify the secant modulus, that corresponds to the slope of the line drawn from a stress of zero to a compressive stress of $0.40f'_c$. For concretes with a density, γ_c, between 1500 and 2500 kg/m^3 the equation for E_c is:

[2.1] $$E_c=(3300\sqrt{f'_c}+6900)\left(\frac{\gamma_c}{2300}\right)^{1.5}$$

Alternatively, for normal density concretes with compressive strengths from 20MPa to 40MPa:

[2.2] $$E_c=4500\sqrt{f'_c}$$

It is implied in A23.3 that the empirical relationship for E_c given in Eq. [2.1] is preferred. For normal density concretes, however, Eq. [2.2] predicts more conservative E_c values at low compressive strengths and is therefore used in the analysis of very young concretes.

The CSA A23.3-14 (CSA 2014) equation for the modulus of rupture, f_r, is:

[2.3] $$f_r=0.6\sqrt{f'_c}$$

The modulus of rupture is proportional to the square root of the compressive strength and the proportionality constant of 0.6 is intended to represent a lower bound of the experimental data (CSA 2014).

The stress-strain relationship of concrete is necessary to derive the moment-curvature relationship for a section in flexure. The Todeschini and Modified Hognestad

relationships have been commonly used to idealize the stress-strain relationship for normal strength concrete in compression and have longstanding credibility in this role (MacGregor & Bartlett 2000). The flexural behaviour of sections at young ages can therefore be quantified given variations of the concrete stress-strain relationship. This also facilitates verification of various common simplifications of the flexure theory, such as the compressive stress block idealization in CSA A23.3-14 (2014), at young ages.

Deflections depend on member stiffness and so on the flexural rigidity, E_cI_{cr}. Therefore, to compute accurate deflections, both the elastic modulus and cracked moment of inertia must be accurate. For a rectangular cross section without compression reinforcement, the cracked moment of inertia, I_{cr}, is given (e.g., MacGregor & Bartlett 2000) by:

[2.4] $$I_{cr}=\frac{b(kd)^3}{3}+nA_s(d-kd)^2$$

where b is the section width, d is the depth to the reinforcement, n is the modular ratio, E_s/E_c, A_s is the area of steel and kd is the depth to the neutral axis. The factor k, used to locate the neutral axis depth, is computed as:

[2.5] $$k=\sqrt{2\rho n+(\rho n)^2}-\rho n$$

2.1.2 Chapter Objectives

The main objective of this chapter is to determine if the material properties conventionally assumed for deflection calculations are accurate when the concrete is very young. The specific objectives of this chapter are as follows:

1. To determine the age at which the experimental stress-strain data (e.g., Khan 1995, Jin et al. 2005) can be reasonably modeled using the Todeschini (1964) and the Modified Hognestad (1951) compressive stress-strain relationships.

2. To determine if experimentally determined material properties (e.g., Khan 1995, Jin et al. 2005) can be reasonably modeled using the CSA A23.3-14 empirical relationships for the elastic modulus, Eq. [2.2], and modulus of rupture, Eq. [2.3].

3. To determine if the moment-curvature response derived from experimental stress-strain data (e.g., Khan 1995, Jin et al. 2005) can be reasonably modeled using typical simplified idealizations commonly adopted in the theory of flexure for reinforced concrete (e.g., MacGregor & Bartlett 2000).

4. To quantify any differences in the flexural rigidity, E_cI_{cr}, for varying material properties, concrete ages, and reinforcement ratios, as computed using the A23.3 (CSA 2014) empirical equation for the elastic modulus of concrete, Eq. [2.2], or using secant moduli computed from experimental data for young age concretes.

2.2 STRESS-STRAIN CURVES FOR EARLY-AGE CONCRETE

Stress-strain relationships, and empirical relationships for predicting concrete material properties, such as the elastic secant modulus and the modulus of rupture, have been developed for mature concrete using the 28-day specified concrete compressive strength, f'_c. For the purposes of the present study, very young concrete is deemed to be less than 24 hours old, and young concrete is considered to be from one to three days old.

2.2.1 Todeschini and Modified Hognestad Stress-Strain Relationships

The Todeschini relationship provides a convenient idealization of concrete in compression. As shown in Table 2-1 and Figure 2-1, the entire stress-strain curve is given by one continuous function. It provides convenient closed-form solutions for the magnitude and location of the resultant concrete force at a given extreme fibre strain. The concrete stress, f_c, is a function of the 28-day specified concrete compressive strength, f'_c, for a given compressive strain, ε, Eq. [2.6]. The strain at peak stress, ε_0, is also a function of f'_c, and the elastic modulus, E_c, Eq. [2.7]. The ultimate extreme fibre strain, ε_{ult}, is limited to 0.0035 as prescribed in A23.3-14 (CSA 2014). For the analysis of young concretes, f'_c was taken as the maximum concrete stress, f_0, at a given age from the experimental data, and the elastic modulus was determined using Eq. [2.2].

Table 2-1: Todeschini and Modified Hognestad Stress-Strain Relationships

Relationship	Concrete Stress, f_c (MPa)	Eq.	Strain at Peak Stress, ε_0	Eq.	Ultimate Strain, ε_{ult}
Todeschini (1964)	$f_c = \frac{2f'_c(\varepsilon/\varepsilon_0)}{1+(\varepsilon/\varepsilon_0)^2}$	[2.6]	$\varepsilon_0 = 1.71 f'_c/E_c$	[2.7]	$\varepsilon_{ult} =$ 0.0035
Modified Hognestad (1951)	$f_c = f'_c\left[\frac{2\varepsilon_c}{\varepsilon_0}-\left(\frac{\varepsilon_c}{\varepsilon_0}\right)^2\right]$ for $f_c < f'_c$ $f_c = f'_c\left[1-.15\left(\frac{\varepsilon_c-\varepsilon_0}{\varepsilon_{ult}-\varepsilon_0}\right)\right]$ for $f_c > f'_c$	[2.8]	$\varepsilon_0 = 1.8 f'_c/E_c$	[2.9]	$\varepsilon_{ult} =$ 0.0038

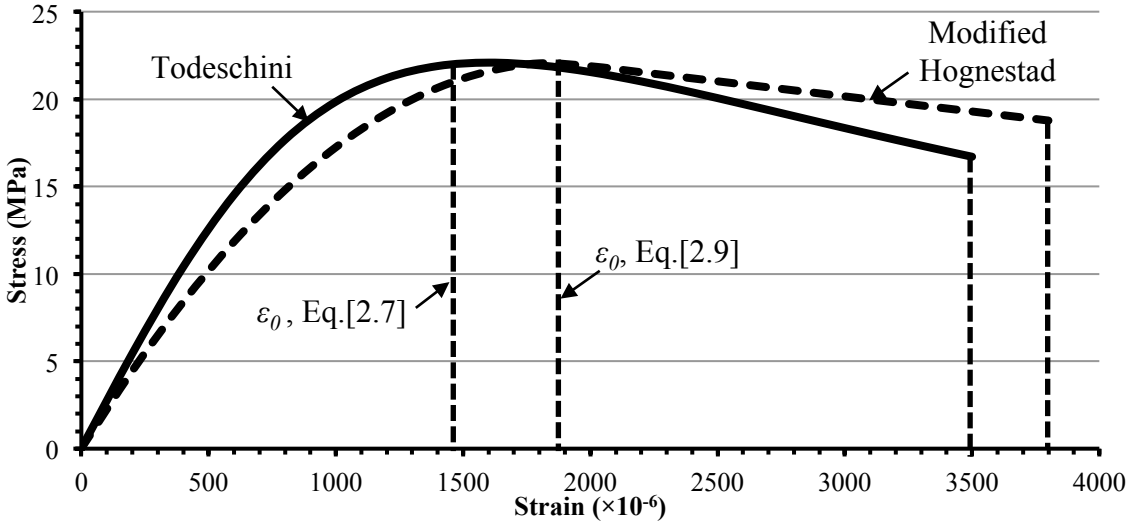

Figure 2-1: Todeschini (1964) and Modified Hognestad (1951) Stress-Strain Relationships

The Modified Hognestad stress-strain relationship, also shown in Table 2-1 and Figure 2-1, consists of a parabola to a maximum stress at a strain, ε_0, computed using Eq. [2.9], that is 5.2% larger than the ε_0 value assumed in the Todeschini relationship, Eq. [2.7]. The descending branch is linear to 85% of the maximum stress at an ultimate strain of 0.0038. When using the Modified Hognestad stress-strain relationship for young concretes the 28-day specified concrete strength, f'_c, was taken as the maximum concrete stress, f_0, at a given age from the experimental data.

Others have investigated empirically the stress-strain response of concrete at early ages. The experimental data obtained as part of the studies by others was used for analysis, and was not experimentally obtained as part of this investigation. Khan (1995) performed modulus of rupture tests and investigated the compressive stress-strain responses of 30, 70 and 100MPa strength concretes at ages from 72 hours to 91 days, and a total of approximately 300 cylinders were tested in compression. The study also investigated the

influence of temperature-matched, sealed, and air-dried curing conditions on the initial temperature rise after casting. For the purposes of the present study, the sealed specimens with a 28-day concrete strength of 30MPa were investigated because this strength is typical for concrete floor slabs and the sealing procedure will limit significant shrinkage effects.

Concrete cylinders, 100×200mm, and flexural beams were cast in plastic moulds that enabled demoulding at very early ages without disturbing the concrete. The cylinders were end-capped with a sulphur-based capping compound prior to testing. Compressive strength and modulus of rupture tests were carried out at 9.7, 14.5 and 17.7 hours, and at least three cylinders were tested at each of 1, 1.24, 3, 7, 14, 28, and 91 days. To determine the compressive strengths at very early ages (i.e., less than 24 hours), more sensitive load cells were used.

Figure 2-2 shows the observed compressive stress-strain responses at various ages. From an age of one day and beyond, the stress-strain response conforms generally to the Todeschini or Modified Hognestad relationships: initially linear with reduced modulus to the maximum stress followed by strain softening. At an age of 9.7 hours, however, there is no strain softening, so neither the maximum stress nor the corresponding strain at maximum stress is well defined.

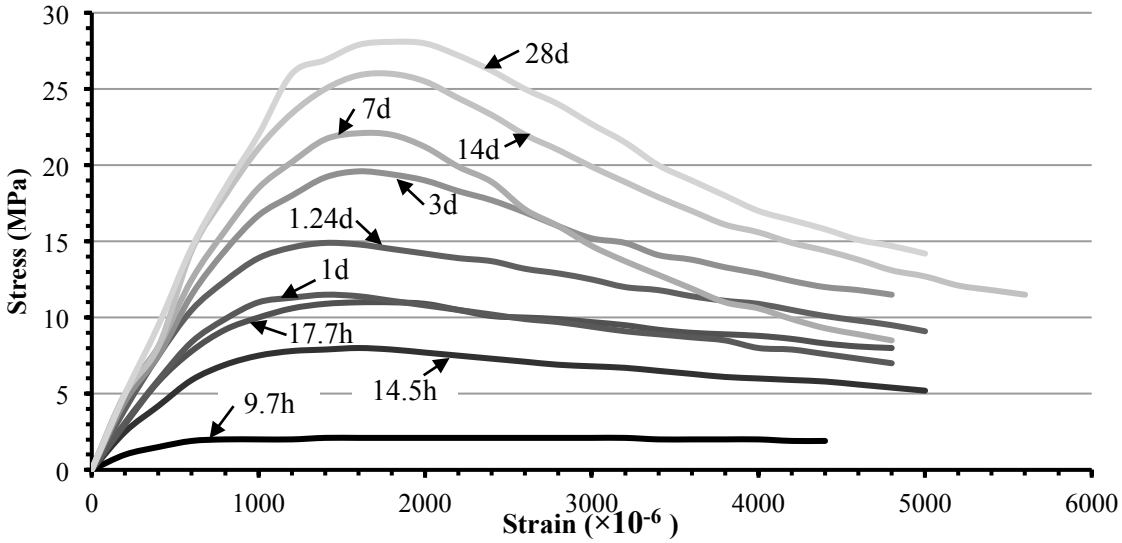

Figure 2-2: Stress-Strain Data (Khan 1995)

Jin, Shen and Li (2005) investigated the behaviour of high- and normal-strength concretes at ages between 12 hours and 28 days. The study included compression and splitting tension tests. The cylinder specimens, 100×200mm, were covered with a wet cloth until demoulding, at which point the specimen was either tested or transferred to a climate-controlled curing room. Splitting tension tests were performed on three cylinder specimens at each age. Figure 2-3 shows the complete stress-strain responses that were obtained at ages of 18 hours, 1, 2, 3, 7 and 28 days. To eliminate the influence of any heterogeneous behaviour of the cement gel on the linearity of the stress–strain curve, four loading-unloading cycles at 40% of desired maximum load were applied to the test specimen before the actual test. The complete stress–strain curve was measured after the pre-loading cycle. The compressive stress-strain curve at three days is again generally consistent with the Todeschini and Modified Hognestad relationships. While the sample sizes are relatively small, the data can be used with confidence because both studies were

independently performed a decade apart and show similar trends. Both studies indicate that very young concrete does not strain soften, and does not show a clear maximum stress or corresponding strain at maximum stress. Strain softening was observed the young age of three days in both studies.

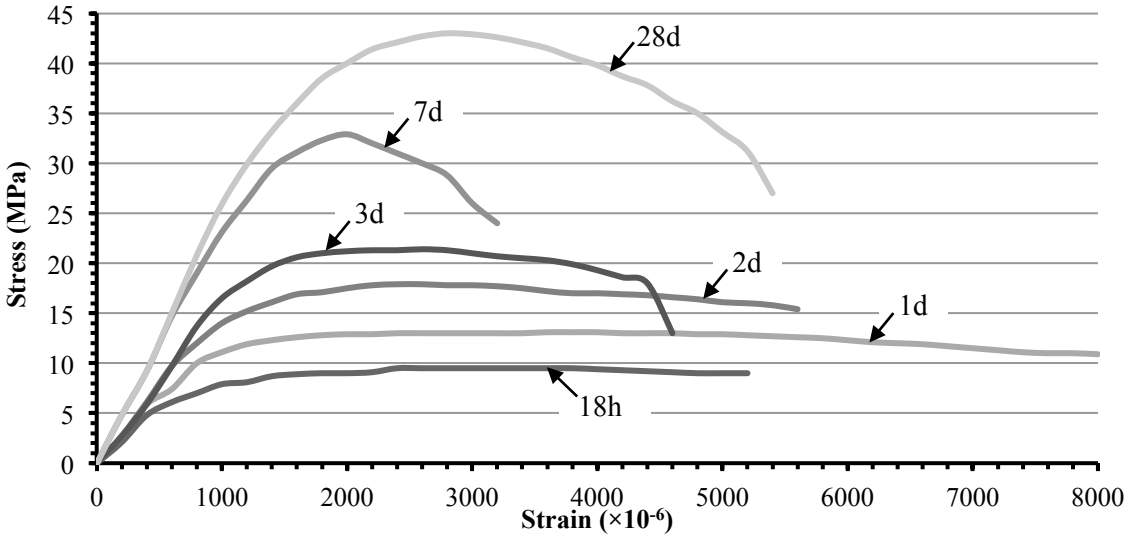

Figure 2-3: Stress-Strain Data (Jin et al. 2005)

2.2.2 Early-Age Stress Strain Curves

The experimental stress-strain response from Khan (1995) at 9.7 hours is shown in Figure 2-4(a) and (b) with the Todeschini and Modified Hognestad stress-strain curves for the experimentally observed maximum stress, 2.1MPa, and the corresponding strain at peak stress computed using Eq. [2.7] or Eq. [2.9], respectively. Both the Todeschini and Modified Hognestad relationships overestimate the stress in the ascending portion of the curve and predict significant strain softening. The strain softening in the Modified Hognestad relationship is less than that in the Todeschini relationship so the fit of the descending branch to the data is better. If the strain at peak stress, ε_0, is obtained from the

experimental data and the Todeschini and Modified Hognestad relationships are recalculated [shown as the Adjusted Todeschini, and Adjusted Modified Hognestad responses in Figure 2-4(a) and (b), respectively], the fit to the data is better. However, this causes the stress in the ascending portion of the stress-strain curve to be underestimated, and there is no simple procedure to determine an appropriate strain-at-peak-stress value.

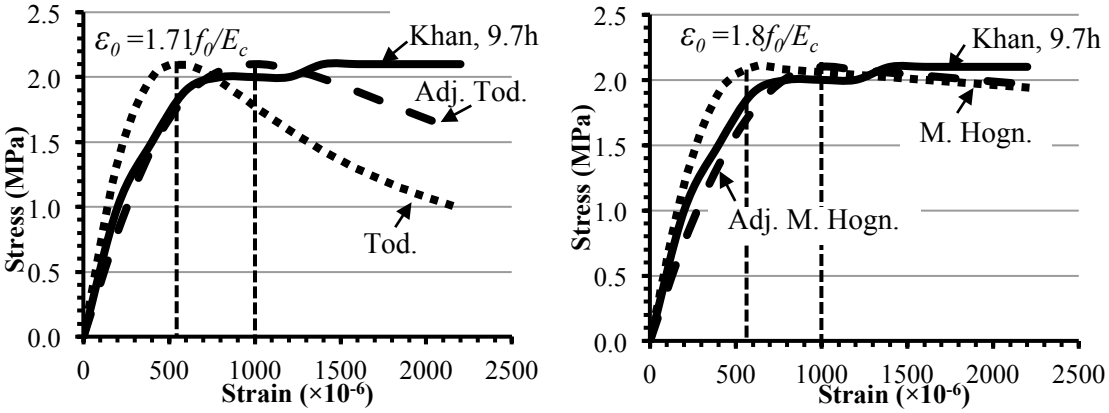

a) Todeschini *b) Modified Hognestad*

Figure 2-4: Stress-Strain Curves, Khan 9.7h

It is unlikely that formwork will be removed from concrete that is only 9.7 hours old. It is therefore useful to determine the age at which the unmodified Todeschini and Modified Hognestad relationships accurately simulate the observed responses. Figure 2-5 shows the stress-strain data reported by Khan (1995) superimposed on the Todeschini and Modified Hognestad relationships at ages of 9.7 hours, 1, 7 and 28 days. At slightly older ages the ascending branch of the data is bounded by the Todeschini and Modified Hognestad relationships: the Todeschini relationship slightly overestimates and the Modified Hognestad relationship slightly underestimates the stress at a given strain in the

ascending portion of the response. This is attributed to the differences in the calculated strains at peak stress, ε_0. The value computed using Eq. [2.7] for the Todeschini relationship is 5% lower than that computed using Eq. [2.9] for the Modified Hognestad relationship. Generally, both relationships overestimate the strain softening of young concrete and underestimate the strain softening of mature concrete. However, the descending branch of the stress-strain curve has no impact on deflection calculations.

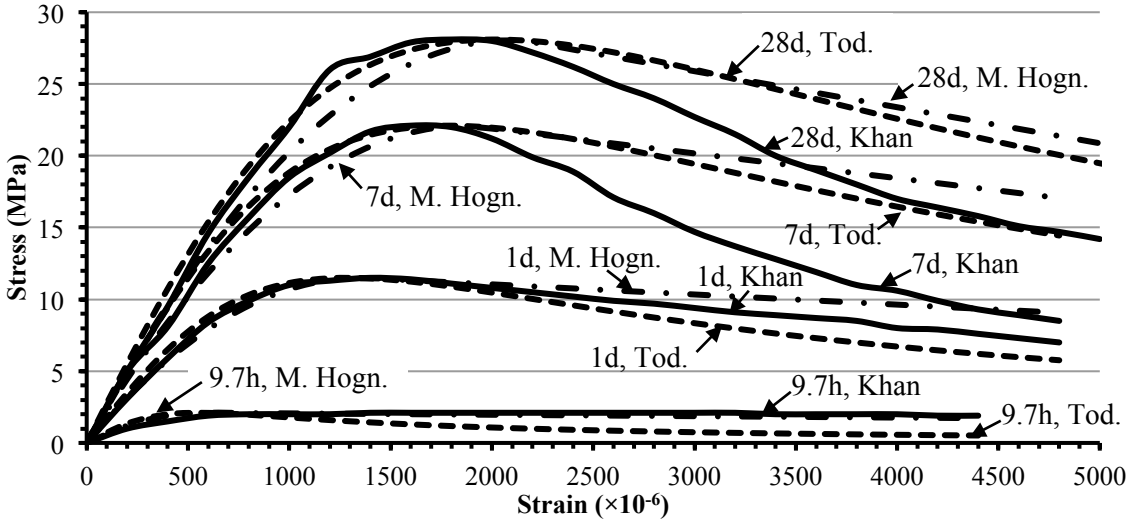

Figure 2-5: Stress-Strain from Data, Todeschini & Modified Hognestad Relationships, Khan

Figure 2-6 shows the stress-strain curves normalized by the maximum stress, f_0, at ages of 9.7 hours and one day. This figure and Figure 2-5 indicate that shortcomings of the Todeschini and Modified Hognestad relationships tend to disappear when the concrete is one day old, when the observed response starts to exhibit strain softening. A practitioner should be cautious when using either the Todeschini or Modified Hognestad relationship to predict the stress-strain responses of very young age concretes: the accuracy of these relationships depend heavily on the value of strain at peak stress. However, for more

realistic young ages, i.e. between one and three days old, the relationships reasonably predict the observed stress-strain response.

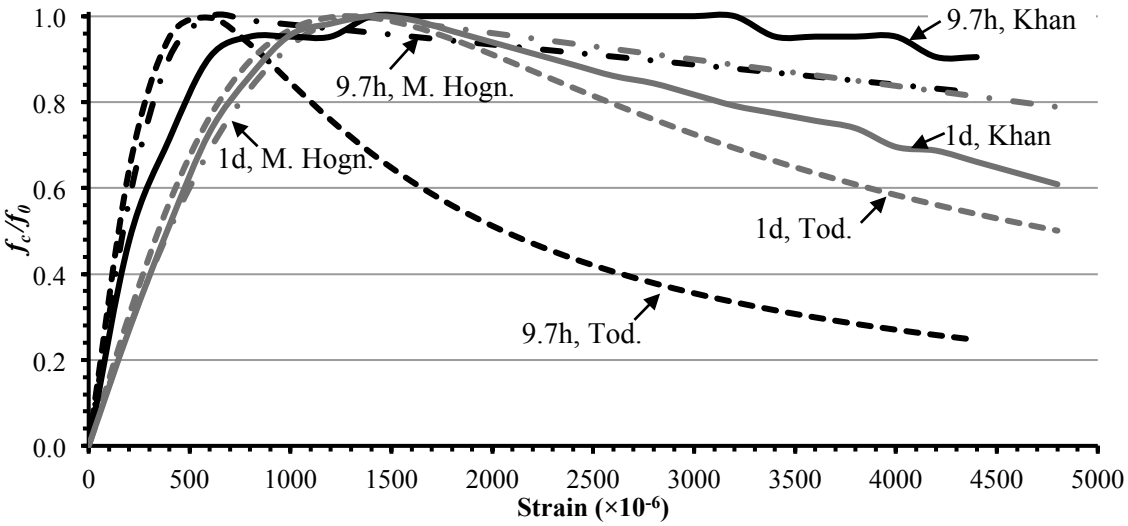

Figure 2-6: Normalized Stress-Strain Curves from Data, Todeschini & Modified Hognestad Relationships, Khan 9.7h & 1d

2.2.3 Elastic Secant Modulus at Young Ages

The elastic secant modulus was computed as the slope of the line drawn from a stress of zero to a compressive stress of $0.40f_0$. Table 2-2 and Table 2-3 compare the moduli computed at various ages from the Khan (1995) and Jin et al. (2005) data, respectively, to values predicted using the simple equation given in A23.3, Eq. [2.2], and the various Todeschini and Hognestad relationships. At very young ages, Eq. [2.2] overestimates the elastic modulus by up to 30%. Similarly the Todeschini and Modified Hognestad relationships also overestimate the elastic modulus because, for the data from both sources, they overestimate the stress at a given strain in the ascending portion of the stress-strain relationship. The Adjusted Todeschini and Adjusted Modified Hognestad

relationships, with larger strains at the maximum stress, underestimate the observed elastic moduli by up to 40%.

Table 2-2: Comparison of Elastic Secant Moduli with Khan (1995)

		Test/Predicted E_c				
Age	**E_c (MPa) Khan**	**A23.3 Eq [2.2]**	**Todeschini**	**Adjusted Todeschini**	**Modified Hognestad**	**Adjusted Hognestad**
9.7h	5,000	0.77	0.74	1.25	0.83	1.36
14.5h	11,300	0.89	0.81	1.19	0.92	1.29
17.7h	14,700	0.98	0.89	1.12	1.01	1.21
1d	15,000	0.98	0.89	0.97	1.01	1.04
1.24d	19,100*	1.10	0.99	0.95	1.13	1.03
3d	18,800	0.94	0.85	0.81	0.96	0.87
7d	20,400	0.96	0.86	0.78	0.98	0.84
14d	22,000	0.96	0.86	0.80	0.98	0.86
28d	24,000	1.01	0.90	0.81	1.03	0.87

*Results at 1.24d represent a local stiffness maximum, and therefore may be unreliable.

Table 2-3: Comparison of Elastic Secant Moduli with Jin et al. (2005)

		Test/Predicted E_c				
Age	**E_c (MPa) Jin et al.**	**A23.3 Eq. [2.2]**	**Todeschini**	**Adjusted Todeschini**	**Modified Hognestad**	**Adjusted Hognestad**
18h	11,700	0.84	0.74	1.24	0.87	1.39
1d	14,600	0.90	0.78	1.13	0.92	1.26
2d	15,600	0.82	0.71	0.97	0.83	1.09
3d	15,900	0.76	0.66	0.75	0.77	0.84
7d	24,200	0.94	0.81	0.74	0.96	0.83
28d	25,400	0.86	0.74	0.83	0.88	0.94

The Khan (1995) data show that when the age reaches 17.7 hours, the simple A23.3-14 equation, Eq. [2.2], gives a good estimate of the elastic modulus and gives results within 6% of the observed elastic moduli for concrete ages from 3 to 28 days. The Modified Hognestad relationship gives consistent results within 5% of the observed elastic moduli for concrete ages from 3 to 28 days and gives similar results as the A23.3 equation at all ages. For an age of one day the Modified Hognestad, Adjusted Todeschini and Adjusted

Modified Hognestad relationships all give consistent values for E_c. For concrete ages from 3 to 28 days the observed elastic moduli are consistently less than those predicted using the Todeschini, Adjusted Todeschini and Adjusted Modified Hognestad relationships.

The Jin et al. (2005) data show that there is great variability in the predicted elastic secant moduli at all ages and the predicted values using all relationships overestimate the observed elastic moduli for concrete ages of three days and older. The discrepancies between the observed values and those predicted using the A23.3 equation, Eq. [2.2], and the Todeschini, and Modified Hognestad relationships show no clear trend with increased concrete age. The Adjusted Todeschini and Adjusted Modified Hognestad relationships underestimate the observed elastic moduli at very young ages and overestimate the observed elastic moduli for ages older than two days. The discrepancies between the observed values and those predicted using the A23.3 equation and the Modified Hognestad relationship are similar at all ages.

Figure 2-7 compares the observed elastic moduli as fractions of the 28-day value from both studies with values computed using Eq. [2.2] for ages up to seven days. Even at very young ages, Eq. [2.2] adequately predicts the elastic moduli computed from the Khan (1995) stress-strain data. Equation [2.2] is less adequate predicting the elastic moduli from the Jin et al. (2005) stress-stain data, however, until the concrete reaches an age of seven days.

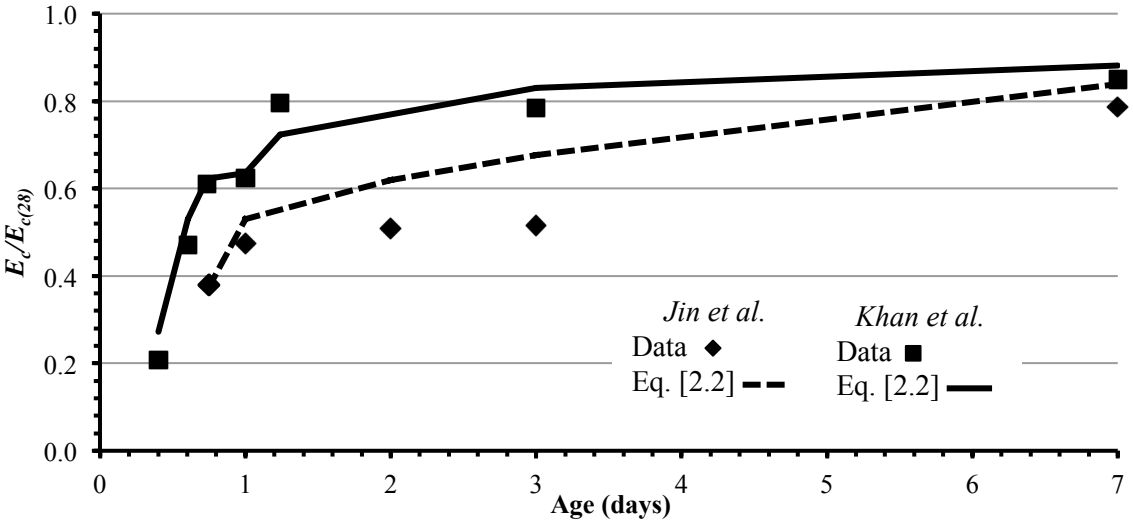

Figure 2-7: Comparison of Observed and Computed Normalized Elastic Moduli

2.2.4 Modulus of Rupture at Young Ages

Khan (1995) conducted modulus of rupture tests to determine the tensile strengths. This test subjects flexural specimens to significant strain gradients and flexural cracking and, therefore, is more relevant for determining deflections of flexural members. The mean modulus of rupture is typically taken to be proportional to square root of the compressive strength, i.e., (MacGregor & Bartlett 2000):

[2.10] $$\overline{f}_r = 0.69\sqrt{f'_c}$$

Jin et al. (2005) performed splitting tension tests, which yield the splitting tensile strength, f_{ct}, that approximate the shear strength of concrete (MacGregor & Bartlett 2000). The mean split cylinder strength is also often assumed to be proportional to square root of the compressive strength, i.e., (MacGregor & Bartlett 2000):

[2.11] $$\overline{f}_{ct} = 0.53\sqrt{f'_c}$$

Figure 2-8(a) and (b) show the variation of proportionality constants in Equations [2.10] and [2.11] observed in the Khan (1995) and Jin et al. (2005) data, respectively, for ages up to 7 days. The proportionality constants for the modulus of rupture computed from the Khan (1995) data, Figure 2-8(a), compare very well to the values of 0.6 and 0.69, used in Equations [2.3] and [2.11], respectively, even at very young ages. For these data, the A23.3 equation for the modulus of rupture, Eq. [2.3], is conservative for concrete ages of 14.5 hours or older. The proportionality constants for the splitting tensile strength computed from the Jin et al. (2005) data, Figure 2-8(b), approximate the values of 0.6 and 0.53 used in Equations [2.3] and [2.10], respectively, when the age exceeds 2 days.

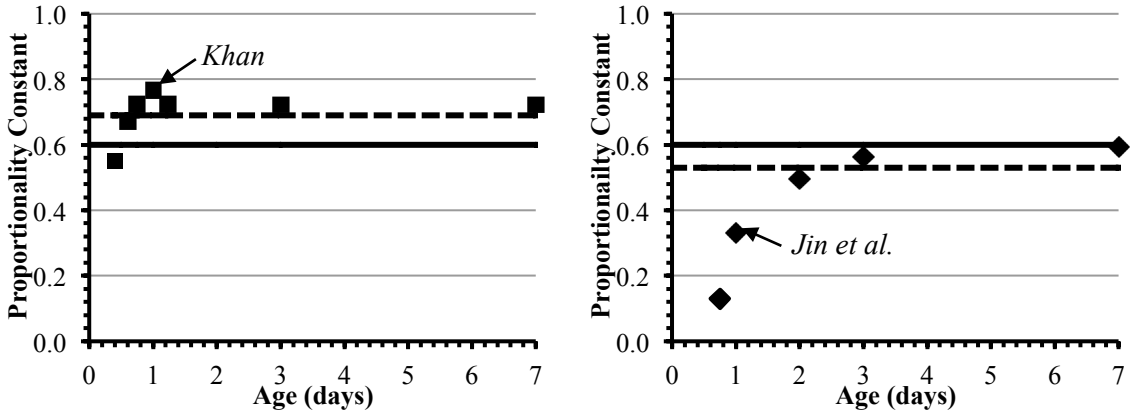

a) Modulus of Rupture Test, Khan (1995) *b) Splitting Tension Test, Jin et al. (2005)*

Figure 2-8: Proportionality Constant at Various Ages

2.3 MOMENT-CURVATURE ANALYSIS

The observed stress-strain relationships for very young and mature concretes are different. Moment-curvature analyses were therefore performed to determine the impact of this difference on the flexural response for a range of concrete ages and reinforcement

ratios. A rectangular cross section of 300×600mm was used and the parameters and associated ranges of variation were as follows:

- *Concrete age* – the concrete ages investigated ranged from 9.7 hours to 28 days.
- *Material properties* – for each age investigated, the concrete compressive strength, f_0, and elastic modulus, E_c, were determined from the stress-strain data obtained by Khan (1995) and Jin et al. (2005).
- *Reinforcement Ratios* – values of ρ were chosen to be 0.5%, 1% and 1.5%, reflecting a realistic range from lightly reinforced two-way slabs to more heavily reinforced beams.

Figure 2-9 shows the procedure for computing the moment and associated curvature for each increment of concrete extreme-fibre compressive strain. The calculation of the concrete compressive stress and force, indicated by the shaded box, can be based on simplified idealizations commonly assumed in practice, experimental concrete stress-strain data, or the Todeschini or Modified Hognestad relationships. Appendix A provides the detailed steps used to conduct the moment-curvature analysis and example calculations of the concrete compressive stresses and force using concrete stress-strain data and the Todeschini and Modified Hognestad relationships.

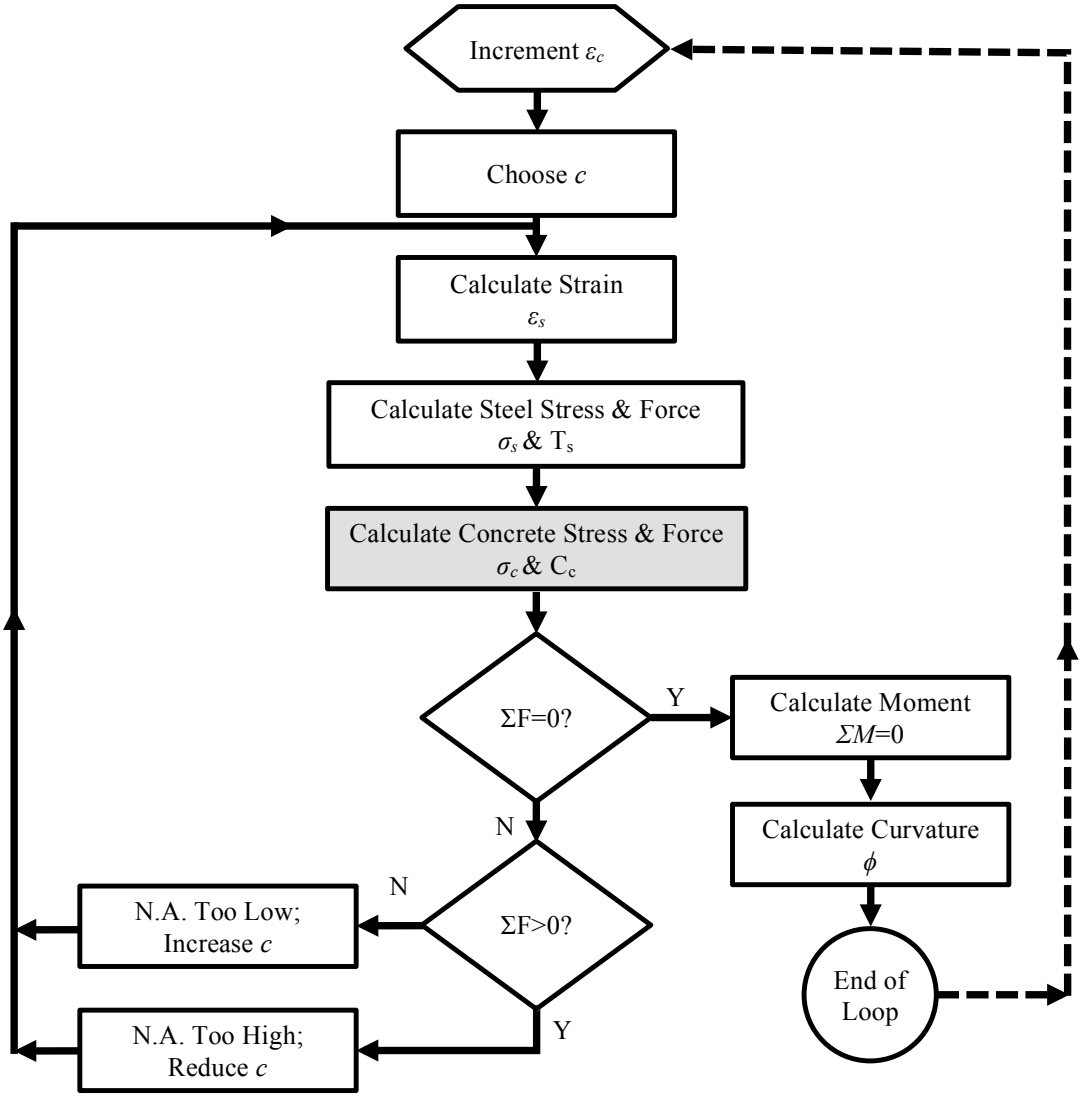

Figure 2-9: Moment-Curvature Analysis Flowchart

The applicability of conventional simplifying approximations adopted for the flexural analysis of reinforced concrete was investigated, specifically the assumptions of the linear-elastic response before cracking, the linear-elastic cracked response before the reinforcement yields and the stress block idealization (CSA 2014) at ultimate. This trilinear idealization of the moment-curvature relationship, shown in Figure 2-10, was computed manually and using a MS Excel (2011) spreadsheet. The limits of the response

are defined by the cracking, yielding and nominal ultimate moments, M_{cr}, M_y and M_n, respectively, and the associated curvatures, ϕ.

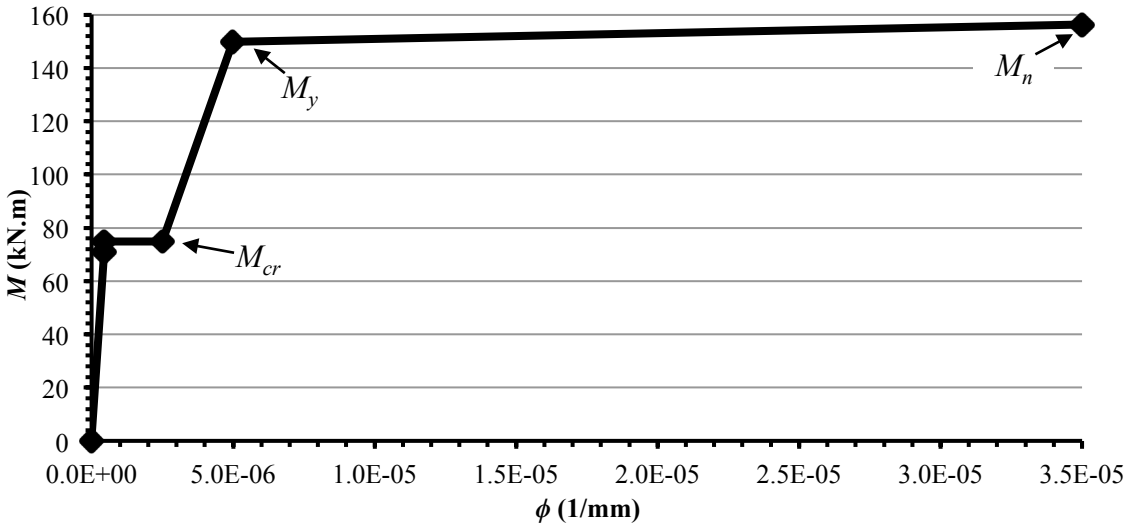

Figure 2-10: Trilinear Moment-Curvature Relationship Derived Using Conventional Simplifying Approximations

Figure 2-11 shows the effective cross sections, strain distributions and stress distributions assumed for the three phases of the trilinear idealization as follows:

- *Linear-uncracked analysis* – the applied moment is less than the cracking moment, $M_a < M_{cr}$. The section is therefore uncracked at this stage, as shown in Figure 2-11(a). Transformed section properties were computed using the modular ratio, n, which ranged from 31 at an age of 9.7 hours to 8.4 at an age of 28 days.
- *Linear-cracked analysis* – the applied moment exceeds the cracking moment but is less than the yield moment, $M_{cr} \leq M_a \leq M_y$. The section is now cracked, with the concrete and steel exhibiting linear-elastic responses as shown in Figure 2-11(b). The neutral axis depth in the uncracked section, kd, was calculated to satisfy horizontal force equilibrium using Eq. [2.5]. Then the cracked moment of inertia

was used to compute curvatures to satisfy moment equilibrium. The moment at which the steel yields (i.e. stress in the steel reaches f_y) and the corresponding curvature were also determined. The maximum concrete stresses was computed and compared to f_0 from the experimental data to check the assumption of a linear-elastic concrete response at steel yielding.

- *Nonlinear-cracked analysis* – the applied moment approaches the nominal ultimate capacity, $M_a \approx M_n$. The equivalent rectangular concrete stress block idealization from A23.3 (CSA 2014) was used to determine the nominal moment capacity and associated curvature as shown in Figure 2-11(c). The maximum neutral axis depth, *c/d,* limit for flexural members in CSA A23.3 (2014) was checked to verify that the steel yields. Resistance factors were neglected to facilitate comparison with experimental results.

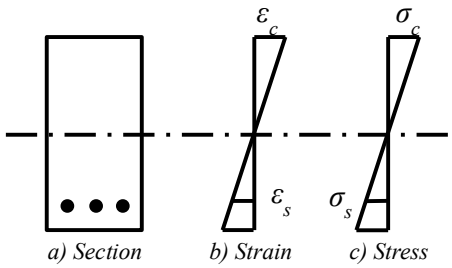

a) Linear-Uncracked Analysis

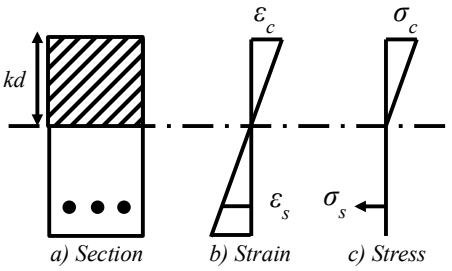

b) Linear-Cracked Analysis

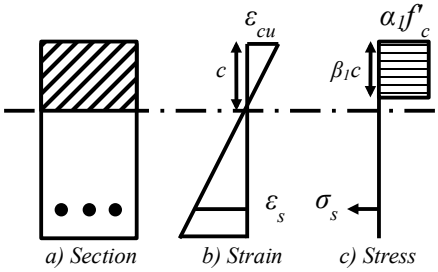

c) Nonlinear-Cracked Analysis

Figure 2-11: Conventional Simplifying Approximations

The analysis highlighted the pitfalls of applying these simplifying approximations to very young concretes. Figure 2-12 shows that, for 9.7-hour old concrete analysed using f_0 and E_c values from the Khan (1995) data, for the simplified trilinear idealization the maximum concrete compressive stress at cracking is $0.66f_0$. At greater curvatures, the assumption of a linear-elastic stress-strain relationship for concrete in compression is doubtful, even for a reinforcement ratio of 0.5%. The computed maximum concrete compression stress at steel yield greatly exceeds the compressive strength, so the estimation of the yield moment using linear-elastic cracked section analysis is incorrect.

The limit for *c/d* at ultimate is exceeded so the steel cannot be assumed to yield but section failure is instead initiated by the concrete crushing in compression. Whitney (1937) gives the following equation for the nominal moment of a section with compression-initiated failure:

[2.12] $$M_n = 0.333 f'_c b d^2$$

As shown in Figure 2-12(a), the nominal moment capacity obtained using this equation is conservative.

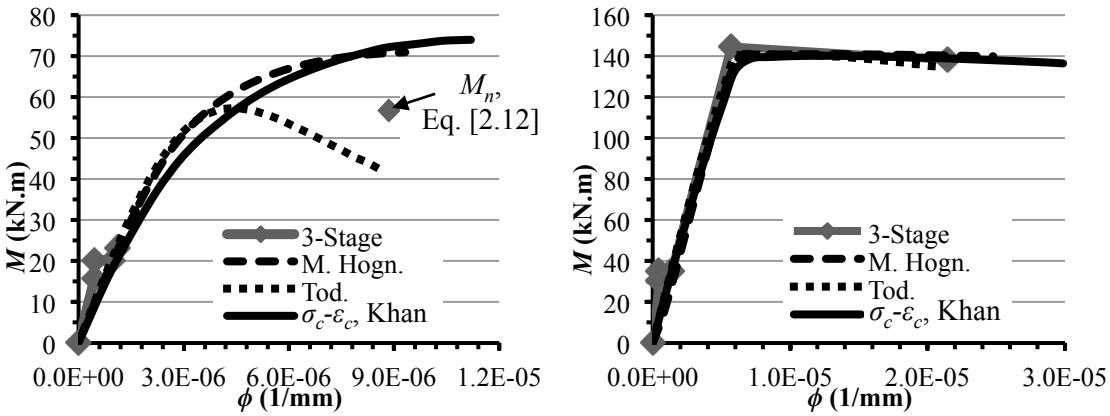

a) 9.7h *b) 14.5h*

Figure 2-12: Moment-Curvature for Various Stress-Strain Relationships, ρ=0.5%

Figure 2-12(a) also shows the moment-curvature response computed from the Khan stress-strain data (σ_c-ε_c, Khan), the Todeschini relationship (Tod.) and the Modified Hognestad relationship (M. Hogn.). The shape of the moment-curvature response computed from the Khan stress-strain data at an age of 9.7 hours, shown in Figure 2-12(a), differs from that of mature concrete. Because the steel stress never reaches yield, the neutral axis depth, *c,* increases when the extreme fibre strain exceeds ε_0, the strain corresponding to the maximum concrete compressive stress. In the moment-curvature

analysis of a section containing mature concrete, the neutral axis depth, *c,* begins to decreases after the steel yields.

Figure 2-12(b) shows the moment-curvature response when the concrete stress-strain response corresponding to that observed by Khan (1995), at a concrete age of 14.5 hours. In this case, the concrete has sufficient compressive strength to ensure steel yield at ultimate, and the ultimate nominal moment computed from the CSA A23.3 (CSA 2014) stress block idealization corresponds well to that computed from the observed stress-strain data. Close agreement is observed for the moment-curvature relationships computed from the observed stress-strain data reported by Khan, the Todeschini relationship, the Modified Hognestad relationship and the conventional simplifying approximations adopted in practice.

In both Figure 2-12(a) and (b), the moment-curvature relationships computed using the concrete stress-strain data reported by Khan or the Modified Hognestad relationship are similar, particularly in the region of maximum moment. The Modified Hognestad relationship works well because it accurately models the descending branch of the concrete stress-strain relationship observed by Khan as shown in Figure 2-6. The moment-curvature response computed using the Todeschini relationship shows significant strength loss beyond the maximum moment. As shown in Figure 2-13, the depth of the compression region is required to be much larger to satisfy force equilibrium using the Todeschini relationship. The resultant compressive force obtained assuming the Todeschini relationship is located much further from the extreme compression fibre than

that obtained for the Modified Hognestad relationship. Hence the moment arm between the resultant tension and compression forces is reduced, and so the resisting moment is also reduced.

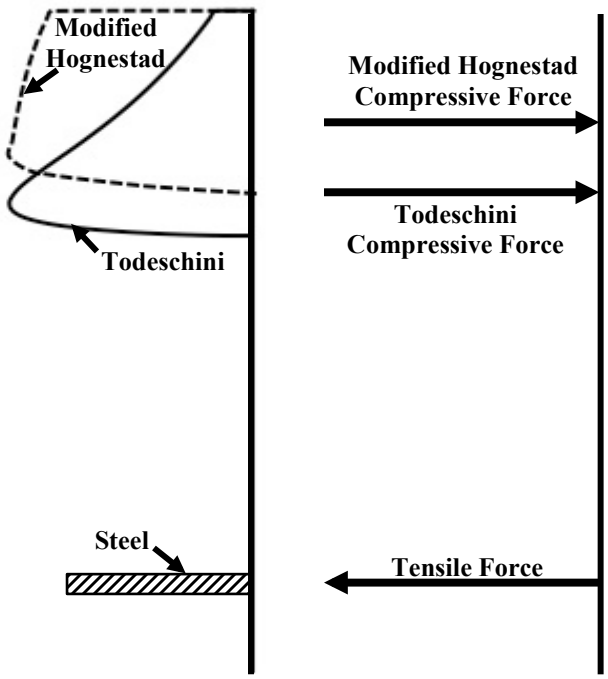

Figure 2-13: Force Equilibrium

Table 2-4 shows the variation of nominal ultimate moments and associated curvatures, ϕ_n, computed for a beam with 9.7 hour-old concrete. The result using the conventional simplifying approximations is based on a maximum concrete compressive strain of 0.0035 as specified in A23.3 (CSA 2014) with M_n computed using Eq. [2.12]. The Todeschini relationship assumes strain softening for strains greater than ε_0 so the nominal ultimate moment occurs at a much lower curvature and smaller ultimate extreme fibre compressive strain, ε_{ult}. The Modified Hognestad relationship more accurately simulates the observed descending branch of concrete in compression, Figure 2-6, and so yields a

higher nominal ultimate moment and associated ultimate curvature that are close to those computed using the concrete stress-strain data.

Table 2-4: Nominal Ultimate Moment and Curvature

Relationship	ε_{ult}	ϕ_n (1/mm)	M_n (kN.m)
Data, Khan	0.0044	11.2×10^{-6}	74.0
Conventional Simplifying Approximations	0.0035	9.16×10^{-6}	56.7
Todeschini	0.0013	4.35×10^{-6}	57.3
Modified Hognestad	0.0038	9.94×10^{-6}	71.0

A similar result is obtained at a slightly older concrete age of 18 hours for a cross section analyzed using the concrete stress-strain relationship observed by Jin et al. (2005), as shown in Figure 2-14. The result obtained using the conventional simplifying approximations provides a good approximation of the moment-curvature relationship computed using the concrete stress-strain data reported by Jin et al. (2005). The yield moment exceeds the ultimate nominal moment, however, even for a reinforcement ratio of 0.5%. This solution is inadmissible because the calculated maximum concrete compression stress corresponding to steel yield is 12.7MPa, exceeding f_0 of 9.5MPa. Using the observed concrete compression stress-strain data, the maximum concrete compression stress corresponding to steel yield is 8.1MPa, and the associated yield moment does not exceed the ultimate moment. Thus the conventional simplifying approximations that are the basis of these methods don't always hold for very young concretes. The idealization of concrete in compression as a linear-elastic material to compute the yield moment is not valid if the maximum concrete stress exceeds the elastic

limit, typically 0.6-0.7f_0 (MacGregor & Bartlett 2000), let alone the compressive strength, f_0.

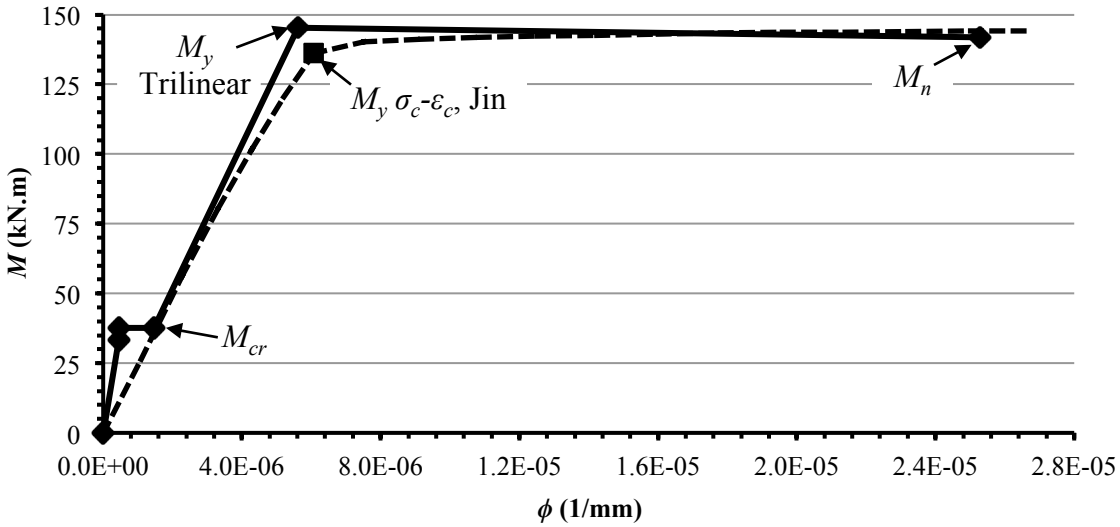

Figure 2-14: Trilinear Moment-Curvature Relationship, Jin et al. 18h

Figure 2-15(a) shows the effect of varying reinforcement ratio on the moment-curvature relationships calculated for a section consisting of 9.7 hour-old concrete. As the area of steel increases, the shortcomings of the Todeschini and Modified Hognestad relationships are amplified. The higher reinforcement ratios cause the strain softening-deficiencies of the Todeschini relationship to have an even greater impact on the nominal ultimate moment. For all reinforcement ratios, use of the Todeschini and Modified Hognestad relationships tend to overestimate the moments in the ascending portion of the moment-curvature relationship because, as shown in Figure 2-6, both imply a greater secant modulus than observed.

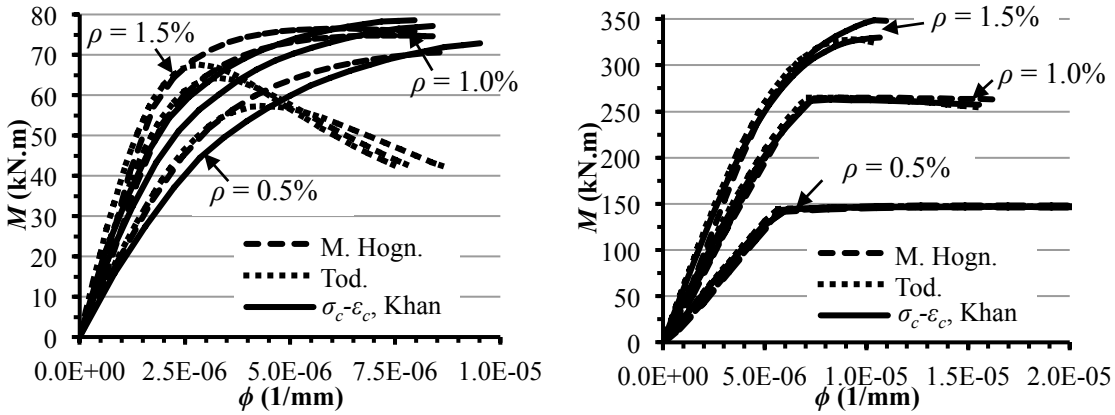

a) 9.7h *b) 1d*

Figure 2-15: Effect of Reinforcement Ratio, Khan

Figure 2-15(b) shows that, when the concrete age is only one day, the computed moment-curvature relationships for reinforcement ratios of 0.5%, and 1.0% are consistent. For the reinforcement ratio of 1.5% the flexural capacity of the section is initiated by compression failure, and the steel never reaches yield, as indicated by the shape of the moment-curvature response.

For very young concretes and associated low concrete strengths, it is prudent to check that the yield moment, M_y, computed using conventional elastic-cracked analysis is an admissible solution. The maximum neutral axis depth at ultimate requirement, *c/d*, (CSA 2014) may also be violated, causing the flexural capacity to be governed by compression-initiated failure. In this case, Whitney's Equation (1937), Eq. [2.12], should be used to determine the nominal moment capacity, M_n, of the section.

When the flexural capacity of a concrete member is governed by tension-initiated failure, the Todeschini and Modified Hognestad relationships predict moment-curvature

relationships and yield moments that closely approximate those computed from the stress-strain data. For very young concretes, the flexural capacity is likely governed by compression-initiated failure; in this case, the moment-curvature relationship computed using Modified Hognestad idealization is best to simulate that computed using the stress-strain data.

2.3.1 Flexural Rigidity at Young Ages

The flexural rigidity, E_cI_{cr}, of the member, and the ascending portion of the moment-curvature response, are of particular interest for deflection calculations. This section will therefore investigate whether the computed moment-curvature response for young-age concretes is well approximated by the flexural rigidity, E_cI_{cr}, computed as the product of the elastic secant modulus and the cracked moment of inertia using conventional simplifying approximations.

Figure 2-16(a) shows the moment-curvature relationship calculated for a concrete age of 9.7 hours using the Khan (1995) stress-strain data. Superimposed on the figure are the flexural rigidities obtained using an elastic modulus, E_c, computed using either Eq. [2.2] or the Khan (1995) stress-strain data and cracked moments of inertia computed using Eq. [2.4]. The difference between these computed flexural rigidities is negligible. Both computed flexural rigidities correlate well to the moment-curvature relationship at lower moment values. This may seem surprising given that Table 2-2, Table 2-3 and Figure 2-7 indicated that Eq. [2.2] tends to overestimate the observed elastic secant modulus for very young concretes. The explanation is clear from Table 2-5: the greater E_c computed using

Eq. [2.2] reduces the modular ratio, n, and so causes the cracked moment of inertia, I_{cr} to be lower. The resulting product, E_cI_{cr}, computed using the conventional simplifying approximations is only 9.6% greater than that obtained from the moment-curvature relationship derived using the Khan (1995) stress-strain data.

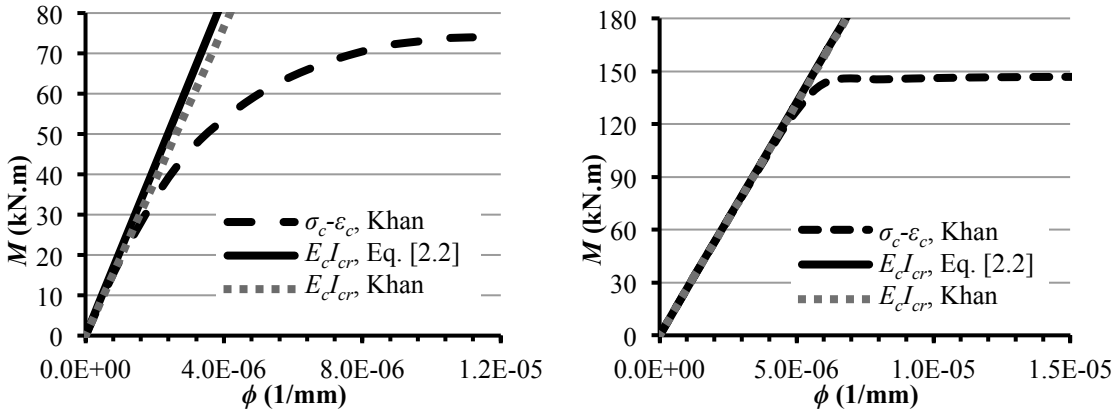

a) 9.7h *b) 1d*

Figure 2-16: Flexural Rigidity Based Moment-Curvature Relationships, Khan

Table 2-5: Flexural Rigidity Comparison

	Concrete age of 9.7 hours				**Concrete age of 1 day**			
	E_c (MPa)	**n**	**I_{cr} ($\times 10^6$mm^4)**	**E_cI_{cr} (kN.m^2)**	**E_c (MPa)**	**n**	**I_{cr} ($\times 10^6$mm^4)**	**E_cI_{cr} (kN.m^2)**
Khan Data	5000	40.0	3830	19100	14900	13.4	1770	26300
Conventional Simplifying Approximations	6520	30.7	3220	21000	15300	13.1	1730	26500

Figure 2-16(b) shows a similar comparison for one-day-old concrete, the difference between flexural rigidities computed using E_c from Eq. [2.2] or from the Khan (1995) stress-strain data and I_{cr} from Eq. [2.4] is again negligible. Both computed flexural rigidities correlate very well to the moment-curvature relationship derived using the Khan (1995) stress-strain data. The data in Table 2-5 confirm that any differences between E_c, I_{cr} and, therefore, E_cI_{cr}, are negligible.

The impact of the reinforcement ratio on the flexural rigidity at various concrete ages was also explored. Table 2-6 shows the ratio of E_cI_{cr} calculated using the conventional simplifying approximations or the Todeschini or Modified Hognestad relationships with that computed from the stress-strain data for concrete ages of 9.7 hours, 14.5 hours, 17.7 hours and one day. The E_c values shown correspond to the early-age secant moduli as previously shown in Table 2-2. At very young ages the elastic moduli computed using Eq. [2.2] and the Modified Hognestad relationship cause the cracked stiffness, E_cI_{cr}, to exceed that computed from the Khan data. Increasing the reinforcing ratio very slightly increases this difference. The cracked stiffness computed using the Todeschini relationship underestimates the flexural rigidity computed using the Khan data and this difference is again slightly greater as ρ increases. However, even when the concrete reaches the very young age of 14.5 hours, the cracked stiffnesses computed using the various procedures converge. When the concrete is one day old, with a strength of 38% of the 28-day specified strength, the differences between the flexural rigidities using the various procedures are negligible.

Table 2-6: Effect of ρ on E_cI_{cr}

		E_cI_{cr}/(Khan, t)		
Age	**ρ**	**Conventional Simplifying Approximations**	**Todeschini**	**Modified Hognestad**
9.7h (f'_c = 2.1MPa)	0.5%	1.10	0.92	1.07
	1.0%	1.13	0.89	1.09
	1.5%	1.15	0.88	1.10
14.5h (f'_c = 8.0MPa)	0.5%	1.03	0.95	1.02
	1.0%	1.04	0.94	1.03
	1.5%	1.05	0.93	1.03
17.7h (f'_c = 11.0MPa)	0.5%	1.00	0.97	1.00
	1.0%	1.01	0.96	1.00
	1.5%	1.01	0.96	1.00
1d (f'_c = 11.5MPa)	0.5%	1.00	1.01	1.00
	1.0%	1.01	1.01	1.00
	1.5%	1.01	1.01	1.00

2.4 SUMMARY & CONCLUSIONS

This chapter presented an investigation into the early-age material properties of concrete that impact computed instantaneous deflections. The experimental stress-strain response and material properties reported by others (Khan 1995, Jin et al. 2005) included concrete from ages of 9.7 hours to 91 days. In the present study, concrete ages up to 28 days were investigated, very young concrete is deemed to be less than 24 hours old, and young concrete is considered to be from one to three days old. The accuracy of the Todeschini (1964) and Modified Hognestad (1951) stress-strain relationships to model the experimental stress-strain responses was investigated because the behaviour of concrete at very young ages may differ markedly from that of mature concrete (MacGregor & Bartlett 2000). The flexural behaviour of sections at young ages can be quantified given variations in the concrete stress-strain relationship, so moment-curvature analyses based on conventional simplifying approximations, the reported concrete stress-strain data, and the Todeschini and Modified Hognestad relationships were performed. Deflections depend on member stiffness and so on the flexural rigidity, $E_c I_{cr}$. Early-age flexural rigidities obtained from moment-curvature analysis for rectangular cross sections with varying reinforcement ratios were also explored.

The conclusions concerning the compressive stress-strain response are as follows:

1. For concrete ages less than one day, the observed stress-strain responses reported by Khan (1995) and Jin et al. (2005) do not exhibit strain softening. The Todeschini and Modified Hognestad relationships simulate strain softening and so are not accurate for very young concretes.

2. The accuracy of the Todeschini and Modified Hognestad relationships for very young concretes also depends on ε_0, the strain corresponding to the maximum stress. It is concluded that:
   i) Conventional equations to compute ε_0 underestimate the observed ε_0 values.
   ii) Increasing ε_0 improves the fit of the adjusted stress-strain relationships to the observed data but also causes the elastic modulus, E_c, to be underestimated.
   iii) Very young age concretes do not exhibit a clear maximum compressive stress, so quantifying ε_0 is challenging.
3. The simple CSA A23.3 (2014) empirical equation, Eq. [2.2], overestimates E_c for very young concretes, and so is unconservative. At ages of one day or greater, the strength gain is sufficient for the A23.3 equation to predict accurately E_c values observed by Khan (1995).
4. The CSA A23.3 (2014) empirical equation for the modulus of rupture accurately quantifies the flexural strengths observed by Khan (1995) if the concrete is at least 14.5 hours old.

The conclusions drawn from the moment-curvature analyses are as follows:

5. Conventional simplifying approximations adopted for flexural analysis do not apply to very young concrete. The computation of M_y based on elastic-cracked analysis may be inaccurate because the assumption of linear-elastic response of concrete in compression is wrong. The low compressive strength of young age concrete makes it is prudent to check that the maximum *c/d* limit in A23.3-14 is

satisfied. If the flexural capacity is controlled by compression-initiated failure, M_n may be computed using Whitney's Equation (1937).

6. Use of the Todeschini and Modified Hognestad relationships overestimates the initial rigidity in the ascending portion of the moment-curvature response at very young ages. When the concrete age exceeds 14.5 hours, this difference becomes negligible.
7. The Todeschini relationship predicts significant strain softening and so underestimates the nominal ultimate moments and the associated curvatures and extreme fibre concrete strains for very young concretes. The Modified Hognestad relationship predicts less strain softening, and more closely approximates these quantities even for very young age concrete.
8. The conventional procedures to compute the cracked stiffness, E_cI_{cr}, give acceptable results even for very young concretes. For a concrete age of 9.7 hours, the difference between E_cI_{cr} computed using conventional procedures or that with E_c computed from the stress-strain data is less than 10%. For a concrete age of one day or older, this difference is 1%. Although E_c is underestimated for very young concretes, the modular ratio, n, is overestimated thus I_{cr} is overestimated. Thus the product E_cI_{cr} is more accurate than either E_c or I_{cr}.

CHAPTER 3: INSTANTANEOUS DEFLECTIONS COMPUTED USING DISCRETIZED ANALYSIS

3.1 METHODS OF DEFLECTION CALCULATION

Flexural cracking of a reinforced concrete member occurs at discrete locations along the span length where the applied moment, M_a, exceeds the cracking moment, M_{cr}, given by:

[3.1] $$M_{cr}=\frac{f_r I_g}{y_t}$$

where f_r is the modulus of rupture, I_g is the gross moment of inertia, and y_t is the distance from the section centroid to the extreme tension fibre. At these locations the cracked moment of inertia, I_{cr}, applies and for a rectangular cross section without compression reinforcement is given by Eq. [2.4]. Between cracks, the moment of inertia approaches the gross moment of inertia, I_g: this is widely known as the tension stiffening effect (e.g., MacGregor & Bartlett 2000).

3.1.1 Equations for Deflection Calculation

Branson (1965) proposed that the rigidity of a reinforced concrete beam with cracks at discrete locations could be quantified using an effective moment of inertia, I_e, computed as:

[3.2] $$I_e=\left(\frac{M_{cr}}{M_a}\right)^m I_g + [1-\left(\frac{M_{cr}}{M_a}\right)^m]I_{cr}$$

where the exponent, m, was determined empirically. Branson recommended m of 3 to determine an overall average effective moment of inertia when the member is idealized as a single element. To determine effective moments of inertia at individual sections

when a member is idealized as discretized elements Branson recommended m of 4. In either case, as the applied moment increases, the tension stiffening effect is reduced and I_e approaches I_{cr}.

Bischoff (2005) has highlighted the need for better methods for evaluating instantaneous deflections for Fibre-Reinforced Polymer (FRP) and lightly reinforced steel concrete beams. The Branson Equation was empirically derived from tests of concrete beams with steel reinforcement ratios, ρ, between 1 and 2%. Within this range, the equation is adequate but for lower reinforcement ratios, it overestimates the tension stiffening effect. The mechanical model of the Branson Equation is wrong, incorrectly idealizing the cracked and uncracked regions as springs in parallel, when they should be in series. Thus the equivalent stiffness incorrectly approaches the uncracked stiffness when the cracked stiffness approaches zero (Bischoff 2007). For lightly reinforced members, such as slabs, with reinforcement ratios less than 1%, the ratio of I_g/I_{cr} increases, I_e is overestimated, and the deflection is underestimated using the Branson Equation (Bischoff 2005).

Bischoff proposed the following equation for I_e that correctly idealizes the uncracked and cracked regions as springs in series (Bischoff 2007). For $M_{cr}/M_a \leq 1$:

[3.3] $$I_e = \frac{I_{cr}}{[1 - (1 - \frac{I_{cr}}{I_g})(\frac{M_{cr}}{M_a})^2]}$$

For $M_{cr}/M_a > 1$, the effective moment of inertia computed using Eq. [3.3] may be negative, in which case I_e should be taken equal to I_g.

To account for tensile stresses in flexural elements due primarily to restraint of shrinkage, A23.3-14 (CSA 2014) requires that the cracking moment be calculated using a reduced modulus of rupture, f_r. When using the Branson Equation, Eq. [3.2], A23.3 requires M_{cr} to be computed using $0.5f_r$ for beams, one-way and two-way slabs. The coefficient of 0.5 is also intended to compensate for the unconservativism of the Branson Equation at low reinforcement ratios. When using the Bischoff Equation, Eq. [3.3], Scanlon and Bischoff (2008) recommend that M_{cr} be calculated using $0.67f_r$. Figure 3-1 shows the variation of I_e/I_g calculated from Eq. [3.2] (with m of 3) and Eq. [3.3] using both the full and reduced moduli of rupture. For ρ greater than 1%, the four approaches yield virtually identical results, as they require I_e equal to I_{cr}. For ρ between 0.2 and 0.7%, the I_e value computed using the Branson Equation, Eq. [3.2], with the full modulus of rupture is markedly greater than that computed using the Bischoff Equation, Eq. [3.3], with the full modulus of rupture. Using the reduced moduli of rupture the Branson and Bischoff Equations yield similar I_e values (CAC 2016).

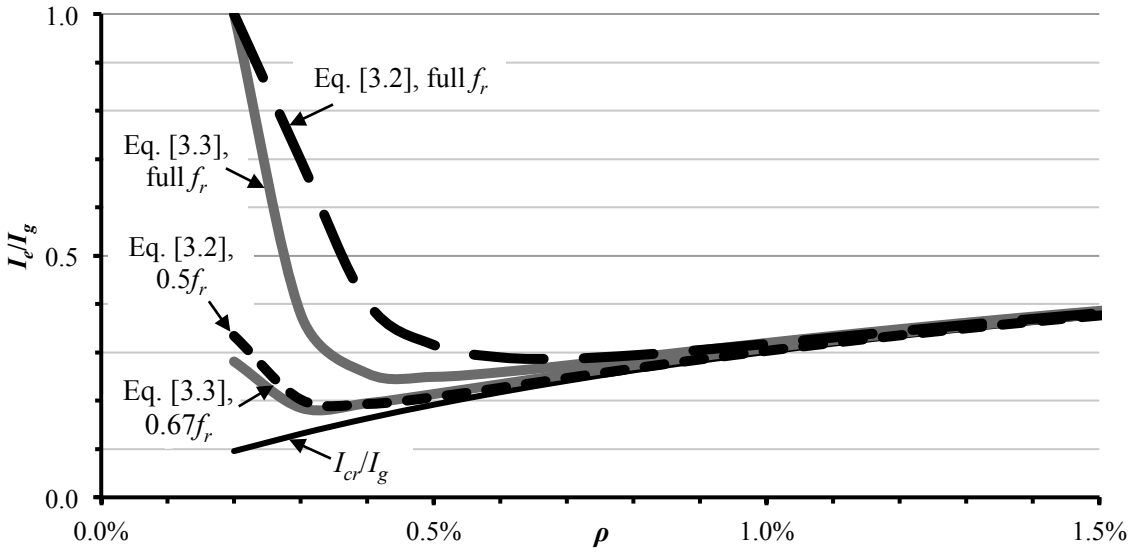

Figure 3-1: Variation of I_e/I_g with Reinforcement Ratio (after CAC 2016)

3.1.2 Member Idealization for Deflection Calculation

Deflection analyses can be carried out by idealizing the member as a single element with an average effective moment of inertia, as shown in Figure 3-2(a), or as a number of discretized elements with unique effective moments of inertia, as shown in Figure 3-2(b). Table 3-1 presents the equations given in A23.3-14 to determine the average effective moment of inertia of a continuous member using the mid-span value, $I_{e(m)}$, and end values, $I_{e(1)}$ and $I_{e(2)}$.

Table 3-1: Equations for Weighted Average I_e for Continuous Spans (CSA 2014)

Displacement Boundary Condition	Equation	Note
One end continuous	$I_e = 0.85I_{em} + 0.15I_{ec}$ where I_{em} is the value of I_e at midspan, and I_{ec} is the value of I_e at the continuous support	A23.3-14 Eq. 9.4
Both ends continuous	$I_e = 0.70I_{em} + 0.15(I_{e1} + I_{e2})$ where I_{e1} is the value of I_e at the left support, and I_{e2} is the value of I_e at the right support	A23.3-14 Eq. 9.3

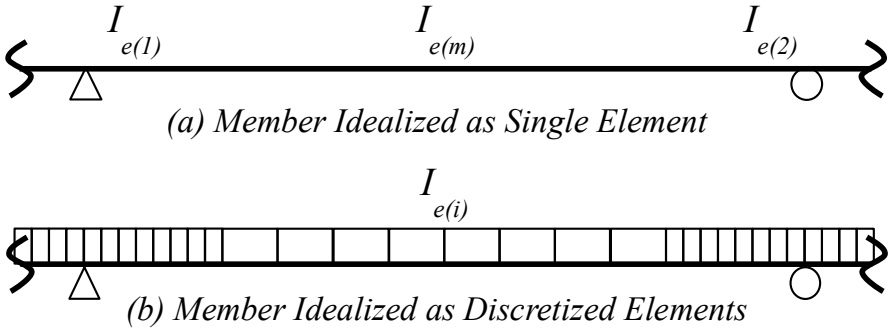

Figure 3-2: Member Idealizations for Deflection Calculation

The I_e computed for a single-element idealization is therefore a weighted average of the values computed at locations of maximum applied moments (i.e., large positive moments at mid-span and large negative moments at the supports). When the member is idealized using discretized elements, a more stringent criterion, and so a reduced I_e, is required for

the cracked regions because the discrete analysis also captures the effect of the uncracked regions that contribute little to the deflection. As already noted, Branson (1965) recognized the need for stricter criteria for discretized analysis and recommended that the exponent used for the single-element idealization, m=3, be increased to 4.

Bischoff's proposed equation is comparable to the Branson 3rd power equation in that it gives an average effective moment of inertia for the single-element idealization. To allow the Bischoff Equation to be used to in a discretized analysis, a similar modification to the exponent m should be investigated. The two equations, two member idealizations and the corresponding exponents are summarized in Table 3-2.

Table 3-2: Member Idealization & Equations for I_e

Equation	Exponent Used For		Comment
	Single-Element Idealization	Discretized-Element Idealization	
Branson (1965)	3	4	Springs in parallel
Bischoff (2005)	2	?	Springs in series

Because a discretized-element idealization involves computing a unique effective moment of inertia at individual sections another important aspect of the analysis is the selection an appropriate element length. The chosen mesh size will impact the accuracy of the results and the computational demand of the analysis. Using an extremely fine mesh that involves longer run times may not be practical for design office use, thus a mesh sensitivity analysis is needed to determine an adequate mesh size that balances accuracy and practicality.

3.1.3 Chapter Objectives

The main objectives of the research reported in this chapter are:

1. To determine, through a mesh sensitivity analysis, the largest practical mesh size that will still yield accurate results for in-office use.
2. To verify the value of m=4 in the Branson Equation for use in a discretized analysis.
3. To determine m for use in the Bischoff Equation for use in a discretized analysis.

To achieve these objectives a mesh-sensitivity analysis was performed and test cases with variable reinforcement and live-to-dead load ratios were devised. This chapter describes the procedures followed and the findings obtained concerning the instantaneous deflections of concrete members computed using discretized analysis.

3.2 MESH SENSITIVITY

When discretizing a member, choosing an optimal mesh size to achieve a proper balance between accuracy and computing requirements is necessary (Cook et al. 2002). A fine mesh yields more accurate results, but at a higher computational cost (i.e., longer analysis run times), so an investigation of the sensitivity of the discretized analysis result to element length was performed. This is an important exercise as element length, or more generally mesh size, plays a significant role in the accuracy of results.

The case of a three-span continuous member was explored first. The member was designed for three different negative reinforcement ratios, i.e., ρ^- of 0.5%, 1% and 1.5%.

Service loads were determined for three live-to-dead load ratios, i.e., w_L/w_D of 0.5, 1.0 and 1.5. The details of the general design procedure are presented in Section 3.0 of this chapter and the additional steps taken for the three-span continuous member are outlined in Section 3.3. Different mesh sizes were considered for the nine different loading and reinforcement ratio combinations using the Branson 4th power equation because it has been previously verified for discrete analysis (Branson 1965).

A Microsoft Excel (2011) spreadsheet was developed to perform a deflection calculation using both the single- and discretized-element idealizations. The spreadsheet used in the discretized-element idealizations was verified by setting $I_e=I_g$ and checking that the discretized-element results from the spreadsheet equalled those computed from standard deflection equations. The resulting differences, shown in Appendix B**,** are less than 0.25%.

Figure 3-3 shows schematically the mesh sizes investigated. Figure 3-3(a) shows the applied moment variation normalized by the nominal moment, M_0, resulting from the total applied uniformly distributed load, $wL^2/8$. Figure 3-3(b) shows the meshes using elements of uniform length with 50 elements in each half-length of beam, $L/2$. Uniform-length element meshes with 20, 10, 7 and 5 elements in each half-length of beam were also investigated. The benefit of uniform-length element meshes is that they are readily specified by the analyst and can be automatically implemented in most proprietary analysis software packages. The normalized bending moment diagram, Figure 3-3(a), shows a higher moment gradient in the negative moment regions near the supports, which

suggests that smaller elements lengths may be needed in this region to capture accurately the member response. Thus variable-length element meshes, as shown in Figure 3-3(c), were also explored. For each combination of the live-to-dead load ratio and reinforcement ratio, the location of the point of inflection was calculated. The region from the support to the point of inflection was idealized using 2, 4, or 6 elements and the region from the point of inflection to midspan was idealized using 3, 12 and 7 elements, respectively. The particular case of six elements in the negative moment region and seven elements in the positive moment region from the point of to midspan is shown in Figure 3-3(c).

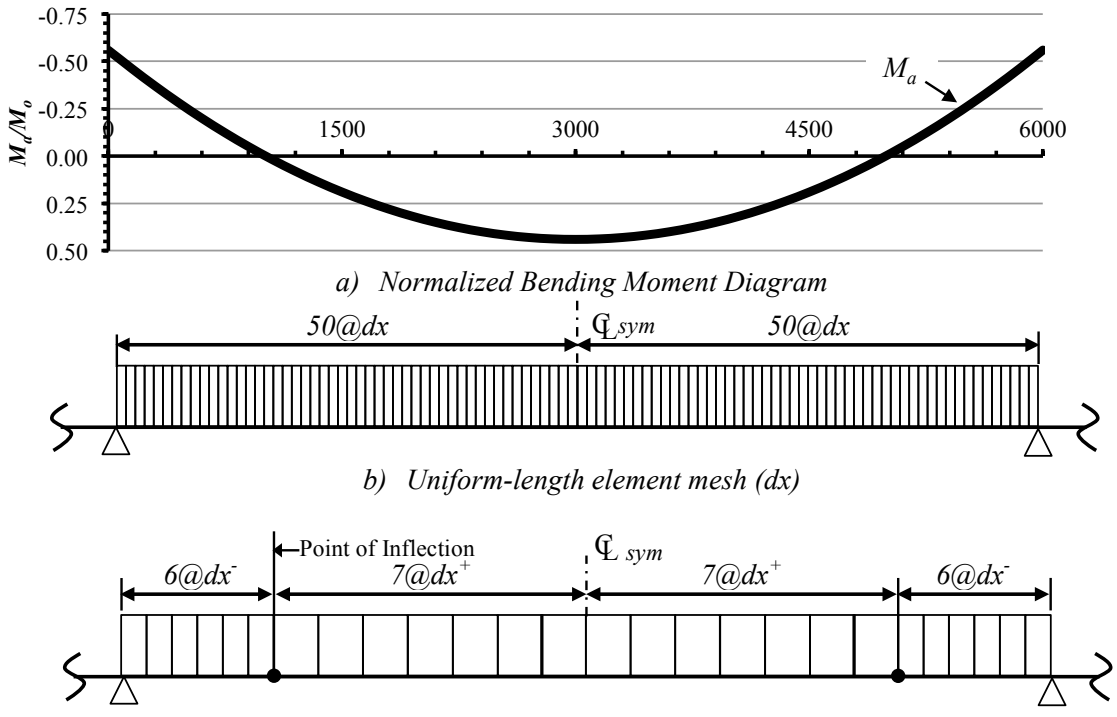

a) Normalized Bending Moment Diagram

b) Uniform-length element mesh (dx)

c) Variable-length element mesh (dx^+ and dx^-)

Figure 3-3: Mesh Sizes

Treating the finest mesh with 50 elements as the "gold standard", Table 3-3 compares the maximum deflection computed using the coarser meshes to that computed using the 50-

element mesh. Positive differences indicate that the maximum deflection computed using the 50-element mesh is greater than that computed using the coarser meshes. Clearly, decreasing the number of elements will increase the underestimation of the deflection, which is not desirable. For the uniform-length element meshes, the underestimation of the deflection is less than 6% if at least 5 elements are using in each half-span. For practical design office purposes, increasing the mesh size to 10 uniform-length elements per half-span may be satisfactory for this type of discretized sectional analysis as the maximum difference in deflection is within 2.2% of that computed using the 50-element mesh. In the context of the statement by ACI Committee 435 (1995) that "the magnitude of actual deflections in concrete structural elements...can only be estimated within a range of 20-40 percent accuracy", this percentage error is insignificant.

Table 3-3: Sensitivity of Maximum Deflection to Mesh Size

	% Difference with respect to the 50 Element Result								
	w_L/w_D = 0.5			**w_L/w_D = 1.0**			**w_L/w_D = 1.5**		
# of Elements	**ρ = 0.5%**	**ρ = 1.0%**	**ρ = 1.5%**	**ρ = 0.5%**	**ρ = 1.0%**	**ρ = 1.5%**	**ρ = 0.5%**	**ρ = 1.0%**	**ρ = 1.5%**
50	0.0%	0.0%	0.0%	0.0%	0.0%	0.0%	0.0%	0.0%	0.0%
20	0.2%	0.2%	0.2%	0.2%	0.1%	0.1%	0.2%	0.1%	0.2%
10	2.2%	0.6%	1.3%	1.0%	0.7%	0.3%	0.6%	0.5%	0.8%
7	4.3%	2.2%	1.2%	2.2%	0.5%	1.9%	1.7%	1.3%	0.8%
5	5.7%	3.8%	1.6%	3.9%	2.1%	3.0%	2.8%	2.1%	3.7%
$6^-\_12^+$	0.8%	0.3%	0.0%	0.3%	0.3%	0.1%	0.2%	0.2%	0.1%
$4^-\_12^+$	1.6%	0.1%	0.6%	0.5%	0.1%	0.3%	0.3%	0.2%	0.2%
$6^-\_7^+$	1.4%	0.4%	0.6%	0.4%	0.4%	0.4%	0.3%	0.4%	0.4%
$2^-\_3^+$	5.2%	3.6%	2.2%	3.6%	1.9%	1.8%	3.8%	1.4%	1.8%

The trend for the variable-length element meshes shown in Table 3-3 is similar. The maximum deflection computed using $6^-\_7^+$ mesh gives better results than that computed using the $2^-\_3^+$ mesh because the former is finer. The $2^-\_3^+$ mesh generally gives

computed deflections that more closely approximate those computed using the uniform-length 5-element mesh. This indicates that the effect of the moment gradient near the supports is marginally important.

The variable-length $6^{-}\_7^{+}$ mesh with 13 elements in the half-span, the $4^{-}\_12^{+}$ mesh with 16 elements and the $6^{-}\_12^{+}$ mesh with 18 elements yield similar deflections. Not surprisingly, the constant-length 10- and 20-element meshes bound these results. The deflections obtained using the variable-length $4^{-}\_12^{+}$ and $6^{-}\_12^{+}$ meshes are very similar and are typically within 1% of the deflections computed using the constant-length 50-element mesh. This again indicates that capturing the effect of the greater moment gradients near the supports is marginally important. In practice the effort required to locate the point of inflection likely outweighs any benefit attributable to the use of a finer mesh in the negative moment region.

Figure 3-4 shows the variation of moment and I_e/I_g as computed using different meshes for ρ of 0.5% and w_L/w_D of 0.5, which typically shows the greatest mesh sensitivity. Figure 3-4(a) shows a symmetric bending moment diagram and that the applied moment exceeds the cracking moment within approximately 800mm from each support and within approximately 1000mm of midspan.

The I_e/I_g values for constant-length 50-, and 5-element meshes are compared on left side of Figure 3-4(b). The 50-element mesh more effectively simulates the uncracked region of the member than the coarser 5-element mesh. Similarly, the comparison of I_e/I_g values for the variable-length element meshes, shown on the right side Figure 3-4(b), indicate

that the finer meshes are more efficient in simulating the stiffness in the uncracked region.

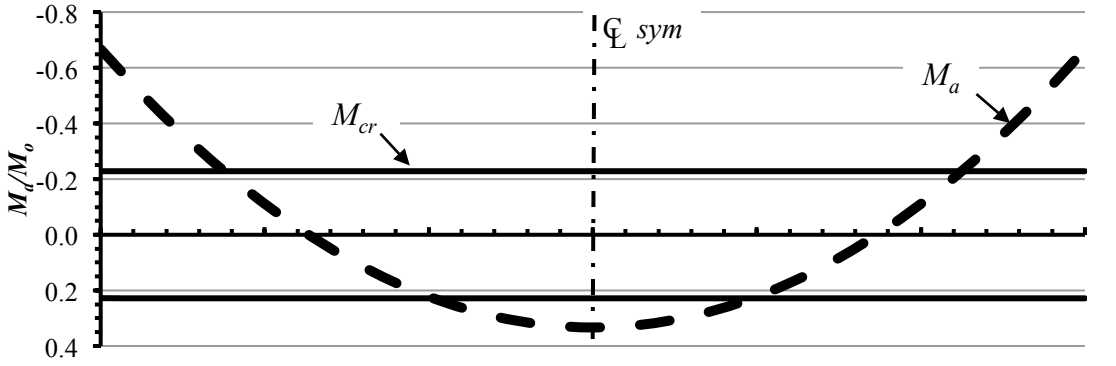

a) Normalized Bending Moment Diagram

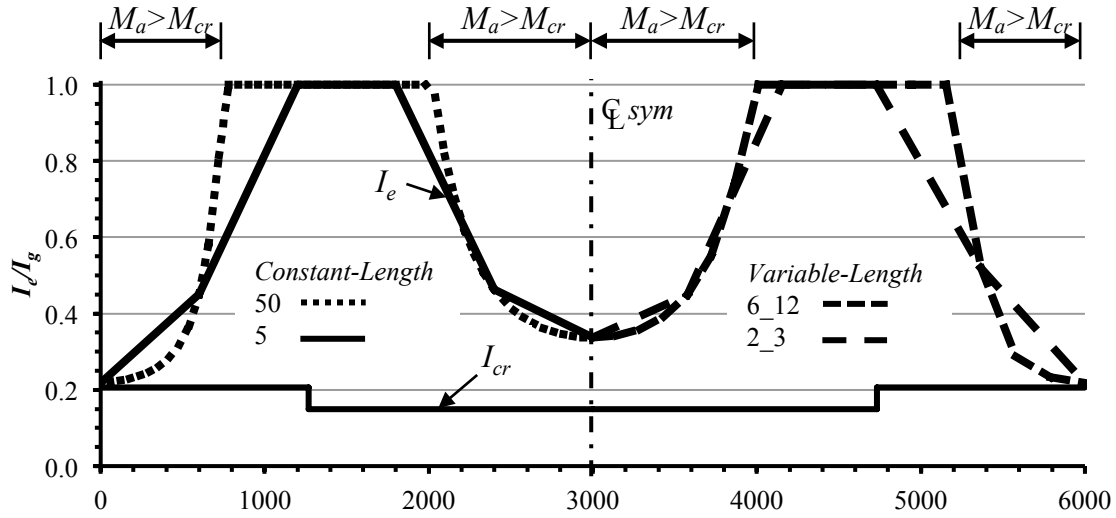

b) Normalized Effective Moments of Inertia

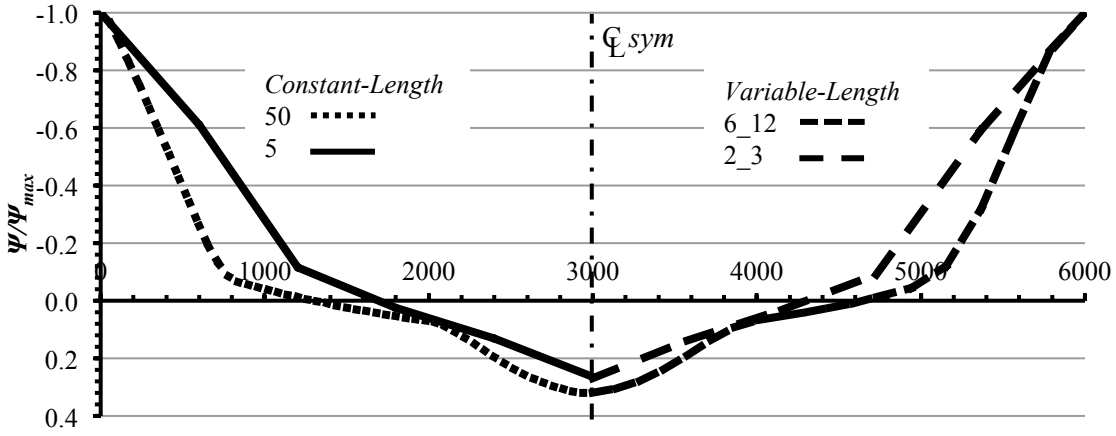

c) Normalized Curvature

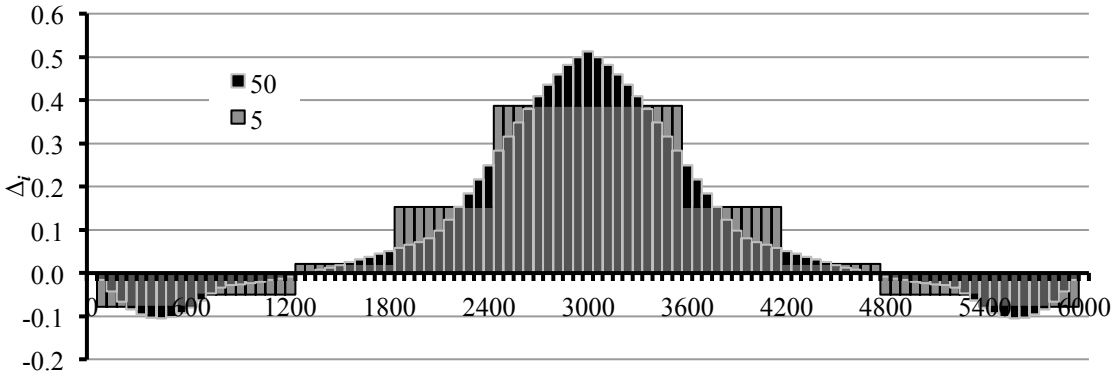

d) Increment of Deflection using Constant-Length Element Mesh

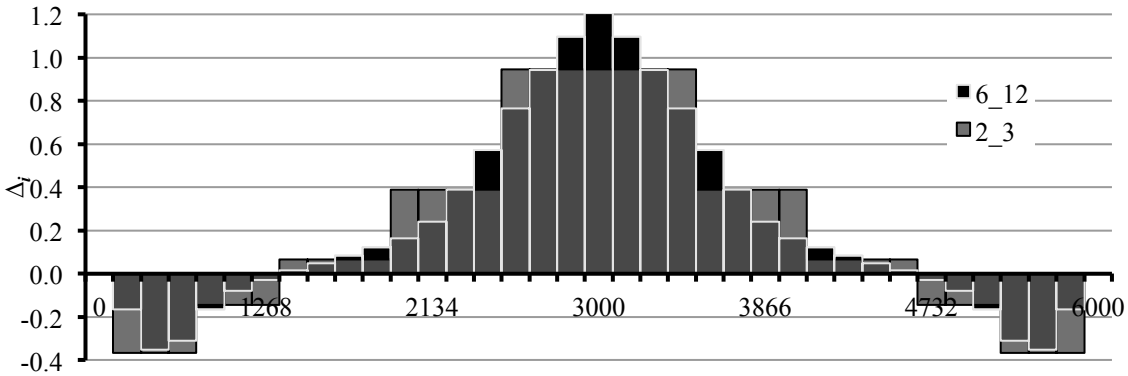

e) Increment of Deflection using Variable-Length Element Mesh

Figure 3-4: Analysis of Discretized Three-Span Beam with Different Meshes, Branson

It may seem that because the finer meshes capture more of the uncracked region that the analysis would show greater member stiffness and therefore, a smaller computed deflection. Figure 3-4(c) shows the computed curvatures, Ψ, normalized by the maximum negative curvature computed at the support. The 5-element mesh predicts the smallest curvature in the positive moment region, near midspan, and the largest curvatures in the negative moment region, near the supports. The total midspan deflection is the summation of the areas under the curvature diagram, and because the coarse mesh over-predicts the curvature near the support and under-predicts the curvature near midspan, the resulting computed deflection is less than that computed using the 50-element mesh.

This point is echoed in Figure 3-4(d) and (e), which shows the incremental deflection using a constant-length and variable-length element mesh, respectively. The coarser constant-length and variable-length element meshes, 5 and $2^{-}\_3^{+}$, respectively, underestimate the increments of deflection in the positive moment region. This region has the greatest contribution to the overall mid-span deflection, therefore, the resulting computed deflection is less than that computed using a finer mesh.

This exercise was repeated for beams loaded with a single point load at midspan. The findings, presented in Appendix C**,** are consistent with those shown in Table 3-3 for uniformly distributed loads. Specifically, computation time can be reduced for a discretized sectional analysis by using 10 constant-length elements in the half-length of the beam and the effect of using different lengths of elements in the positive and negative moment regions on the accuracy of the computed deflections is marginal.

This mesh sensitivity analysis shows that the use of a finer mesh in the negative moment region captures the effect of the higher moment gradient but has little practical impact. This is beneficial because a coarser mesh reduces the computational demand and a constant element length is more practical for in-office use. The use of 10 elements in the half-length of the member seems suitable for practical design office use in this type discretized sectional analysis, and may be more broadly applicable. This mesh size yields deflections that, while unconservative, are within 2.2% of those computed using the 50-element mesh. In the context of the "20-40 percent" range of accuracy of deflection calculation (ACI 435 1995), this percentage error is insignificant. For the present study a

constant-length element mesh of 20 elements in the half-length of the member was used, as the extra computational demand is not onerous and the computed deflections are within 0.2% of those computed using the constant-length 50-element mesh.

The mesh sensitivity analysis was repeated for the simply supported case because the member is subjected only to single curvature, so a variable-length element has no practical advantage. The results, presented in Appendix D, show a coarser mesh can reduce computation time while still providing accurate results, and a mesh of 10 constant-length elements in the full span gives results within 1% of the finest mesh. In this chapter, to verify the exponent *m* in the Branson and Bischoff Equations for a discretized-element idealization the finest mesh of 40 constant-length elements was used.

3.3 VERIFICATION AND COMPARISON OF SINGLE- AND DISCRETIZED-ELEMENT IDEALIZATIONS

To verify the accuracy of the Branson Equation with *m* of 4 and to determine an appropriate exponent in the Bischoff Equation, deflection calculations were carried out and compared using both equations for both single-element and discretized-element idealizations. The initial assumption was that an exponent of 3 in the Bischoff Equation for a discretized-element idealization would yield comparable results to those for a single-element idealization using an exponent of 2. A thorough investigation into the suitable value for *m* was also performed using the MS Excel SOLVER function and is detailed in Appendix E.

The scope of the investigation addressed the following three parameters:

- *Support Conditions* – simply supported, two spans continuous over the interior support, and three spans continuous over the interior supports were investigated.
- *Reinforcement Ratios* – others (Scanlon and Bischoff 2008) have shown that for ρ greater than 1.5% I_e approaches I_{cr} using either the Branson or Bischoff Equations. Therefore, values of ρ were chosen to be 0.5%, 1% and 1.5%. For continuous members, the reinforcement to resist negative moments at the interior supports was chosen to be 0.5%, 1% or 1.5%, and the positive-moment-resisting steel was proportioned to resist the positive moment demand.
- *Live-to-Dead Load Ratios* – from probability-based building code calibration it has been found that for reinforced concrete members the typical range for w_L/w_D is 0.5 to 1.5 (Ellingwood et al. 1980) and so, the chosen values were 0.5, 1.0 and 1.5.

Typical material properties for reinforced concrete members were used. The specified 28-day concrete compressive strength, f'_c, was chosen to be 30MPa and the yield strength of steel, f_y, was 400MPa. Section 3.4 presents the results for members reinforced with ASTM A1035/A1035M Grade 100 (690) steel with yield strength, f_y, of 690MPa. Span lengths were chosen so that the minimum thickness requirements in A23.3-14 (CSA 2014) are violated and deflection computations are therefore required. For members with ρ of 0.5% and w_L/w_D of 1.5 the computed applied dead load, w_D, is less than the self-weight of the member. The solution is therefore inadmissible but is presented for illustrative purposes.

For the various combinations of parameters, the common steps in the procedure are as follows:

1. Determine the factored flexural resistance, M_r, at the critical cross section(s) of the member. The service loads were computed from the known live-to-dead load ratio by setting the factored demand, M_f, exactly equal to the resistance M_r. Then the corresponding service moments, M_a, were calculated at various locations along the member.
2. Calculate the gross and cracked transformed section properties for the known reinforcement in the positive and negative moment regions and included I_g, M_{cr}, I^+_{cr}, and I^-_{cr}.
3. Calculate the maximum deflection for the single-element idealization, using either the Branson Equation, Eq. [3.2], with m=3 or the Bischoff Equation, Eq. [3.3], with m=2. For continuous beams the average effective moment of inertia was calculated using the equations given in Table 3-1. Conventional linear-elastic deflection equations (e.g., CAC 2016) were used to calculate the maximum deflection.
4. Calculate maximum deflection using the discretized-element idealization. Based on the mesh sensitivity analysis present in Section 2.0, each half member was discretized into 20 elements of uniform length. The Branson Equation, Eq. [3.2], with m of 4 and Bischoff Equation, Eq. [3.3], with m of 3 were used to compute the effective moment of inertia specific to each discrete element. Deflections were calculated using the moment-area theorem (e.g., Hibbeler 2012).

Additional details concerning the discretized analysis procedure for the various end fixity conditions are described in the following sections.

3.3.1 Simply Supported Beam

Table 3-4 summarizes the results of the nine combinations of ρ and w_L/w_D for the simply supported case. This is the simplest analysis because the member is subjected only single curvature, and is statically determinate. In all cases, the member width and thickness were kept constant at 1000mm and 200mm, respectively. The minimum thickness requirement if deflections are not to be checked is *L/20* for simply supported one-way slabs (CSA 2014). The member length was therefore chosen to be 4.5m, resulting in *L/23*, so the computation of deflection is required.

Figure 3-5 shows the results using the modified Bischoff Equation, Eq. [3.3], for a discretized simply supported beam with a reinforcement ratio of 0.5% and live-to-dead load ratio of 0.5. Figure 3-5(a) shows the cracking moment computed using the reduced modulus of rupture, $0.67f_r$, and the applied moment variation normalized by $M_0=wL^2/8$. Figure 3-5(b) shows variation of the effective moment of inertia calculated using the modified Bischoff Equation, Eq. [3.3], with m of 3, normalized by I_g and the ratio of I_{cr}/I_g. Figure 3-5(c) shows the member curvature, $\Psi=M/E_cI$, normalized by the maximum curvature, Ψ_{max}, and Figure 3-5(d) shows deflected shape normalized by Δ_{max} for the member. In regions where the applied moment is less than the cracking moment, the effective moment of inertia is equal to the gross moment of inertia. In regions where the applied moment exceeds the cracking moment I_e rapidly approaches I_{cr}.

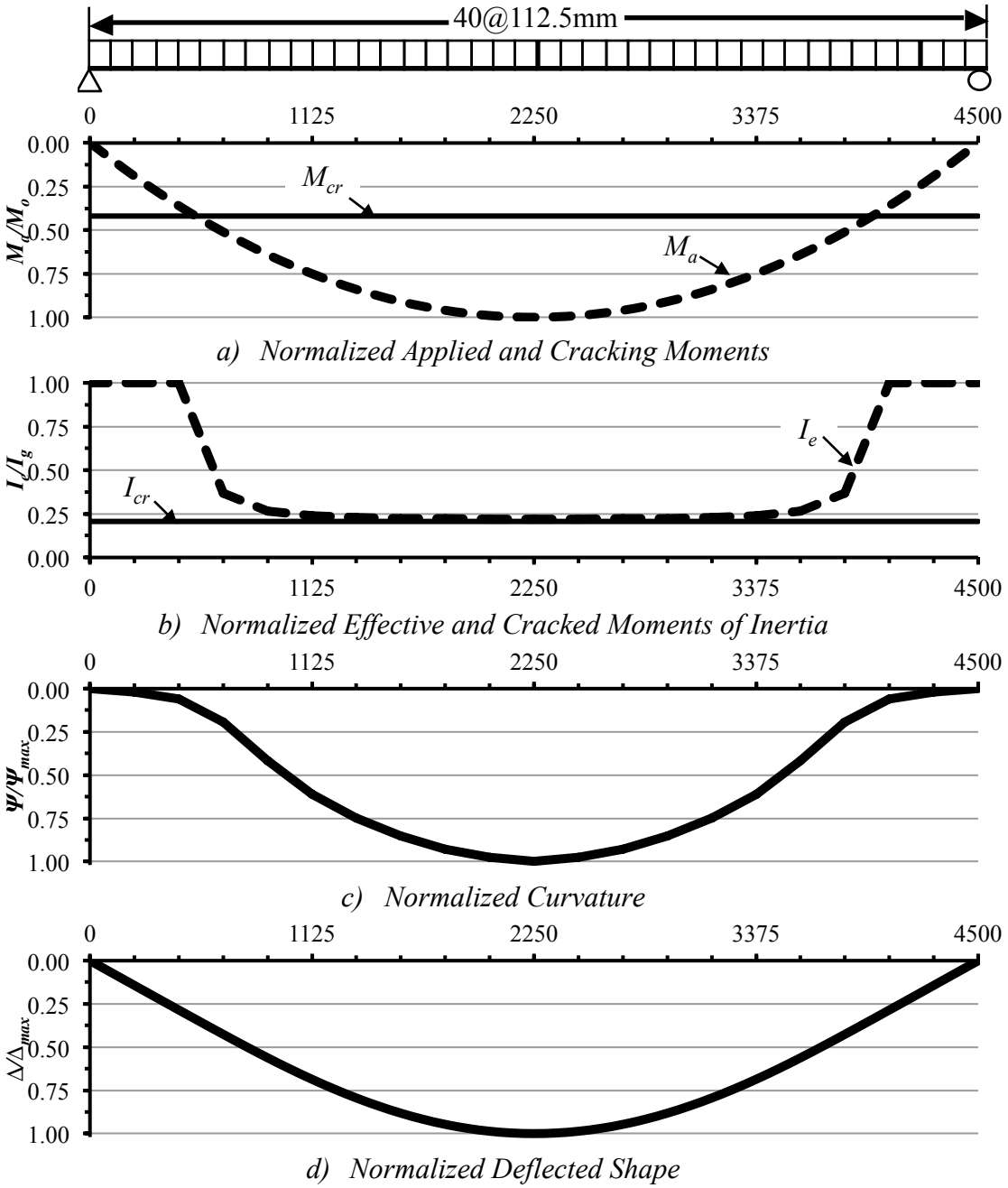

Figure 3-5: Analysis of Discretized Simply Supported Beam, Bischoff

Table 3-4 compares the deflections computed for the single-element and discretized-element idealizations using the Branson, Eq. [3.2], and Bischoff, Eq. [3.3], Equations with reduced moduli of rupture. The differences between the single-element and

discretized-element results are shown, where a positive difference corresponds to the deflection for the single-element idealization exceeding that for the discretized-element idealization. In all cases, the use of m=4 in the Branson Equation or m=3 in the Bischoff Equation for discretized-element analysis yields deflections that are very close to those using single-element analysis. The deflections computed using the Branson Equation with M_{cr} computed using a modulus of rupture of $0.5f_r$ are very close to, and slightly greater than those computed using the Bischoff Equation with M_{cr} computed using a modulus of rupture of $0.67f_r$. The computed deflections increase as the reinforcement ratio increases because the member capacity and the applied moment will increase while the cracking moment remains the same. This means that the ratio M_{cr}/M_a will decrease for higher ρ values and, although I_{cr} is also higher, the effective moment of inertia will decrease and a greater length of the beam is cracked thus the midspan deflection will increase. The deflections associated with a given reinforcement ratio reduce slightly as w_L/w_D increases because the total applied load decreases, and so the cracked length of beam reduces.

Table 3-4: Summary of Simply Supported Beam Computed Deflections

	ρ=0.5%			M_r=46.5kN.m		w_f=18.4kN/m
	Branson			**Bischoff**		
w_L/w_D	***Single Element*** Δ_{MID}	***Discretized*** Δ_{MID}	**% Diff**	***Single Element*** Δ_{MID}	***Discretized*** Δ_{MID}	**% Diff**
0.5	19.4	19.8	-2.3%	18.6	19.1	-2.7%
1	18.6	19.0	-2.4%	17.9	18.3	-2.6%
1.5	18.1	18.6	-2.5%	17.5	17.9	-2.5%
	ρ=1.0%			M_r=87.6kN.m		w_f=34.6kN/m
	Branson			**Bischoff**		
w_L/w_D	***Single Element*** Δ_{MID}	***Discretized*** Δ_{MID}	**% Diff**	***Single Element*** Δ_{MID}	***Discretized*** Δ_{MID}	**% Diff**
0.5	23.5	23.5	0.0%	22.9	23.2	-1.4%
1	22.7	22.8	-0.1%	22.2	22.5	-1.5%
1.5	22.3	22.3	0.0%	21.7	22.1	-1.5%
	ρ=1.5%			M_r=123.5kN.m		w_f=48.8kN/m
	Branson			**Bischoff**		
w_L/w_D	***Single Element*** Δ_{MID}	***Discretized*** Δ_{MID}	**% Diff**	***Single Element*** Δ_{MID}	***Discretized*** Δ_{MID}	**% Diff**
0.5	24.7	24.7	0.0%	24.5	24.6	-0.7%
1	24.0	24.0	0.0%	23.7	23.9	-0.7%
1.5	23.6	23.6	0.0%	23.3	23.5	-0.8%

For the previously described case with ρ of 0.5% and w_L/w_D of 0.5, there is excellent agreement between the two idealization methods and the two equations with the largest difference being 2.7%. In terms of span length, the computed instantaneous deflections range from *L/258* to *L/183*. The provisions of A23.3-14 state that the maximum permissible deflection "after attachment of non-structural elements (sum of the long-term deflection due to all sustained loads and the immediate deflection due to any additional live load)" shall not exceed *L/240* (CSA 2014). The computed instantaneous deflections are due to dead and live load only, long-term deflections, such as those due to the effect of creep and shrinkage, are not considered.

3.3.2 Two-Span Continuous Beam

For the nine combinations of ρ and w_L/w_D considered the member cross section was again assumed constant at 1000mm by 200mm. The span length was chosen to be 6m, corresponding to *L/30*, thus exceeding the minimum thickness requirement of *L/24* for one-way slabs with one end continuous (CSA 2014) so the computation of deflection is again required. The largest deflection of a two-span beam that is continuous over the interior support occurs with dead load on both spans and live load on one span only. The asymmetric loading and the statical indeterminacy therefore complicate the analysis and maximum deflection is not located at mid-span.

This analysis therefore required additional steps as follows:

1. Select reinforcement ratios for positive and negative moment regions. The reinforcement to resist negative moment at the interior support was chosen to be 0.5%, 1% or 1.5% and the factored loads were back-calculated to have M_f equal M_r at this location. The maximum positive and negative factored moments were computed using the approximate moment equations presented in Table 9.1 of A23.3-14, as the member satisfies the requirements of Clause 9.3.3 (CSA 2014). These computed moments provide a bending moment envelope that accounts for the full factored live load applied to either one or both spans. Based on this the positive-moment-resisting steel was selected to provide the necessary resistance.
2. Compute section properties, including I_g, M_{cr} and, for the known reinforcement ratios, I^+_{cr}, and I^-_{cr} for the regions resisting positive and negative moments, respectively. The computed values are shown in Table 3-5.

Table 3-5: Two-Span Continuous Beam Section Properties

ρ^-	ρ^+	M_r^- (kN.m)	M_r^+ (kN.m)	I_{cr}^- (mm^4)	I_{cr}^+ (mm^4)
0.50%	0.40%	46.5	38.0	138×10^6	115×10^6
1.00%	0.82%	87.6	73.7	238×10^6	205×10^6
1.50%	1.18%	123.4	101.0	320×10^6	269×10^6

3. For the single-element idealization:

   3.1. Compute the average effective moment of inertia, $I_{e(avg)}$, for the continuous member using Equation 9.4 from A23.3 (CSA 2014) shown in Table 3-1. This value is applied along the entire member length to compute the maximum deflection.

   3.2. Compute total deflection from the superposition of the dead load and live load deflections using conventional linear-elastic deflection equations (e.g., CAC 2016) as follows:

[3.4] $$\Delta_{max}=5wL^4/384E_cI_{e(avg)}-M^-L^2/16E_cI_{e(avg)}$$

where M^- is the negative moment at the interior support.

4. For the discretized-element idealization:

   4.1. Resolve the indeterminacy of the member. The moment-area theorem (e.g., Hibbeler 2012) was again used to determine rotation at the interior support satisfies the displacement boundary conditions (i.e., zero deflection at the two exterior supports). For this case of live loading on one span only, the associated negative moment over the interior support typically differed slightly from the value obtained using linear-elastic uncracked analysis (e.g., as obtained from Table 1.15 of the Concrete Design Handbook (CAC 2016)). This difference is

due to slight moment redistribution between the span and interior support sections due to non-uniform cracking along the member length.

4.2. Locate the point of zero rotation, which is also the location of the maximum deflection. The adjacent element lengths were adjusted to create a node at this location, and so facilitate computation of the maximum deflection.

Figure 3-6 (a) shows the variation of moment, (b) ratio of I_e/I_g, and I_{cr}/I_g, (c) curvature and (d) the deformed shape along the two-spans with asymmetric loading for ρ of 1.0%, and w_L/w_D of 0.5 using the Bischoff Equation, Eq. [3.3], with m=3 and the cracking moment computed using $0.67f_r$.

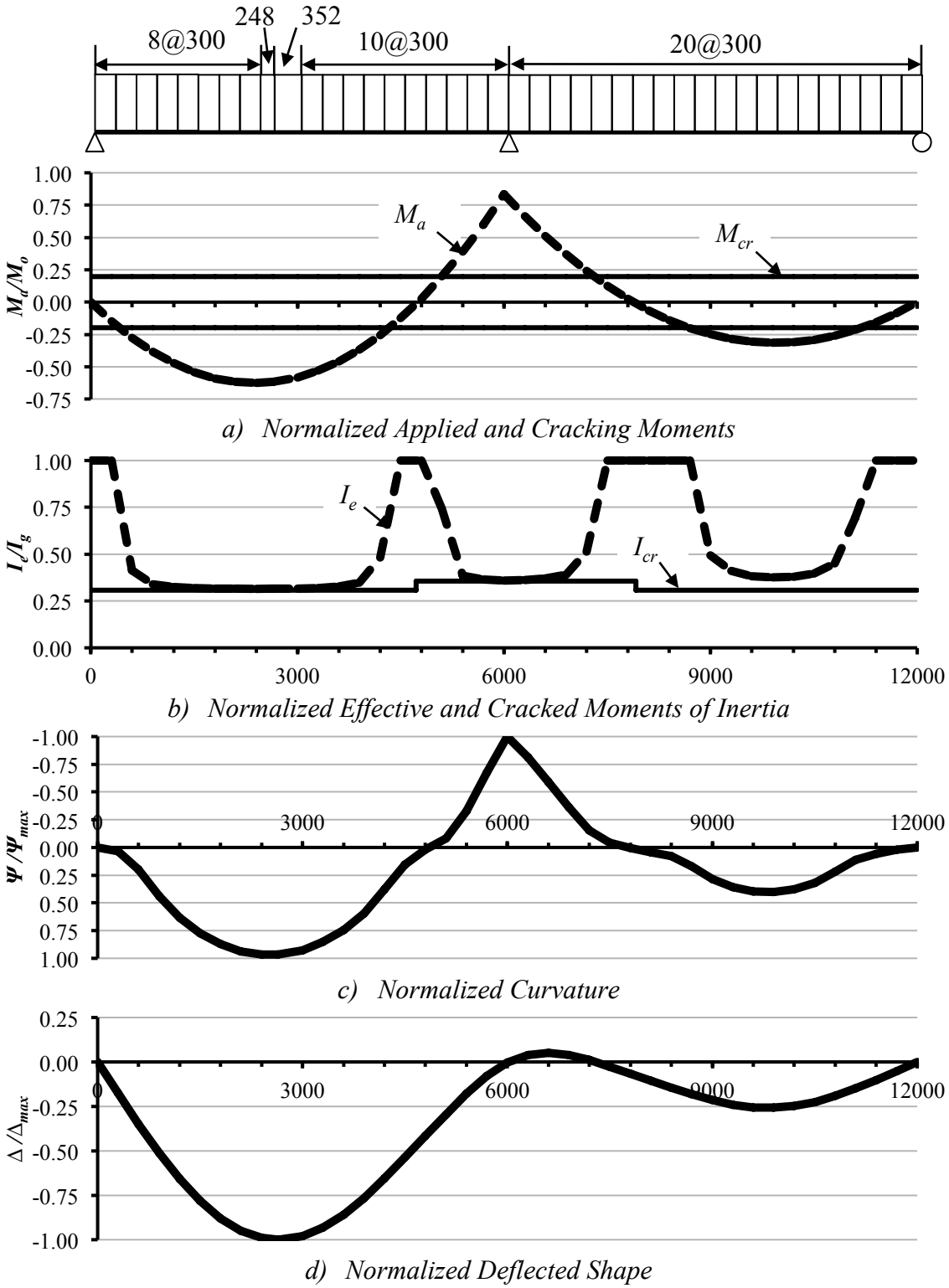

Figure 3-6: Analysis of Discretized Two-Span Continuous Beam, Bischoff

A comparison of the maximum deflection of the two-span beam using both the Branson and Bischoff Equations for both the single-element and discretized-element idealizations is shown in Table 3-6. The computed deflections from the two equations used and the two idealizations are similar. The Branson Equation, whether used for the single-element or discretized-element idealization, typically predicts slightly larger deflections than the Bischoff Equation for either idealization.

Table 3-6: Summary of Two-Span Continuous Beam Computed Deflections

	ρ^- =0.50%	ρ^+=0.40%	M^-_r=46.5kN.m	M^+_r=38.0kN.m	w_f=11.6kN/m	
	Branson			**Bischoff**		
w_L/w_D	***Single Element*** Δ_{MID}	***Discretized*** Δ_{MID}	**% Diff**	***Single Element*** Δ_{MID}	***Discretized*** Δ_{MID}	**% Diff**
0.5	18.3	19.7	-7.5%	18.3	18.8	-2.9%
1	19.6	19.9	-1.4%	19.6	18.9	3.7%
1.5	20.3	20.0	1.7%	20.3	19.0	6.8%
	ρ^- =1.00%	ρ^+=0.82%	M^-_r=87.6kN.m	M^+_r=73.7kN.m	w_f=21.9kN/m	
	Branson			**Bischoff**		
w_L/w_D	***Single Element*** Δ_{MID}	***Discretized*** Δ_{MID}	**% Diff**	***Single Element*** Δ_{MID}	***Discretized*** Δ_{MID}	**% Diff**
0.5	26.1	26.5	-1.8%	25.1	26.0	-3.8%
1	27.8	28.3	-1.6%	26.7	27.6	-3.0%
1.5	28.8	28.9	-0.2%	9.8	28.0	-1.2%
	ρ^- =1.50%	ρ^+=1.18 %	M^-_r =123.5kN.m	M^+_r=101.0kN.m	w_f=30.9kN/m	
	Branson			**Bischoff**		
w_L/w_D	***Single Element*** Δ_{MID}	***Discretized*** Δ_{MID}	**% Diff**	***Single Element*** Δ_{MID}	***Discretized*** Δ_{MID}	**% Diff**
0.5	28.5	28.6	-0.6%	27.9	28.4	-1.9%
1	30.3	30.6	-0.8%	29.7	30.3	-2.0%
1.5	31.4	31.6	-0.5%	30.8	31.1	-1.3%

As for the simply supported beam, increasing the reinforcement ratio increases the member capacity at ultimate and so the applied service moment. As the cracking moment remains the same thus, the maximum deflection again increases. Unlike the simply supported beam, however, increasing the live-to-dead load ratio increases the computed

maximum deflection. Here the full live load is applied to one span only, which increases the maximum positive moment near midspan and decreases the negative moment over the interior support. Typically, the discretized-element idealization gives slightly conservative results with respect to the single-element idealization. In the worst case, the Bischoff Equation using *m* of 3 in a discretized-element idealization gives a deflection 1.3mm (or 6.8%) less than that computed using *m* of 2 in a single-element idealization.

3.3.3 Three-Span Continuous Beam

The maximum deflection for the three-span case is assumed to occur at the centre of the middle span, with the dead load on all three spans and the live load on the middle span only, as shown in Figure 3-7. It is recognized that the deflection of an exterior span is more critical, but this has already been examined in the previous two-span beam case. The symmetry of the negative support moments simplifies the analysis compared to the two-span beam. The bending moment envelope for design of the member at the Ultimate Limit States was determined using the approximate analysis coefficients given in Table 9.1 of A23.3 (CSA 2014), i.e., for an interior span $M^{+}=(w_f L^2/16)$ at mid-span and $M^{-}=(w_f L^2/11)$ at the supports. These coefficients provide a bending moment envelope that accounts for some moment redistribution and slightly differ from those found in Table 1.15 of the Concrete Design Handbook (CAC 2016), as shown in Figure 3-7.

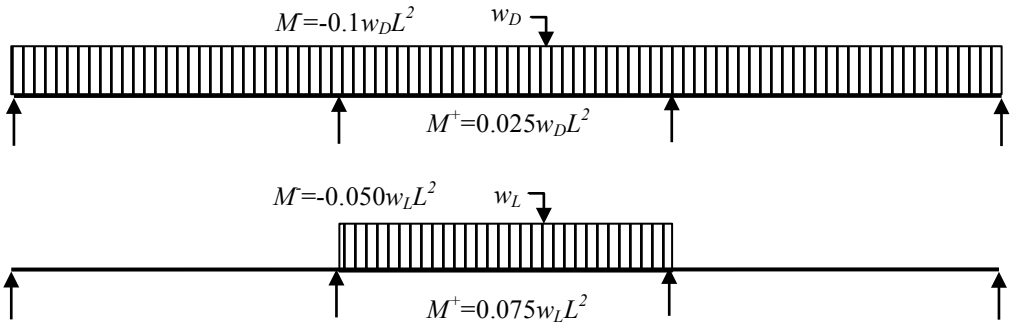

Figure 3-7: Pattern Loading and CAC (2016) Moment Coefficients

The positive moment reinforcement was computed given the negative moment reinforcement following the procedure adopted for the two-span beam case. In the negative moment regions ρ- was set equal to 0.5%, 1.0% or 1.5% and the positive moment reinforcement ρ^+ was to resist the corresponding factored demand. The associated ρ^-, ρ^+, I_{cr}, and I^+_{cr} values are shown in Table 3-7.

Table 3-7: Three-Span Continuous Beam Section Properties

ρ^-	ρ^+	M_r^- (kN.m)	M_r^+ (kN.m)	I_{cr}^- (mm^4)	I_{cr}^+ (mm^4)
0.50%	0.34%	46.5	32.0	138×10^6	99.1×10^6
1.00%	0.66%	87.6	60.2	238×10^6	172×10^6
1.50%	1.00%	123.4	87.6	320×10^6	238×10^6

The deflections were computed for the single-element and discretized-element idealizations using both the Branson and Bischoff Equations with the reduced moduli of rupture. Figure 3-8 shows the variation of moment, effective moment of inertia, curvature and deflected shape along the member length for ρ of 1.5%, and w_L/w_D of 1.0 using the Bischoff Equation.

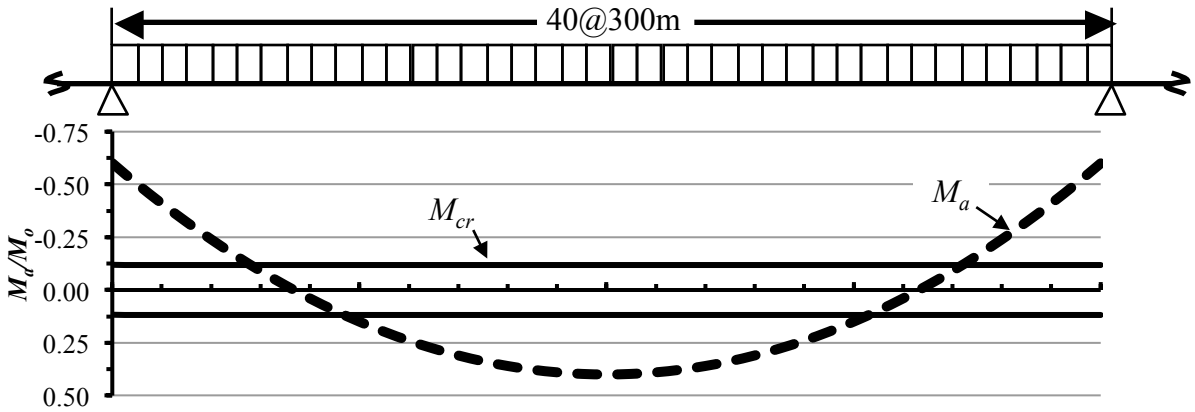

a) Normalized Applied and Cracking Moments

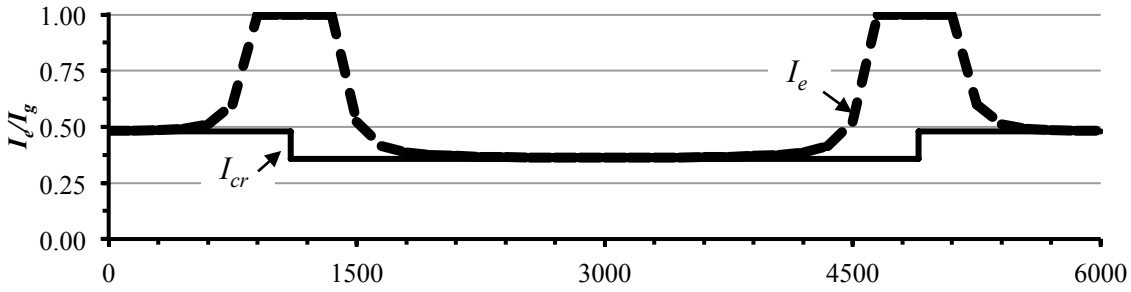

b) Normalized Effective and Cracked Moments of Inertia

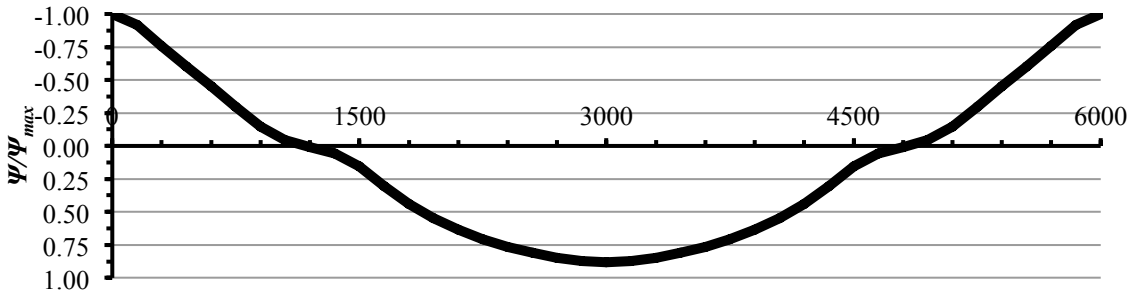

c) Normalized Curvature

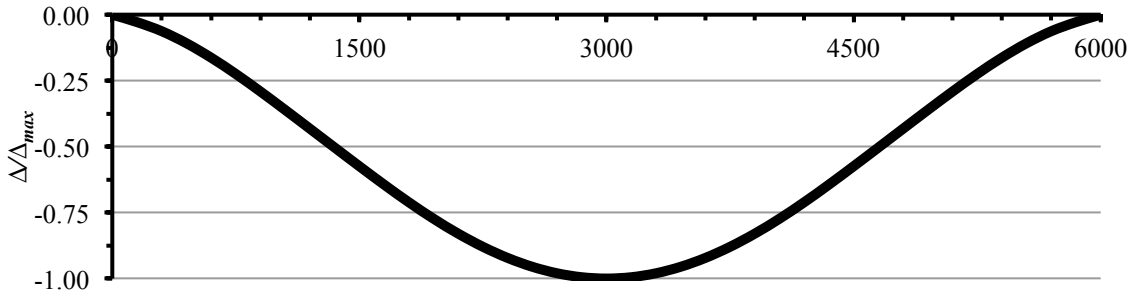

d) Normalized Deflected Shape

Figure 3-8: Analysis of Discretized Three-Span Continuous Beam, Bischoff

When the applied negative moment exceeds the cracking moment, Figure 3-8(a), the ratio of I_e/I_g is less than 1, Figure 3-8(b), and I_e equals I^-_{cr} at the supports. Similarly, the positive applied moment exceeds M_{cr} in the midspan region and I_e approaches I^+_{cr} at midspan.

A comparison of the maximum deflections computed using the two equations and two idealizations for the various three-span cases is shown in Table 3-8. The maximum deflection of the centre span increases as w_L/w_D increases because the pattern-live loading increases the applied mid-span positive moment at that location. The greatest difference between the single-element idealization and discretized-element idealization occurs with the lowest values of ρ and w_L/ w_D, 0.5% and 0.5, respectively. These deflections are in the range of *L/600* to *L/1000*, however, and so are unlikely to be critical. The reasons for these relatively large differences will be investigated further in Section 3.4.

Table 3-8: Summary of Three-Span Continuous Beam Computed Deflections

	ρ^- =0.50%		ρ^+=0.34%		M^-_r=46.5kN.m		M^+_r=32.0kN.m		w_f=14.2kN/m	
	Branson					**Bischoff**				
w_L/w_D	***Single Element*** Δ_{MID}	***Discretized*** Δ_{MID}	**% Diff**	**L/ ($\Delta_{m=3}$)**	**L/ ($\Delta_{m=4}$)**	***Single Element*** Δ_{MID}	***Discretized*** Δ_{MID}	**% Diff**	**L/ ($\Delta_{m=2}$)**	**L/ ($\Delta_{m=3}$)**
0.50	5.9	4.6	23.0%	1009	1310	5.0	3.0	40.8%	1194	2018
1.00	9.8	9.1	7.7%	611	662	9.9	8.1	18.4%	603	739
1.50	12.1	12.0	1.0%	494	499	12.5	11.4	9.2%	479	528
	ρ^- =1.00%		ρ^+=0.66%		M^-_r =87.6kN.m		M^+_r=60.2kN.m		w_f=26.8kN/m	
	Branson					**Bischoff**				
w_L/w_D	***Single Element*** Δ_{MID}	***Discretized*** Δ_{MID}	**% Diff**	**L/ ($\Delta_{m=3}$)**	**L/ ($\Delta_{m=4}$)**	***Single Element*** Δ_{MID}	***Discretized*** Δ_{MID}	**% Diff**	**L/ ($\Delta_{m=2}$)**	**L/ ($\Delta_{m=3}$)**
0.50	13.1	14.5	-10.4%	457	414	12.5	13.6	-8.9%	481	442
1.00	18.3	20.3	-10.8%	328	296	17.5	19.4	-10.9%	343	309
1.50	21.3	23.6	-11.0%	282	254	20.3	22.7	-11.7%	295	264
	ρ^- =1.50%		ρ^+=1.00 %		M^-_r =123.5kN.m		M^+_r=87.6kN.m		w_f=37.7kN/m	
	Branson					**Bischoff**				
w_L/w_D	***Single Element*** Δ_{MID}	***Discretized*** Δ_{MID}	**% Diff**	**L/ ($\Delta_{m=3}$)**	**L/ ($\Delta_{m=4}$)**	***Single Element*** Δ_{MID}	***Discretized*** Δ_{MID}	**% Diff**	**L/ ($\Delta_{m=2}$)**	**L/ ($\Delta_{m=3}$)**
0.50	14.5	16.4	-13.5%	726	639	14.0	15.8	-13.4%	752	664
1.00	19.8	22.1	-11.8%	531	475	19.2	21.5	-12.4%	548	487
1.50	22.8	25.3	-11.2%	461	414	22.2	24.9	-12.2%	474	423

Table 3-8 indicates that both the Branson and Bischoff Equations for single-element and discretized-element idealizations typically yield very similar results and the combinations of ρ and w_L/ w_D that cause the greatest percent differences between the single- and discretized-element idealizations are common for both equations. The Branson Equation using m=3 in a single-element idealization and using m=4 in a discretized-element idealization have previously been shown to give similar results (Branson 1965). The Bischoff Equation using m=3 in a discretized-element idealization typically is conservative with respect to using m=2 in a single-element idealization.

3.3.4 Computed Deflection Results for Beams Reinforced with ASTM A1035/A1035M Grade 100 (690) Steel

The deflection calculations for single-element and discretized-element idealizations using the Branson and Bischoff Equation with a cracking moment computed using a reduced modulus of rupture were again performed using ASTM A1035/A1035M Grade 100 (690) steel reinforcement. For this steel grade, a reinforcement ratio of 1.5% is not realistic and would not typically be used in practice. Therefore, only ρ of 0.5% and 1.0% were considered with various live-to-dead load ratios, i.e., w_L/w_D of 0.5, 1.0 and 1.5.

Because the yield strength of ASTM A1035/A1035M Grade 100 (690) steel is greater than that of Grade 60 (400) steel the assumption that the steel yields is not valid for the chosen negative reinforcement ratios and cross-section geometry. Strain compatibility and the steel-stress equations recommended in the ACI ITR-6R-10 “Design Guide for the Use of ASTM A1035/A1035M Grade 100 (690) Steel Bars for Structural Concrete” (ACI 2010) were used. To satisfy force equilibrium, the depth to the neutral axis, c, was

iterated then the positive and negative moment resistance, M_{r+} and M_{r-}, respectively, were computed.

The positive reinforcement ratios in the two-span and three-span continuous beams were kept consistent with the values used in the analysis with Grade 60 (400) reinforcing steel and the section properties of the two-span and three-span continuous beams are summarized in Table 3-9 and Table 3-10. These tables and Table 3-5 and Table 3-7 show that although the moment resistance, and so the service loads, for beams reinforced with Grade 100 (690) steel are much larger than those for beams reinforced with Grade 60 (400) steel, the cracked moment of inertia remains the same. Therefore, practitioners should be aware greater service-load deflections are probable in beams reinforced with Grade 100 (690) steel.

Table 3-9: Section Properties of Two-Span Continuous Beams with ASTM A1035/A1035M Grade 100 (690) Steel

ρ-	ρ+	M_r^- (kN.m)	M_r^+ (kN.m)	I_{cr}^- (mm^4)	I_{cr}^+ (mm^4)
0.50%	0.40%	63.0	52.8	138×10^6	115×10^6
1.00%	0.82%	104.6	91.9	238×10^6	205×10^6

Table 3-10: Section Properties of Three-Span Continuous Beams with ASTM A1035/A1035M Grade 100 (690) Steel

ρ-	ρ+	M_r^- (kN.m)	M_r^+ (kN.m)	I_{cr}^- (mm^4)	I_{cr}^+ (mm^4)
0.50%	0.34%	63.0	45.3	138×10^6	99.1×10^6
1.00%	0.66%	104.6	78.3	238×10^6	172×10^6

Table 3-11, Table 3-12 and Table 3-13 show the results of the simply supported, two-span continuous and three-span continuous beams, respectively. The results indicate that for members reinforced with ASTM A1035/A1035M Grade 100 (690) steel both the Branson and Bischoff Equations for single-element and discretized-element idealizations

typically yield similar relative differences to the computed deflections when the member is reinforced with Grade 60 (400) steel. The combinations of ρ and w_L/w_D that cause the greatest percent differences between the single- and discretized-element idealizations are common for both equations. These results support the previous conclusions, and deflection calculations for beams reinforced with Grade 100 (690) steel can be carried out following the same procedure as for members reinforced with Grade 60 (400) steel.

Table 3-11: Summary of Computed Deflections of Simply Supported Beams with ASTM A1035/A1035M Grade 100 (690) Steel

	ρ=0.5%			M_r=78.4kN.m		w_f=31.0kN/m
	Branson			**Bischoff**		
w_L/w_D	***Single Element*** Δ_{MID}	***Discretized*** Δ_{MID}	**% Diff**	***Single Element*** Δ_{MID}	***Discretized*** Δ_{MID}	**% Diff**
0.5	35.7	35.9	-0.7%	34.7	35.5	-2.1%
1	34.5	34.7	-0.7%	33.6	34.3	-2.1%
1.5	33.8	34.1	-0.8%	32.9	33.6	-2.2%
	ρ=1.0%			M_r=147.0kN.m		w_f=58.1kN/m
	Branson			**Bischoff**		
w_L/w_D	***Single Element*** Δ_{MID}	***Discretized*** Δ_{MID}	**% Diff**	***Single Element*** Δ_{MID}	***Discretized*** Δ_{MID}	**% Diff**
0.5	39.6	39.6	0.0%	39.2	39.5	-0.7%
1	38.4	38.4	0.0%	38.0	38.3	-0.7%
1.5	37.7	37.7	0.0%	37.3	37.6	-0.7%

Table 3-12: Summary of Computed Deflections of Two-Span Continuous Beams with ASTM A1035/A1035M Grade 100 (690) Steel

	ρ^- =0.50%	ρ^+=0.40%		M^-_r=63.0kN.m	M^+_r=52.8kN.m	w_f=15.8kN/m
	Branson			**Bischoff**		
w_L/w_D	***Single Element*** Δ_{MID}	***Discretized*** Δ_{MID}	**% Diff**	***Single Element*** Δ_{MID}	***Discretized*** Δ_{MID}	**% Diff**
0.5	29.6	31.3	-5.6%	29.0	30.7	-5.6%
1	31.7	32.5	-2.5%	31.0	31.5	-1.4%
1.5	32.8	32.8	0.0%	32.1	31.7	1.2%
	ρ^- =1.00%	ρ^+=0.82%		M^-_r=104.6kN.m	M^+_r=91.9kN.m	w_f=26.1kN/m
	Branson			**Bischoff**		
w_L/w_D	***Single Element*** Δ_{MID}	***Discretized*** Δ_{MID}	**% Diff**	***Single Element*** Δ_{MID}	***Discretized*** Δ_{MID}	**% Diff**
0.5	31.4	31.9	-1.4%	30.5	31.4	-3.0%
1	33.5	34.0	-1.4%	32.5	33.5	-3.0%
1.5	34.7	34.9	-0.6%	33.7	34.2	-1.4%

Table 3-13: Summary of Computed Deflections of Three-Span Continuous Beams with ASTM A1035/A1035M Grade 100 (690) Steel

	ρ^- =0.50%	ρ^+=0.34%	M^-_r=63.0kN.m	M^+_r=45.3kN.m	w_f=19.3kN/m	
	Branson			**Bischoff**		
w_L/w_D	***Single Element*** Δ_{MID}	***Discretized*** Δ_{MID}	**% Diff**	***Single Element*** Δ_{MID}	***Discretized*** Δ_{MID}	**% Diff**
0.5	12.0	11.7	3.0%	12.5	11.4	8.4%
1	18.3	19.2	-5.0%	18.7	19.0	-2.1%
1.5	21.8	23.6	-8.1%	22.1	23.4	-5.9%
	ρ^- =1.00%	ρ^+=0.66%	M^-_r=104.6kN.m	M^+_r=78.3kN.m	w_f=32.0kN/m	
	Branson			**Bischoff**		
w_L/w_D	***Single Element*** Δ_{MID}	***Discretized*** Δ_{MID}	**% Diff**	***Single Element*** Δ_{MID}	***Discretized*** Δ_{MID}	**% Diff**
0.5	16.2	18.3	-13.0%	15.6	17.5	-12.2%
1	22.4	25.1	-12.0%	21.6	24.3	-12.6%
1.5	25.9	29.0	-11.9%	25.0	28.2	-12.7%

3.4 FURTHER INVESTIGATION OF LIGHTLY REINFORCED BEAM RESULTS

The results shown in Table 3-4, Table 3-6, and Table 3-8 indicate the deflections obtained using either the Bischoff or Branson Equation with either the single-element or discretized-element idealization are generally comparable. The largest relative differences occur for lightly reinforced beams, particularly for the three-span continuous beam case, where the discretized-element idealization yields unconservative results using both the Bischoff and Branson Equations. The underlying mechanics of the incremental deflection analysis, and beam curvature will be investigated to gain insight into these differences.

Figure 3-9(a) and (b) show the variation of normalized moment and normalized effective moment of inertia computed using the Bischoff Equation, respectively, for ρ of 0.5% and w_L/w_D of 0.5. For this small reinforcement ratio, the corresponding loading is also small and the applied moment exceeds the cracking moment for only short regions at the

supports and mid-span. As shown in Figure 3-9(b), the discretized-element idealization accurately captures the effect of the significant uncracked length of the beam. The effective moment of inertia, $I_{e(avg)}$, used in the single-element idealization is computed based on the maximum moments at the supports and midspan to yield the constant average value shown. At the supports, this values exceeds the effective moment of inertia for the discretized-element idealization, $I_{e,d}$, but in the positive moment region, $I_{e,d}$ is typically much greater than $I_{e(avg)}$ because the member is uncracked. Thus $I_{e(avg)}$ markedly underestimates the overall member stiffness because it is computed using only the maximum moment values at the supports and midspan.

The impact of these differences is further explored by comparing the curvatures based on $I_{e(avg)}$ and $I_{e,d}$, in Figure 3-9(c). The average effective moment of inertia, $I_{e(avg)}$, overestimates the member stiffness at the supports resulting in lower curvatures and markedly underestimates the member stiffness in the positive moment region resulting in larger curvatures and, therefore, larger deflections. Figure 3-9(d) shows the increment of deflection contributed by each element along the beam length. These increments can be computed using the Moment Area Theorem in the discretized-element idealization: the summation of the increments from the support to mid-span in Figure 3-9(d) is the mid-span deflection. Clearly the incremental deflections in the positive moment region have the largest impact on the overall deflection calculated. The use of the single-element average effective moment of inertia, $I_{e(avg)}$, underestimates the actual value close to the supports, where the member is cracked, but markedly overestimates the actual value in

the positive moment region, leading to a greater maximum deflection (5.0mm) than that calculated from the discretized analysis (3.0mm).

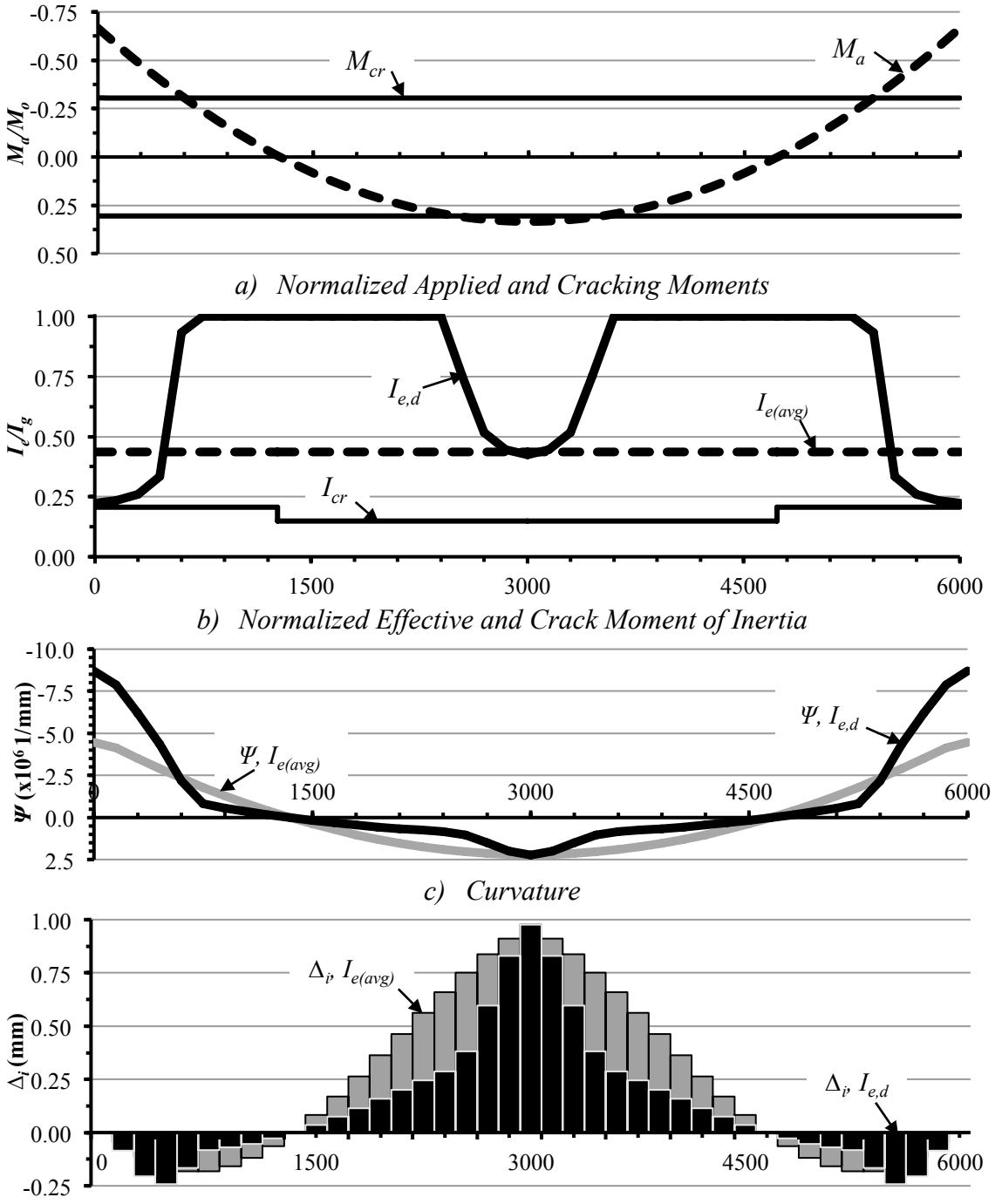

Figure 3-9: Analysis of Discretized Three-Span Continuous Beam, Bischoff, ρ^-=0.5%

Figure 3-10 compares the single- and discretized-element idealization results obtained using the Bischoff Equation for a larger reinforcement ratio, ρ of 1.5%, and w_L/w_D of 0.5. The positive and negative moment resistances are also larger, so the applied moment exceeds the cracking moment over long regions at the supports and mid-span, Figure 3-10(a). Figure 3-10(b) shows the variation of normalized effective moment of inertia computed using the Bischoff Equation. The single-element idealization effective moment of inertia, $I_{e(avg)}$, gives a value less than I_{cr}^- at supports, but in the positive moment region, $I_{e(avg)}$ is generally greater than $I_{e,d}$, thus overestimating the member stiffness. Because the member is cracked over large regions $I_{e,d}$ rapidly approaches I_{cr}^- at supports and I_{cr}^+ at mid-span. The relative difference between $I_{e(avg)}$, and $I_{e,d}$ at the support and at mid-span, is -15% and 12%, respectively, and, looking at the curvatures in Figure 3-10(c), these differences may seem trivial. However, Figure 3-10(d) shows that because single-element average I_e underestimates the incremental deflection in the positive moment region, it predicts a lower maximum deflection (14.0mm) than that calculated from the discretized-element idealization (15.8mm). The summation of these minor differences leads to a relative difference of 13% between the single- and discretized-element idealization results computed using the Bischoff Equation.

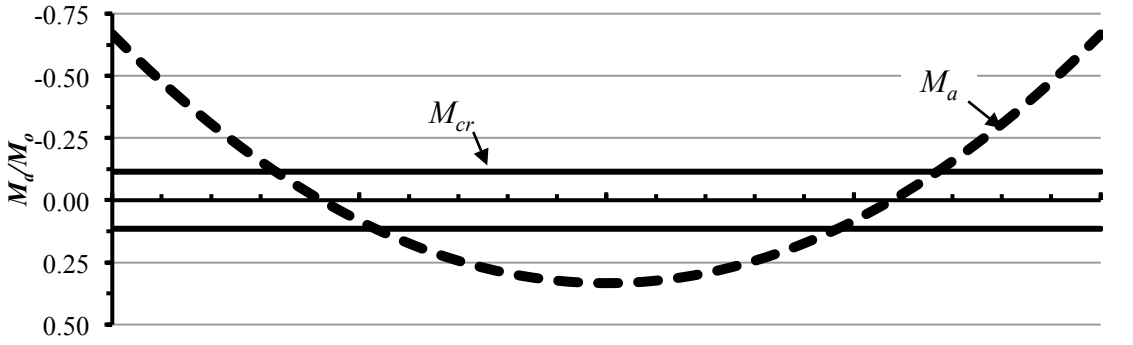

a) Normalized Applied and Cracking Moments

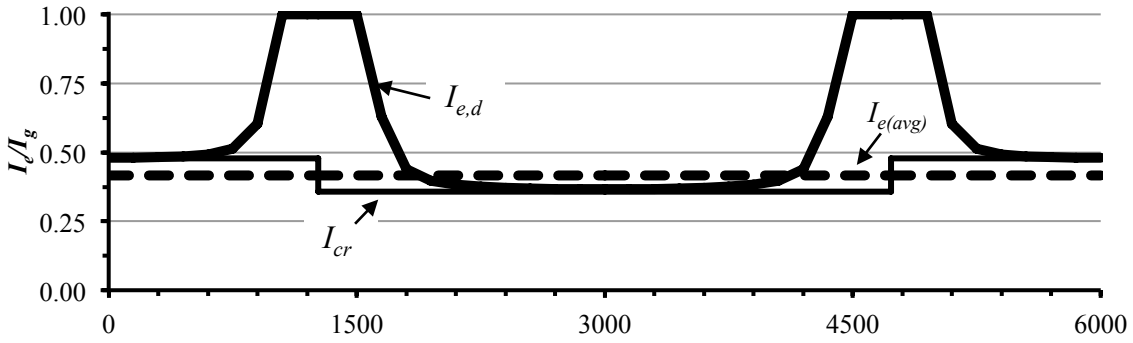

b) Normalized Effective and Crack Moment of Inertia

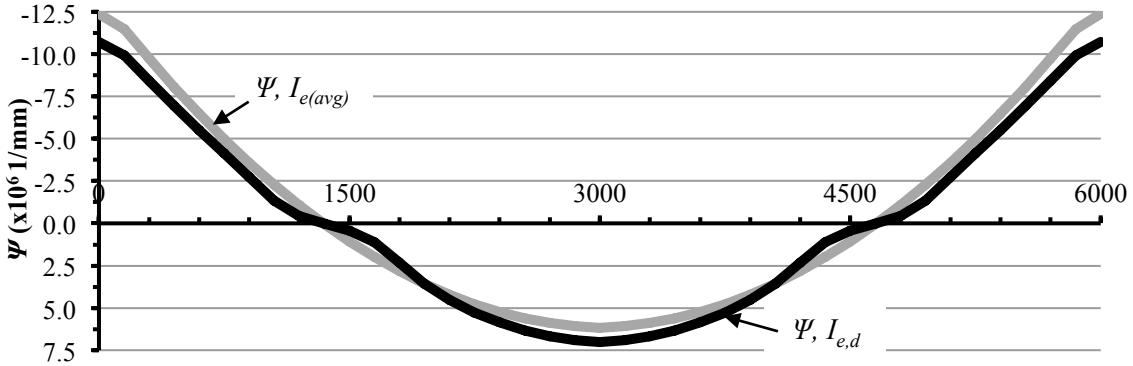

c) Curvature

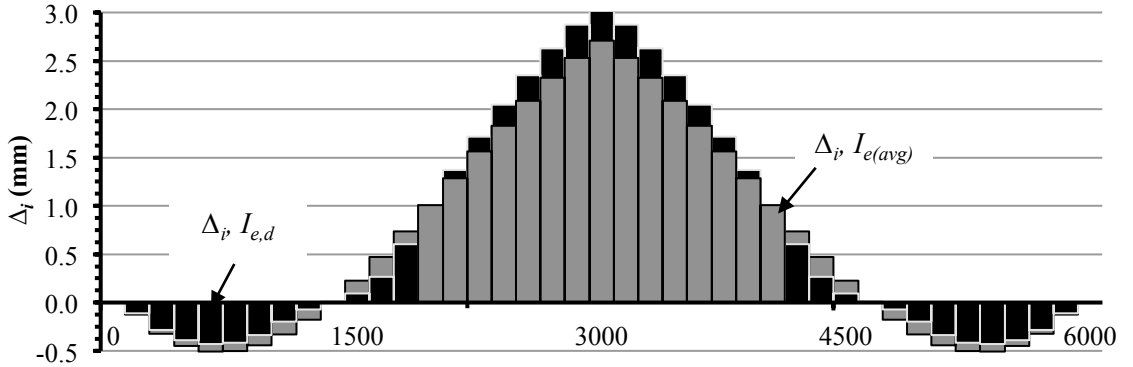

d) Increment of Deflection using various I_e

Figure 3-10: Analysis of Discretized Three-Span Continuous Beam, Bischoff, ρ^-=1.5%

3.5 SUMMARY, CONCLUSIONS & RECOMMENDATIONS

The research presented in this chapter compared single-element and discretized-element idealizations for deflection calculation with the effective moment of inertia computed using the Branson or Bischoff Equations. A mesh sensitivity analysis was performed to determine an acceptable mesh size for practical design office use. MS Excel spreadsheets were developed for the various deflection calculations. Parametric analyses were conducted that investigated the effect of various support conditions, reinforcement ratios and live-to-dead load ratios on the computed deflections. The nine combinations of reinforcement ratio and live-to-dead load ratios, ρ of 0.5%, 1.0% and 1.5%, and w_L/w_D of 0.5, 1.0 and 1.5, respectively, were investigated for simply supported beams, two spans continuous over the interior support, and three spans continuous over the interior supports Modifications to the Bischoff Equation were investigated to extend its application to discretized-element idealizations.

The conclusions of this research are as follows:

1. Use of a uniform-length element mesh with 20 elements in each member yields deflections that are, in the worst case, within 3% of those computed using a uniform-length element mesh with 100 elements in each member.
2. The use of a variable-length element mesh, with shorter elements in the negative moment regions, can capture the effect of the moment gradient near the supports. However, the improvement of the accuracy is marginal and the additional effort required to locate the point of inflection makes this optional unattractive for design-office use.

3. The Branson Equation with m of 4 and the cracking moment computed using a reduced modulus of rupture, $0.5f_r$, in a discretized-element idealization yields deflections that closely approximate those obtained using a single-element idealization using the Branson Equation with m of 3. Excluding any outlier cases, the average differences were: -0.8% for a simply supported beam, -0.7% for a two-span continuous beam, and -11.4% for a three-span continuous beam where the negative difference indicates that the deflection for the discretized-element idealization exceeds that for the single-element idealization.
4. The Bischoff Equation with a modified m equal to 3 and the cracking moment computed using a reduced modulus of rupture, $0.67f_r$, in a discretized-element idealization yields deflections that closely approximates those obtained a single-element idealization using the Bischoff Equation with m of 2. Excluding any outlier cases, the average differences were: -1.6% for a simply supported beam, -1.5% for a two-span continuous beam, and -11.6% for a three-span continuous beam where the negative difference indicates that the deflection for the discretized-element idealization exceeds that for the single-element idealization.
5. Others have shown the Branson Equation with $0.5f_r$ gives results in a single-element idealization that are similar to the Bischoff Equation with $0.67f_r$ (e.g., Scanlon & Bischoff 2008, CAC 2016). Similarly, the Branson Equation with m=4 and $0.5f_r$ gives results in a discretized-element idealization that are similar to the Bischoff Equation with m=3 and $0.67f_r$.

CHAPTER 4: VERIFICATION OF DEFLECTION CALCULATION PROCEDURES

4.1 INTRODUCTION

The research presented thus far has shown that using the Branson or Bischoff Equation for the effective moment of inertia using either a single-element or discretized-element idealization provides comparable results if the recommended reduced tensile strengths are used to compute the cracking moment. ACI Committee 435 (1995) cautions "the magnitude of actual deflections in concrete structural elements...can only be estimated within a range of 20-40 percent accuracy". Therefore, the primary objective of this chapter is to quantify the accuracies of deflections computed using the various idealizations and effective moment of inertia equations using experimentally observed values.

The existing database of experimental results were typically published between 1950 and 1970 and primarily focused on deflections due to sustained loads on simply supported members (Espion 1988). Espion (1988) also cites three experimental investigations of two-span continuous beams by Branson (1965), Washa and Fluck (1952), and Bakoss et al. (1982). More recent studies of continuous beams rarely focus exclusively on steel-reinforced concrete members, but rather on FRP-reinforced concrete. However, these studies typically include steel-reinforced control specimens (i.e., Habeeb 2008, El-Mogy 2011) that are relevant for the present investigation.

In this chapter, deflections are computed for a total of 65 test specimens that cover a wide range of reinforcement ratios, span-to-depth ratios, and section geometries, subjected to varying curing conditions and applied loading. As in Chapter 3, deflections are computed using the following alternative deflection calculation procedures: computing the effective moment of inertia using the Branson or Bischoff Equations accounting for single- or discretized-element idealizations; and, computing the cracking moment using the full or reduced modulus of rupture. Inaccurate predictions and discrepancies between results obtained using the alternative deflection calculation procedures are further investigated to determine the underlying cause.

4.1.1 Chapter Objectives

The main objectives of the research reported in this chapter are:

1. To determine, through comparison to experimental results, the optimal idealization, effective moment of inertia equation, and modulus of rupture value with respect to experimentally observed deflections.
2. To quantify the accuracy of these alternative deflection calculation procedures.
3. To identify circumstances where it is appropriate to use the reduced modulus of rupture.
4. To identify factors that have a major impact on the accuracy of computed deflections.

To achieve these objectives, deflections were calculated using the reported material properties, section geometries, applied loadings and other relevant data. A comparison

was performed using a database of: 42 rectangular simply supported members, 4 T-beam simply supported members, 11 rectangular two-span continuous members and 8 simply supported T-beams with cantilevers at one support. The discretized-element idealization for simply supported members was performed using a constant-length element mesh of $L/20$ in the full span, the two-span members were discretized into a constant-length element mesh of $L/20$ in each span, and the simply supported T-beam members with a cantilever at one support were discretized into a constant-length element mesh of $L/20$ in the main span and cantilever.

4.2 SIMPLY SUPPORTED MEMBERS

The investigation of simply supported members involves experimental data from the ten studies shown in Table 4-1. Table 4-1 summarizes the curing conditions, applied loading and other relevant data for the 46 simply supported specimens investigated. Generally, the specimens were wet cured and the applied loading was typically uniformly distributed two point loads that simulate the bending moment diagram of a specimen under uniform loading. The specimens cover a wide range of reinforcement ratios, $0.29\% \leq \rho \leq 3.05\%$, and wide range of span-to-depth ratios, $9 \leq L/h \leq 30$. The last two studies shown, denoted with *, are presented in detail in Appendix F.

Table 4-1: Summary of Simply Supported Studies

Study	Comment	Curing	Applied Loading	No. of Specimens	ρ^+	*L/h*
Gilbert & Nejadi (2004a) Short Term	Special care to prevent shrinkage	Kept moist (covered in wet Hessian) for a period of 28d	Point Loads @ *L*/3	4-Beam	0.53%	10 & 11
			UDL	6-Slab	0.30%-0.60%	22
Gilbert & Nejadi (2004b) Sustained	Special care to prevent shrinkage	Kept moist (covered in wet Hessian) for a period of 14d	Point Loads @ *L*/3	6-Beam	0.53%-0.80%	10 & 11
			UDL	6-Slab	0.29%-0.59%	22
Washa & Fluck (1952)	Higher ρ, $I_e \rightarrow I_{cr}$ irrespective of the f_r	Cured under wet canvas 5d, then concrete was exposed to air on all surfaces except the bottom.	UDL	5	1.47%-1.58%	20 & 30
El-Nemr (2013)	Steel control specimen	No info given	2 Pt. Loads near midspan	1	0.43%	9
Branson (1965)	Equation based on test results and full f_r	No info given	UDL	2	0.69%-2.07%	22
Washa (1947)	M_{cr} sensitive to f_r	Cured in moulds 3-7d. "Sealed" specimens painted with bakelite lacquer. "Dry" slabs were only sealed on edges, top and bottom exposed to air	UDL	2-Dry & 2-Sealed	0.80%	30
Corley & Sozen (1966)	Higher ρ, $I_e \rightarrow I_{cr}$ irrespective of the f_r	Wet burlap 24h, fog room 7d, open lab 21d	Point Loads @ *L*/4	3	1.36%-3.05%	12 & 17
Yu (1959)	T-Beams	Cast in T-shaped forms, covered with waterproof membrane for 3d, forms were removed, controlled climate for 18d. Lab for 7d and tested at 28d	UDL	4	0.50%-0.83%	14 - 30
*Park et al. (2012)	Early-age loading, 3d or 7d	Cured at low temp, <17˚C	2 Pt. Loads near midspan	4	0.50%-1.04%	28
*Bakoss et al. (1982)	Higher ρ, $I_e \rightarrow I_{cr}$ irrespective of the f_r	Moist cured 14d, kept in climate-controlled lab	Point Loads @ *L*/3	1	1.74%	29

4.2.1 Study by Gilbert & Nejadi (2004a, 2004b)

Gilbert and Nejadi (2004a, 2004b) conducted two studies on the flexural cracking in reinforced concrete members, one focusing on short-term loads, UNICIV Report No. R-434 (2004a), and the other on sustained loads, UNICIV Report No. R-435 (2004b). While the second study focused on the behaviour under sustained loads, instantaneous deflections were also recorded, and so are relevant for the present study. In both studies:

- Twelve prismatic singly reinforced concrete specimens (six beams and six slabs) were all simply supported on a 3.5 m span with span-to-depth ratios, L/h, of 10 or 11 for beams and 22 for slabs.
- All specimens were kept moist (covered in wet Hessian) to minimise the loss of moisture, for a period of 28 days in the short-term load study and for 14 days in the sustained-load study.
- Material properties, including the compressive strength, tensile strength and elastic modulus, were tested at various ages.
- In the short-term load study, the specimens were tested to failure using two equal point loads applied at the third points of the span at ages ranging from 42 to 63 days.
- In the sustained-load study, the specimens were initially loaded at an age of 14 days. The six beams were subjected to two equal point loads applied at the third points of the span, and the six slabs were each subjected to a sustained uniformly distributed superimposed load. Two identical specimens, “a” and “b”, were

constructed for each combination of parameters, but subjected to different sustained load levels.

Table 4-2 shows deflection test-to-predicted ratios for the single- and discretized-element idealizations, and the Bischoff and Branson Equations for the short-term load study (Gilbert & Nejadi 2004a). Care was taken to prevent moisture loss and, therefore, the tensile stresses due to restraint of shrinkage were likely slight. The predicted deflections are therefore also computed using cracking moments calculated using the full modulus of rupture. In this case, the deflections predicted using the Bischoff Equation with the full f_r, for either the single-element idealization or discretized-element idealization, most closely approximate the observed values: the test-to-predicted ratios range from 0.68 to 1.09. The coefficient of variation, CoV, for deflections computed using the Bischoff Equation is low, confirming its accuracy. For the lightly reinforced members, the Branson Equation with full f_r is unconservative using either idealization and has a relatively high coefficient of variation, confirming that it is less accurate than the Bischoff Equation. When the recommended f_r reductions are applied, the two equations and two idealizations give very similar results that are consistent (i.e., low CoVs) and conservative (i.e., means less than 1).

Table 4-2: Results of UNICIV Report No. R-434 (Gilbert & Nejadi 2004a)

Specimen	ρ (%)	Test Δ_{MID} (mm)	Test-to-Predicted From Different Methods							
			$0.5f_r$		$0.67f_r$		Full f_r			
			Branson		Bischoff		Branson		Bischoff	
			m=3	m=4	m=2	m=3	m=3	m=4	m=2	m=3
B1-a	0.53%	7.6	0.85	0.83	0.88	0.86	1.44	1.38	1.09	1.07
B1-b	0.53%	6.8	0.76	0.75	0.79	0.77	1.31	1.25	0.98	0.97
B2-a	0.53%	8.1	0.87	0.87	0.91	0.89	1.29	1.24	1.08	1.06
B2-b	0.53%	7.5	0.81	0.80	0.85	0.83	1.19	1.15	1.00	0.98
S1-a	0.30%	9.9	0.60	0.55	0.57	0.55	1.83	1.87	1.01	1.03
S1-b	0.30%	9.4	0.57	0.53	0.54	0.53	1.78	1.83	0.98	1.01
S2-a	0.45%	19.1	0.80	0.79	0.83	0.81	1.23	1.16	0.97	0.95
S2-b	0.45%	16.9	0.71	0.70	0.73	0.72	1.09	1.03	0.86	0.84
S3-a	0.60%	15.5	0.61	0.62	0.64	0.63	0.74	0.72	0.69	0.68
S3-b	0.60%	15.5	0.62	0.62	0.64	0.63	0.74	0.72	0.70	0.68
	Mean		0.72	0.71	0.74	0.72	1.27	1.24	0.94	0.93
	Std. Dev.		0.11	0.12	0.13	0.13	0.36	0.39	0.14	0.15
	CoV.		15.7%	17.1%	18.1%	18.1%	28.8%	31.3%	15.1%	15.7%

Table 4-3 shows test-to-predicted ratios for the initial deflections measured in the sustained-load study (Gilbert & Nejadi 2004b). Again steps were taken to prevent shrinkage, so the deflections are calculated using both the reduced and full moduli of rupture. Similar trends to those noted in Table 4-2 emerge: using the reduced modulus of rupture yields conservative and consistent results using either equation or idealization. Using the full modulus of rupture is unconservative, especially for the slab specimens with ρ of 0.29%. There is considerable variability for predicted deflections computed using the full modulus of rupture for Slab S1-a because the applied moment exceeds the cracking moment for only a small region at midspan. The unconservativism of the Branson Equation for lightly reinforced members is very apparent. The single-element idealization provides slightly better predictions than the discretized-element idealization because $I_{e,avg}$ is computed from the lowest ratio of M_{cr}/M_a at midspan where it is less than 1. In contrast, using the discretized-element idealization, the ratio of M_{cr}/M_a is greater

than 1 and, therefore, I_e equals I_g for most of the member length. Thus the effective moment of inertia of the discrete elements in the cracked region near mid-span is overestimated, and the associated deflection is markedly underestimated. This also explains the variability between the results obtained using the different methods for Slab S2-b, as it exhibits a short cracked region at midspan when using the full modulus of rupture to compute the cracking moment.

For Slab S3-b, using the full modulus of rupture to compute the cracking moment yields conservative deflections, but there is variability between the results obtained using the different methods. There is variability for the same reasons as Slabs S1-a and S2-b: the single-element idealization is computed from the lowest ratio of M_{cr}/M_a at midspan, and so yields more conservative results than the discretized analysis where I_e equals I_g for more of the member length. The conservatism is attributed to the ratio of M_{cr}/M_a at midspan. Slabs S2-b and S3-b have the same M_{cr}, similar I_{cr}, $31.2\times10^6\text{mm}^4$ and $39.1\times10^6\text{mm}^4$, and similar ratios of M_s/M_u, 0.34 and 0.32, respectively. However, the ratios of M_{cr}/M_a at midspan differ from 0.93 and 0.76, and so the computed deflections for S3-b are more conservative. When the reduced moduli of rupture are used to compute M_{cr}, I_e approaches I_{cr} and there is a consistent level of conservatism in the results for these slabs.

Table 4-3: Results of UNICIV Report No. R-435 (Gilbert & Nejadi 2004b)

Specimen	ρ (%)	Test Δ_{MID} (mm)	Test-to-Predicted From Different Methods							
			$0.5f_r$		$0.67f_r$		Full f_r			
			Branson		Bischoff		Branson		Bischoff	
			m=3	m=4	m=2	m=3	m=3	m=4	m=2	m=3
B1-a	0.53%	4.9	0.85	0.83	0.90	0.88	1.69	1.69	1.27	1.28
B1-b	0.53%	2.0	0.67	0.64	0.74	0.74	1.81	1.82	1.81	1.82
B2-a	0.53%	5.0	0.83	0.82	0.88	0.87	1.39	1.38	1.14	1.13
B2-b	0.53%	2.0	0.59	0.58	0.66	0.65	1.60	1.61	1.60	1.61
B3-a	0.80%	5.8	0.88	0.88	0.92	0.91	1.02	1.02	1.01	0.99
B3-b	0.80%	2.0	0.55	0.55	0.60	0.59	0.94	0.96	0.85	0.85
S1-a	0.29%	7.1	0.63	0.61	0.62	0.63	2.13	2.32	1.51	1.84
S1-b	0.29%	3.7	0.59	0.59	0.61	0.68	1.72	1.72	1.72	1.72
S2-a	0.44%	10.6	0.67	0.66	0.70	0.68	1.13	1.16	0.88	0.90
S2-b	0.44%	4.4	0.48	0.47	0.51	0.52	1.34	1.45	1.08	1.26
S3-a	0.59%	11.8	0.77	0.77	0.81	0.80	1.06	1.06	0.95	0.94
S3-b	0.59%	5.0	0.48	0.47	0.51	0.51	0.88	0.94	0.71	0.76
	Mean		0.67	0.66	0.71	0.70	1.39	1.43	1.21	1.26
	Std. Dev.		0.14	0.14	0.14	0.14	0.40	0.42	0.37	0.40
	CoV.		20.8%	21.3%	20.5%	19.3%	28.7%	29.7%	30.3%	31.4%

The results from both studies are consistent with the observations of others. The Branson Equation is unconservative for lightly reinforced members (e.g, Bischoff 2007) and, using the recommended $0.5f_r$ to compute M_{cr} for use in the Branson Equation or $0.67f_r$ to compute M_{cr} for use in the Bischoff Equation will yield similar values for I_e (CAC 2016).

4.2.2 Study by Washa & Fluck (1952)

The focus of the study by Washa and Fluck (1952) was to determine the effect of compressive reinforcement on the creep deflection of concrete beams. However, their reported immediate deflections of singly reinforced specimens are relevant to the present investigation. The geometry of the test specimens differed, but the area of tensile reinforcing steel was fairly consistent, with ρ of 1.5% being typical for beams. The span-to-depth ratios, L/h, ranged from 20 to 70, and for the purposes of the present

investigation the specimens with *L/h* of 20 or 30 were considered. The specimens were covered with wet canvas for five days until the side forms were removed and the concrete was exposed to the air. Two weeks after casting, the specimens were uniformly loaded by their own weight and concrete loading blocks so that the midspan moment approached the limiting design moment of a balanced section designed in accordance with the 1947 ACI Building Code (ACI 1947).

Table 4-4 shows the test-to-predicted ratios for deflections computed using the different methods, again with the cracking moments computed using the full and reduced moduli of rupture. For this higher reinforcement ratio, I_e approaches I_{cr} irrespective of the modulus of rupture assumed, and the discrepancies between the deflections computed using the Branson and Bischoff Equations are slight. There is low variability, as indicated by the low coefficient of variation, suggesting that accurate results can be obtained using either equation or idealization for members with ρ of 1.5%. This is again consistent with the observations by others (e.g., Scanlon & Bischoff 2008, CAC 2016).

Table 4-4: Results of Washa & Fluck (1952)

Specimen	ρ (%)	Test Δ_{MID} (mm)	Test-to-Predicted From Different Methods							
			$0.5f_r$		$0.67f_r$		Full f_r			
			Branson		Bischoff		Branson		Bischoff	
			m=3	m=4	m=2	m=3	m=3	m=4	m=2	m=3
A6	1.58%	17.0	1.06	1.06	1.08	1.07	1.09	1.10	1.12	1.11
B3.B6	1.57%	26.4	1.01	1.01	1.04	1.03	1.06	1.07	1.09	1.07
D3.D6	1.54%	17.8	1.15	1.15	1.17	1.16	1.19	1.19	1.22	1.20
	Mean		1.07	1.07	1.10	1.09	1.11	1.12	1.14	1.13
	Std. Dev.		0.07	0.07	0.07	0.07	0.07	0.07	0.07	0.07
	CoV.		6.4%	6.5%	6.3%	6.4%	5.9%	5.9%	5.9%	6.0%

4.2.3 Study by El-Nemr (2013)

El-Nemr (2013) tested thirty-three simply supported members made of normal- and high-strength concrete with a clear span of 3.75m and cross-section of 200×400mm. Two test specimens were reinforced with Grade 400 10M steel bars and specimen N3#10ST, made of normal-strength concrete (f'_c=33.5MPa), is considered in this study. Two equal concentrated point loads near midspan were applied monotonically, the load corresponding to the first crack was recorded, and the experimental cracking moment was computed to be 14.2kN.m. This observed cracking moment is bounded by those computed using the full or reduced moduli of rupture. Table 4-5 shows the deflections computed using the alternative deflection calculation procedures and using the observed cracking moment. When using the Branson Equation, the actual deflection is bounded by predictions based on using the full and reduced moduli and the most accurate results are obtained with the observed cracking moment. There is high variability in the results suggesting that, for lightly reinforced members, the Branson Equation is particularly sensitive to the computed M_{cr}. When using the Bischoff Equation, the actual deflection is best predicted when using the full modulus and there is little variability in results obtained using the reduced modulus or using observed cracking moment, suggesting that the Bischoff Equation is less sensitive to the computed M_{cr}.

Table 4-5: Results of El-Nemr (2013) – Specimen N3#10ST

		Test-to-Predicted From Different Methods											
	Test	0.5f_r		0.67f_r		Full f_r				Obsv. M_{cr}			
ρ (%)	Δ_{MID}	Branson		Bischoff		Branson		Bischoff		Branson		Bischoff	
	(mm)	m=3	m=4	m=2	m=3	m=3	m=4	m=2	m=3	m=3	m=4	m=2	m=3
0.43%	7.2	0.81	0.80	0.84	0.82	1.31	1.27	0.99	0.99	0.97	0.94	0.86	0.85

Figure 4-1 shows the normalized effective moment of inertia computed using the discretized-element idealization for the Branson and Bischoff Equations based on the observed cracking moment and cracking moment computed using the reduced moduli of rupture on the left side or the full moduli of rupture on the right side. Using the reduced modulus of rupture or the observed cracking moment I_e equals I_{cr} near mid-span. When using the full modulus of rupture, particularly for the Branson Equation, I_e is overestimated at midspan and the extent of cracking is underestimated, yielding unconservative deflections as shown in Table 4-5.

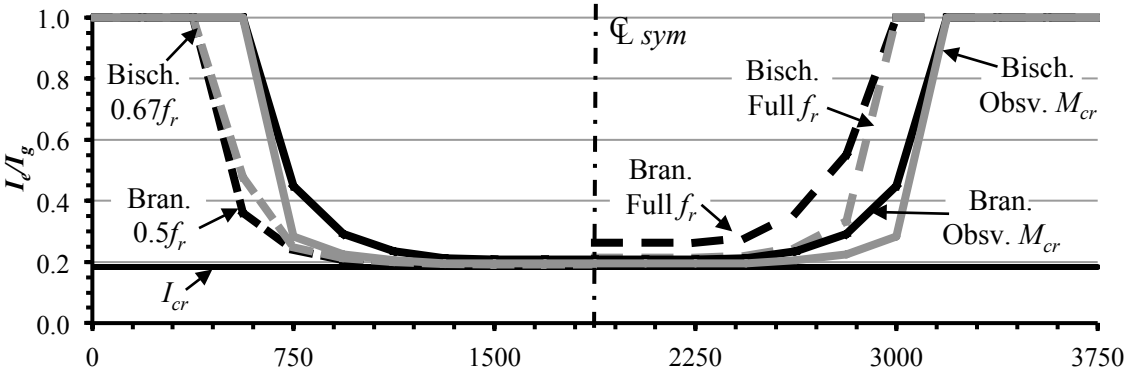

(a) Normalized Effective and Cracked Moments of Inertia

Figure 4-1: Beam N3#10ST – El-Nemr (2013)

4.2.4 Study by Branson (1965)

The Branson Equation for the effective moment of inertia was empirically derived from the test results of Part I of his study in 1963 (1965). This study included simply supported members, SB-1 and SB-3, reinforced with one (ρ = 0.7%) or three (ρ = 2.1%) #3 bars, respectively, spanning 9ft (2.74m) and with a cross section of 4×5in (102×127mm). The specimens were loaded at 28 days with the beam dead load plus a uniformly distributed load applied using iron bricks spaced uniformly along the beams. Superimposed-dead-

load to dead-load ratios, SDL-to-DL, of 2.0 and 5.5 were applied to the one-bar and three-bar beams, respectively.

The left sides of Figure 4-2(a) and (b) show the normalized applied and cracking moments and normalized effective and cracked moments of inertia, respectively, for the lightly loaded member, SB-1. The right sides of Figure 4-2(a) and (b) show the same for the more heavily loaded member, SB-3. For Beam SB-1, the applied moment does not exceed the cracking moment computed using the full modulus of rupture, thus I_e equals I_g in either single- or discretized-element idealizations. For Beam SB-3, the applied moment exceeds the cracking moment, whether computed using full or reduced moduli of rupture, for most of the member length, and so, I_e equals I_{cr} for most of the member length.

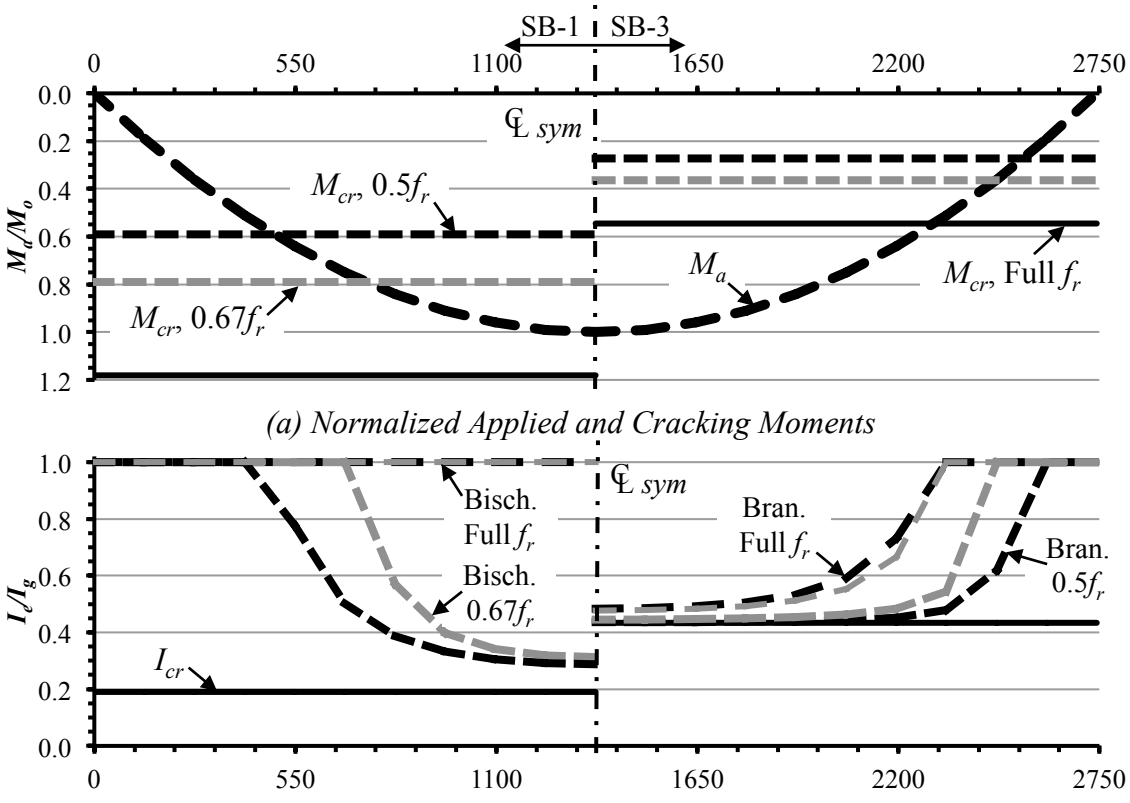

Figure 4-2: Simply Supported Beams SB-1 (left) & SB-3 (right) – Branson (1965)

Table 4-6 shows the test-to-predicted ratios for deflections computed using the alternative deflection calculation procedures. The differences between the single-element and discretized-element idealizations are very slight due to the reasons previously explained. For SB-1, when using the full modulus of rupture the predicted deflections are the same because the ratio of M_{cr}/M_a is greater than 1 along the entire member length, the beam is uncracked and, therefore, I_e equals I_g. When using the reduced moduli, the ratio of M_{cr}/M_a is less than 1 at midspan, implying the member is cracked and the predicted deflections are overly conservative. For SB-3, when using either the full or reduced moduli of rupture the ratio of M_{cr}/M_a is less than 1, and so, the majority of the beam is cracked, therefore I_e approaches I_{cr}. Using the reduced moduli of rupture is very conservative for both members. These results, again, emphasize the importance of accurately predicting the cracking moment, and so, the extent of cracking and the ratio of M_a/M_{cr}.

Table 4-6: Results of Branson (1965)

Specimen	ρ (%)	Test Δ_{MID} (mm)	Test-to-Predicted From Different Methods							
			$0.5f_r$		$0.67f_r$		Full f_r			
			Branson		Bischoff		Branson		Bischoff	
			m=3	m=4	m=2	m=3	m=3	m=4	m=2	m=3
SB-1	0.7%	1.0	0.29	0.29	0.31	0.34	0.82	0.82	0.82	0.82
SB-3	2.1%	3.9	0.62	0.62	0.66	0.65	0.74	0.75	0.73	0.73
	Mean		0.46	0.46	0.48	0.49	0.78	0.78	0.77	0.77
	Std. Dev.		0.24	0.24	0.25	0.22	0.06	0.05	0.06	0.06
	CoV.		51.6%	52.0%	50.8%	43.6%	7.1%	6.3%	7.7%	8.2%

4.2.5 Study by Washa (1947)

The tests performed by Washa (1947) involved thin reinforced concrete slabs loaded for five years. All of the members were very slender with a cross-section of 3×12in

(76×305mm). The span-to-depth ratios, *L/h,* were large, varying from 30 to 70. The reinforcement ratios varied from 0.80% to 1.60%. The present investigation considers the instantaneous deflections of the G and H specimens from Case 3 with *L/h* of 30 and reinforcement ratios of 0.80%. The G and H slabs were identical in all aspects, including a design compressive strength of 2,000psi (13.8MPa), and water-to-cement ratio of 0.84, except the desired concrete slumps were 102mm and 203mm in Slabs G and H, respectively. This slump difference was achieved by different mix design proportions by weight of 1:4.0:6.2 and 1:3.6:5.5, in Slabs G and H, respectively. All slabs were cured in the moulds under damp burlap from 3 to 7 days. After stripping, the specimens were subjected to two curing conditions: half were sealed by a bakelite lacquer and then a paraffin coating; and, the rest were sealed on the edges and ends only to simulate field conditions with the top and bottom exposed to air. The specimens were designated as Sealed or Dry based on their respective curing condition.

Table 4-7 shows the ultimate compressive strength, $f_{c,ult}$ and elastic modulus determined from compressive strength tests performed at 28 days and 5 years on control cylinders for G and H concretes and Sealed and Dry conditions. The Dry specimens have a higher compressive strength at 28 days but the long-term strength of the Sealed specimens is higher. These differences are, however, relatively small.

Table 4-7: Compression Tests of Control Cylinders in study by Washa (1947)

Specimen	Condition	$f_{c,ult}$ (MPa)		E_c (MPa)	
		28 days	5 years	28 days	5 years
G	Dry	19.0	23.2	21,100	24,900
	Sealed	18.8	24.5	20,100	26,300
H	Dry	23.4	24.4	23,000	28,100
	Sealed	21.1	26.6	23,800	31,200

Figure 4-3(a) shows the normalized applied moment variation and M_{cr} computed using the full or reduced f_r for Beam 3-G-Dry. The cracking moments computed using the reduced moduli of rupture cause the length of the cracked region to double and the minimum ratio of M_{cr}/M_a to reduce from 0.80 for the full f_r to 0.53 and 0.40 for $0.67f_r$ and $0.5f_r$, respectively. Figure 4-3(b) shows the normalized effective and cracked moments of inertia computed using the Branson or Bischoff Equations with the full or reduced moduli of rupture used to compute M_{cr}. Using the full modulus of rupture with either the Branson or Bischoff Equation is very unconservative because the extent of the cracked region is underestimated. In this case, the cracked length is the same, and I_e at midspan computed using the Bischoff Equation is markedly less than that computed using the Branson Equation. Using the reduced moduli of rupture increases the extent of the cracked region, especially when using $0.5f_r$ with the Branson Equation. In this case, the effective moments of inertia computed using the Branson and Bischoff Equations are similar.

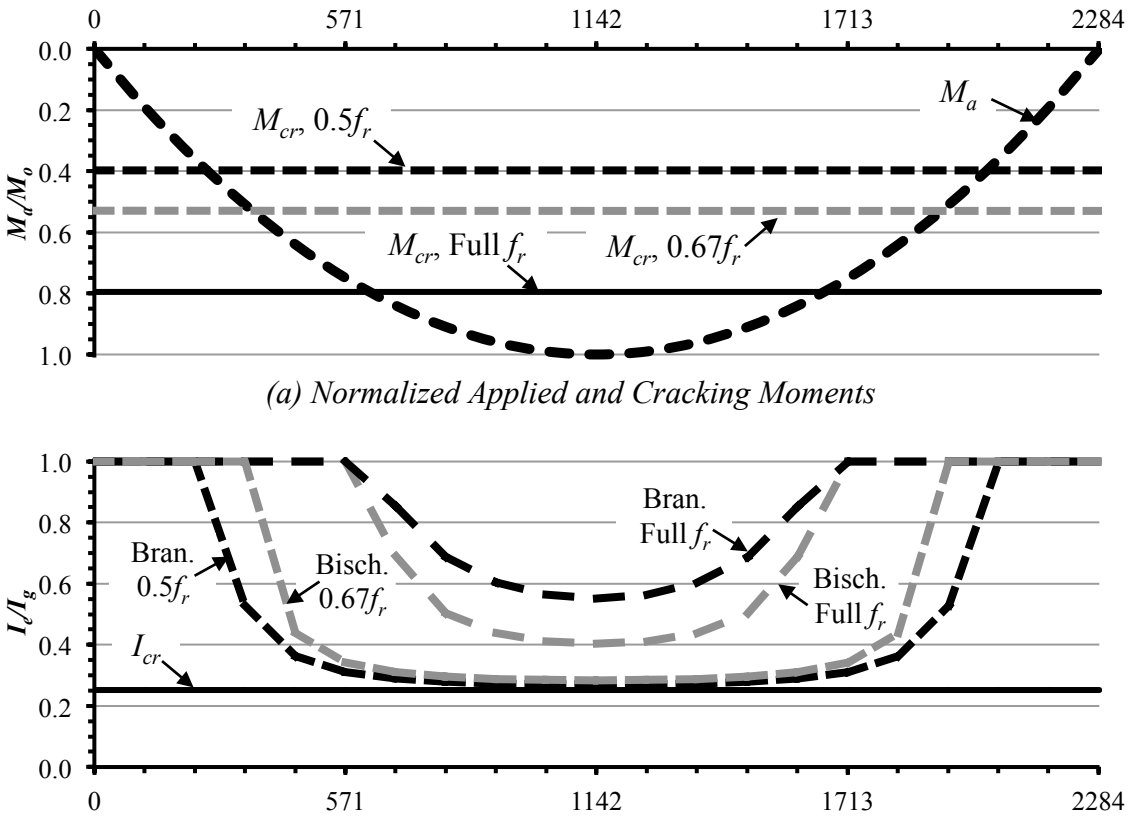

(a) Normalized Applied and Cracking Moments

(b) Normalized Effective and Cracked Moments of Inertia

Figure 4-3: Beam 3-G-Dry – Washa (1947)

Table 4-8 shows the deflection test-to-predicted ratios from the alternative deflection calculation procedures for the Dry and Sealed G and H specimens. The applied moment exceeds the cracking moment computed using the full modulus of rupture for only a small region at midspan. Similar trends to those observed for the Gilbert and Nejadi (2004b) specimen S1-a are seen: there is great variability in the results, the single-element idealization provides slightly better results than the discretized-element idealization with either the Branson or Bischoff Equation, and the Branson is very unconservative for low reinforcement ratios. This confirms that both the ratio of M_{cr}/M_a

at midspan and the length of the cracked region are particularly sensitive parameters in deflection calculations.

When the cracking moments are computed using the reduced moduli, the two idealizations provide consistent results using either the Branson or Bischoff Equations. For Beam 3-G-Dry, the recommended reductions for the modulus of rupture are necessary because, due to drying shrinkage from curing, tensile stresses due to restraint of shrinkage are present. Figure 4-3(a) and (b) show that computing M_{cr} using the full modulus of rupture will, markedly, underestimate the length of the cracked region at midspan and, as Table 4-8 shows, cause the predicted deflections to be very unconservative. For the Sealed specimens, the observed deflections are smaller than those for the Dry specimens because care was taken to prevent shrinkage and so tensile stresses due to restraint of shrinkage. The unconservative results when the full f_r is used to compute M_{cr}, however, suggests that restraint due to shrinkage was reduced but not prevented and tensile stresses are present in the Sealed specimens. The test-to-predicted ratios are smaller for the Sealed specimens because, regardless of curing conditions, the alternative deflection calculation procedures predict very similar deflections for the Dry and Sealed specimens.

Table 4-8: Results of Washa (1947)

Specimen	ρ (%)	Test Δ_{MID} (mm)	Test-to-Predicted From Different Methods							
			$0.5f_r$		$0.67f_r$		Full f_r			
			Branson		Bischoff		Branson		Bischoff	
			m=3	m=4	m=2	m=3	m=3	m=4	m=2	m=3
3-G-Dry	0.80%	6.1	0.79	0.78	0.84	0.83	1.66	1.80	1.26	1.38
3-G-Sealed	0.80%	5.3	0.68	0.67	0.72	0.72	1.39	1.50	1.07	1.17
3-H-Dry	0.80%	7.1	1.01	0.99	1.08	1.08	2.55	2.80	1.96	2.25
3-H-Sealed	0.80%	6.6	0.92	0.90	0.98	0.97	2.21	2.43	1.62	1.84
	Mean		0.85	0.83	0.90	0.90	1.95	2.13	1.48	1.66
	Std. Dev.		0.15	0.14	0.15	0.16	0.53	0.59	0.39	0.48
	CoV.		17.4%	17.1%	17.0%	17.4%	27.0%	27.7%	26.5%	29.1%

4.2.6 Study by Corley & Sozen (1966)

Corley and Sozen (1966) investigated time-dependent deflections of four reinforced concrete beams over two years. Specimens C1 and C2 were proportioned as balanced sections, such that the allowable stress limits in the steel and concrete occur simultaneously, with reinforcement ratios of 1.4%. Specimens C3 and C4 were designed following the ultimate strength design theory in accordance with the Appendix to ACI 318-56 (ACI 1956) using minimum load factor of 1.8. Beams C3 and C4 were designed to carry the same moment as C1 but using as small an effective depth, d, as possible with f_y of 60,000psi (414MPa) and 40,000psi (275MPa), respectively, resulting in reinforcement ratios of 2.0% and 3.0%. The beams were covered with wet burlap for 24 hours after casting, then forms were stripped and beams were moved to a fog room for 7 days then moved to the open lab for 21 days. At an age of 28 days, specimens were moved to a climate-controlled room and tested. All beams had a 28-day concrete strength of 3500psi (24MPa), spanned 6ft (1.83m) and were loaded identically by two point loads

at $L/4$. Beam C2 was loaded to cracking, then unloaded and stored to monitor crack widths and the effects of shrinkage and residual stresses with time.

Figure 4-4(a) and (b) show the normalized applied and cracked moments and normalized effective and cracked moments of inertia computed using the Branson or Bischoff Equations and M_{cr} computed using the full or reduced f_r for Beam C1, respectively. The ratio of M_{cr}/M_a is low, and most of the member length at midspan is cracked, thus, I_e quickly approaches I_{cr} irrespective of the modulus of rupture or effective moment of inertia equation assumed. Table 4-9 shows that because M_{cr}/M_a is small whether M_{cr} is computed using either the reduced or full moduli of rupture, the effect on the computed deflections is insignificant. For Specimens C3 and C4, with even higher reinforcement ratios, there is negligible difference between the deflections computed using the single-element and discretized-element idealizations with the Branson or Bischoff Equations. These findings are consistent with those observed when considering the specimen tested by Bakoss et al. (1982) and are further explored in Appendix F.

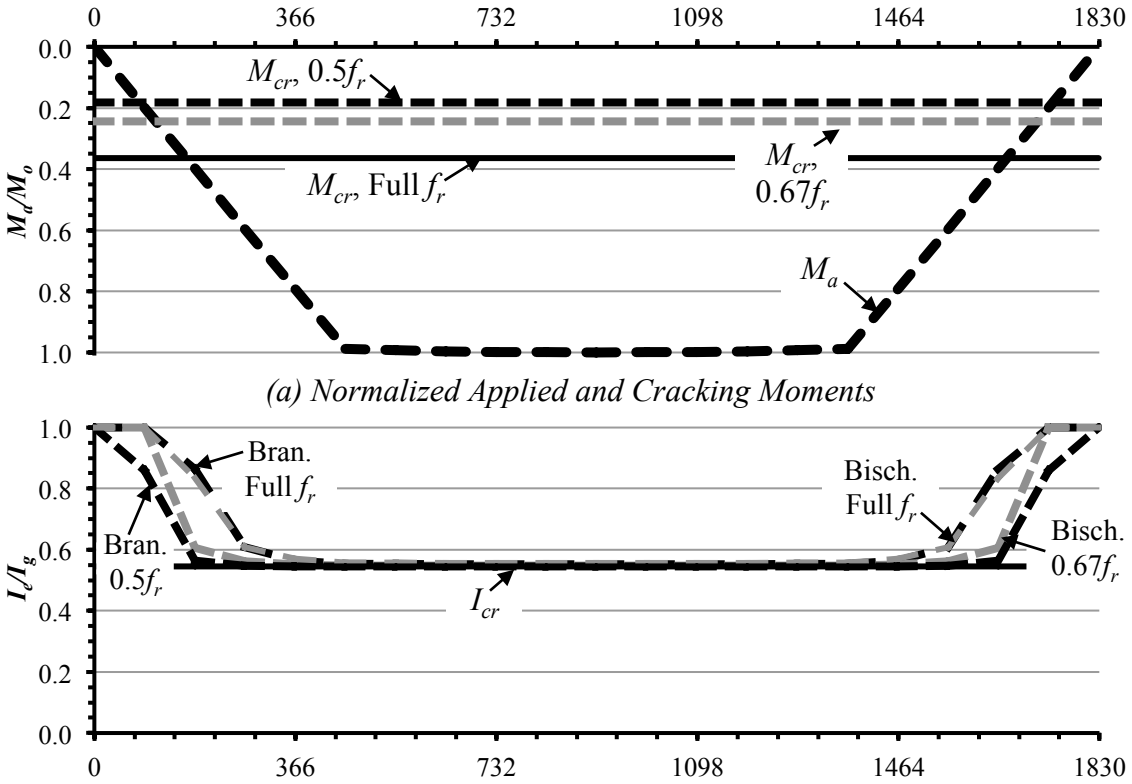

Figure 4-4: Simply Supported Beam C1 – Corley & Sozen (1966)

Table 4-9: Results of Corley & Sozen (1966)

Specimen	ρ (%)	Test Δ_{MID} (mm)	Test-to-Predicted From Different Methods							
			0.5f_r		0.67f_r		Full f_r			
			Branson		Bischoff		Branson		Bischoff	
			m=3	m=4	m=2	m=3	m=3	m=4	m=2	m=3
C1	1.4%	3.0	0.97	0.97	0.99	0.97	1.00	0.99	1.02	1.00
C3	2.0%	7.9	1.00	1.00	1.00	1.00	1.00	1.00	1.01	1.00
C4	3.0%	6.1	1.00	1.00	1.00	1.00	1.00	1.00	1.00	1.00
	Mean		0.99	0.99	1.00	0.99	1.00	1.00	1.01	1.00
	Std. Dev.		0.02	0.02	0.01	0.01	0.00	0.01	0.01	0.00
	CoV.		1.8%	1.9%	0.8%	1.5%	0.2%	0.6%	1.0%	0.4%

4.2.7 Study by Yu (1960) – T-Beam Member

Yu's (1960) investigation included a series of 12 tests carried out at Cornell University on T-beams, six under short-time loading and six under sustained loading. The six T-beams under short-term loading, A-1, B-1, C-1, D-1, E-1 and F-1, including the two

specimens with compression reinforcement, B-1 and C-1, are deemed to be relevant for the present study as the presence of compression reinforcement is likely not significant for instantaneous deflections of T-beams (CAC 2016). Table 4-10 shows the variable parameters in the study, which included: reinforcement ratio, $\rho^+ = A_s/(b_{fl}d)$; flange-to-web width ratio, b_{fl}/b_w; span-to-depth ratio, L/h; and, the average compressive strength of the control cylinders, f'_c.

Table 4-10: Specimen parameters varied in study by Yu (1960)

Specimen	ρ^+	b_{fl}/b_w	L/h	f'_c (MPa)
A-1	0.50%	2	20	25.4
B-1	0.50%	2	20	26.8
C-1	0.50%	2	20	24.4
D-1	0.52%	4	20	25.4
E-1	0.52%	2	14	29.4
F-1	0.83%	2	30	29.4

All beams were cast in T-shaped forms and covered with waterproof membrane for sealing. After 3 days, the forms were removed and the beams were placed in a controlled climate for 18 days. Beams were then stored in the open laboratory for 7 days. At an age of 28 days the beams were tested under uniform loading. Service loads were computed on the basis of the ultimate strength theory by assuming f_y of 80,000psi (552MPa), a load factor of 1.8, and f'_c as the average compressive strength of the control cylinders, as shown in Table 4-10. For all specimens, the service loading is very high, so the ratio of M_{cr}/M_a is low irrespective of the modulus of rupture assumed as shown in Figure 4-5(a). Figure 4-5(b) shows, for specimen E-1, that I_e approaches I_{cr} over the majority of the member length. Table 4-11 shows the test-to-predicted ratios for the deflections computed from the different methods. The differences in computed deflections are slight,

irrespective alternative deflection calculation procedure used, because the majority of the member length is cracked.

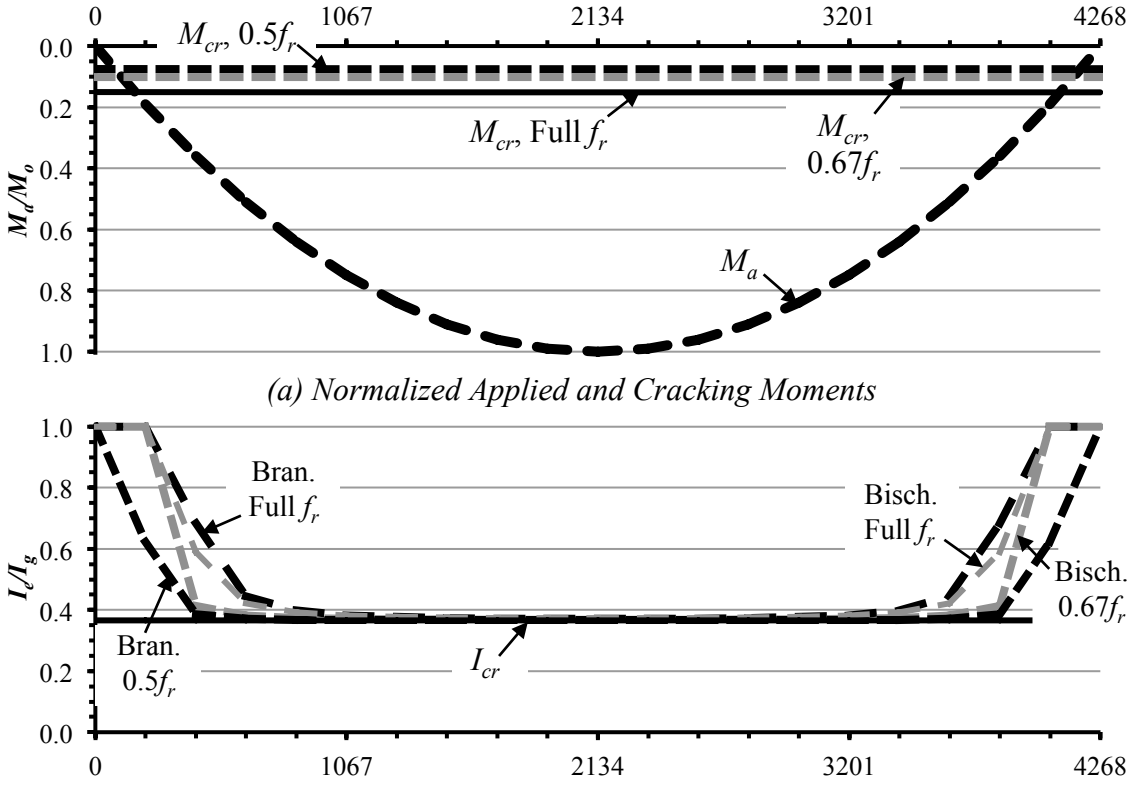

(a) Normalized Applied and Cracking Moments

(b) Normalized Effective and Cracked Moments of Inertia

Figure 4-5: Simply Supported Beam E-1 – Yu (1960)

Table 4-11: Results of Yu (1960)

Specimen	ρ (%)	Test Δ_{MID} (mm)	Test-to-Predicted From Different Methods							
			0.5f_r		0.67f_r		Full f_r			
			Branson		Bischoff		Branson		Bischoff	
			m=3	m=4	m=2	m=3	m=3	m=4	m=2	m=3
A-1	0.50%	34.0	1.01	1.02	1.03	1.02	1.04	1.04	1.05	1.04
B-1	0.50%	31.5	0.93	0.93	0.94	0.94	0.95	0.95	0.96	0.95
C-1	0.50%	30.2	0.90	0.90	0.91	0.90	0.92	0.92	0.93	0.92
D-1	0.52%	32.3	0.92	0.92	0.93	0.92	0.92	0.93	0.93	0.93
E-1	0.52%	13.0	0.78	0.78	0.79	0.79	0.81	0.81	0.82	0.81
F-1	0.83%	55.9	0.93	0.93	0.94	0.93	0.94	0.94	0.95	0.94
	Mean		0.91	0.91	0.92	0.92	0.93	0.93	0.94	0.93
	Std. Dev.		0.08	0.08	0.08	0.08	0.07	0.07	0.07	0.07
	CoV.		8.4%	8.4%	8.2%	8.3%	7.8%	7.8%	8.2%	8.2%

4.2.8 Overall Findings for Simply Supported Members

The investigation of simply supported members has identified some of the key parameters that need to be accurately quantified to predict deflections accurately. Accurate quantification of the cracking moment, especially for lightly reinforced members, is essential. For beams with lower ρ, such as Beam SB-1 tested by Branson (1965), the applied moments at service are relatively small and the ratio of M_{cr}/M_a may vary greatly along the member length. Accurate prediction of M_{cr} is important to determine the cracked and uncracked regions. As the reinforcement ratio increases, the applied moments are much higher, often markedly exceeding the cracking moment for the majority of the member length, such as Beam SB-3 tested by Branson (1965). In this case, I_e approaches I_{cr} irrespective of the assumed M_{cr}. When curing methods cause tensile stresses due to restraint of shrinkage to occur computing the cracking moment based on a reduced modulus of rupture is appropriate.

When examining the individual studies trends emerge: using the reduced modulus of rupture provides consistent and conservative results; the Branson Equation with the full modulus of rupture is unconservative for low reinforcement ratios, and the Bischoff Equation with the full modulus of rupture provides the best results when tensile stresses are slight. These trends are consistent with the overall trends seen when looking at the entire database of test results and with the observations of others (e.g., CAC 2016, Scanlon & Bischoff 2008).

Figure 4-6(a) shows the test-to-predicted ratios for different idealizations and effective moment of inertia equations when using the reduced moduli of rupture to compute the cracking moment for various reinforcement ratios. For lower reinforcement ratios, using a reduced f_r gives conservative results. Typically results for a particular test are superimposed on top of each other indicating results obtained using the different idealizations and effective moment of inertia equations with the reduced modulus of rupture are consistent.

Figure 4-6(b) shows the test-to-predicted ratios for different idealizations and effective moment of inertia equations when using the full modulus of rupture to compute the cracking moment for various reinforcement ratios. For reinforcement ratios less than 1%, using the full f_r typically gives unconservative results, especially when using the Branson Equation. The results of a particular test are scattered indicating the results among the different idealizations and effective moment of inertia equations with the full modulus of rupture for reinforcement ratios less than 1% are variable. For reinforcement ratios greater than 1%, the test-to-predicted ratio approaches 1, and there is virtually no scatter in the data, indicating consistent results among the different idealizations and effective moment of inertia equations.

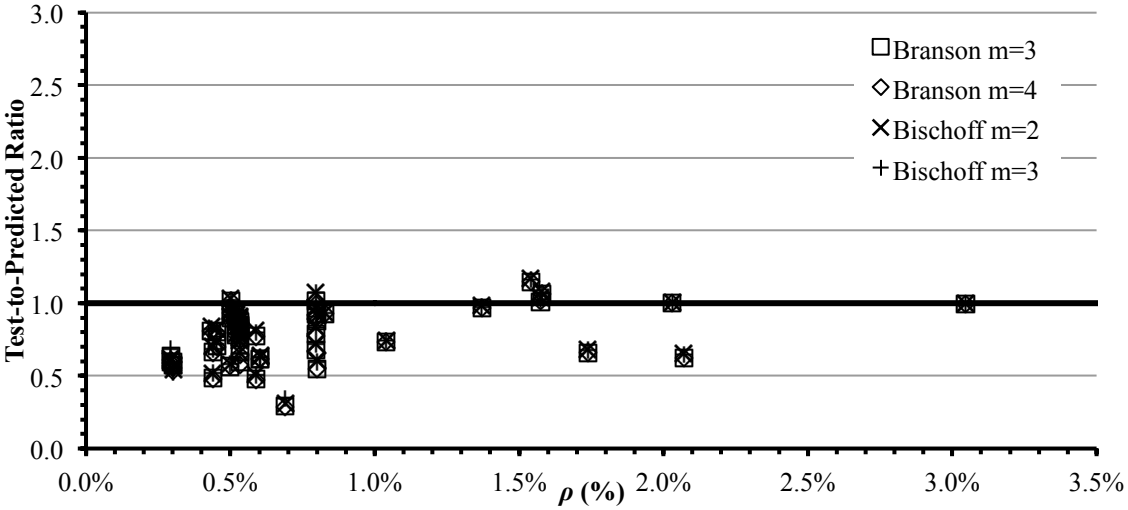

(a) Reduced Modulus of Rupture

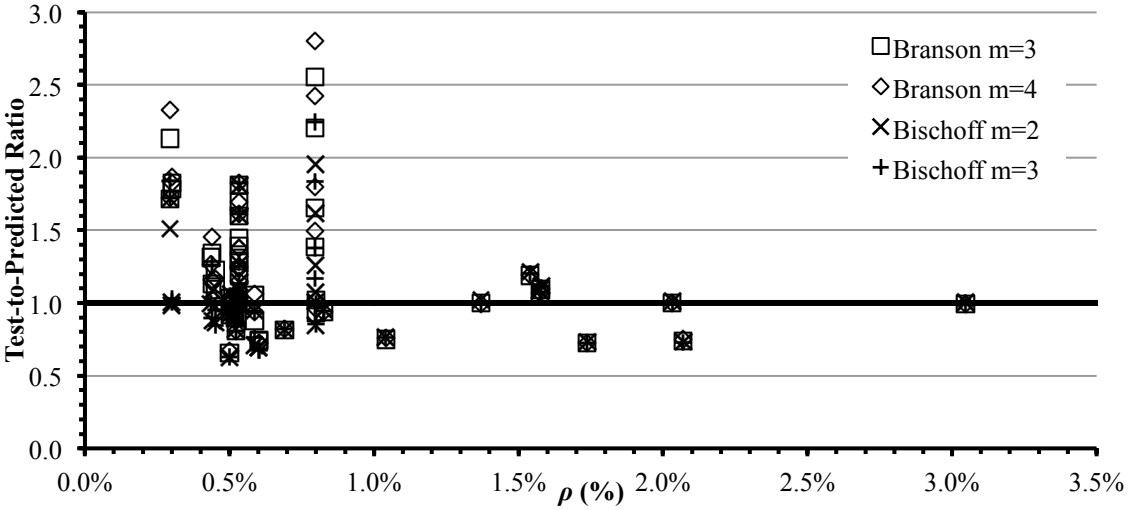

(b) Full Modulus of Rupture

Figure 4-6: Test-to-Predicted Ratios for Various Reinforcement Ratios – Simply Supported Members

Table 4-12 shows the overall mean, standard deviation and coefficient of variation of test-to-predicted ratios computed for the various alternative deflection calculation procedures. The very high mean and standard deviation for deflections computed using the Branson Equation with the full modulus of rupture indicates unconservative and variable results. The Bischoff Equation with a full modulus of rupture in either a single-

element or discretized-element idealization, on average, gives slightly unconservative results that are within 8% of the observed deflections, and the standard deviation is lower than that for the Branson Equation. The single-element idealization with a full modulus of rupture using the Branson or Bischoff Equation gives slightly more accurate results than those computed in a discretized-element idealization. When using the reduced moduli of rupture the difference in the Branson or Bischoff Equations in a single- or discretized-element idealization is slight. The mean values are very consistent for the averaged results of the two idealizations and two equations for the effective moment of inertia, and the coefficient of variation is 22-24%, markedly lower than that for the full modulus of rupture.

Table 4-12: Overall Findings for Simply Supported Members

	Test-to-Predicted From Different Methods							
	$0.5f_r$		$0.67f_r$		Full f_r			
	Branson		Bischoff		Branson		Bischoff	
	m=3	m=4	m=2	m=3	m=3	m=4	m=2	m=3
Mean	0.78	0.77	0.80	0.80	1.22	1.24	1.05	1.08
Std. Dev.	0.18	0.18	0.18	0.18	0.43	0.48	0.30	0.35
CoV.	23.4%	24.0%	22.8%	22.4%	35.4%	38.5%	28.2%	32.3%

Table 4-13 shows the overall mean, standard deviation and coefficient of variation of test-to-predicted ratios for the studies that did not control to prevent shrinkage. The tensile stresses are likely slight in specimens excluded from this table, which include those tested by Gilbert and Nejadi (2004a, 2004b) and the Sealed specimens tested by Washa (1947). When those specimens are excluded the sample size is reduced to 22 specimens. Again, computing M_{cr} using the reduced modulus of rupture provides consistent and conservative results using either effective moment of inertia equation. These values improve, as compared to Table 4-12, because when the studies that

controlled shrinkage are included, computing M_{cr} using the reduced modulus of rupture the tensile stresses due to restraint of shrinkage are accounted for twice and the computed deflections are, therefore, overly conservative. If M_{cr} is computed using the full modulus, the Branson Equation is very inconsistent, as indicated by the very high standard deviation, and associated coefficient of variation. The Bischoff Equation provides the best mean result of all the alternative deflection procedures, and has a lower standard deviation, and coefficient of variation than the Branson Equation. These values also improve compared to those shown in Table 4-12, especially for the values computed using the Branson Equation because the specimens investigated by Gilbert and Nejadi (2004a, 2004b) and Washa (1947) have reinforcement ratios less than 1% and M_{cr} computed using the full modulus of rupture underestimates the length of the cracked region.

Table 4-13: Overall Findings for Simply Supported Members – Excluding Studies

	Test-to-Predicted From Different Methods							
	$0.5f_r$		$0.67f_r$		Full f_r			
	Branson		Bischoff		Branson		Bischoff	
	m=3	m=4	m=2	m=3	m=3	m=4	m=2	m=3
Mean	0.86	0.86	0.88	0.87	1.05	1.07	1.00	1.01
Std. Dev.	0.19	0.19	0.20	0.19	0.40	0.45	0.27	0.32
CoV.	22.7%	22.7%	22.2%	21.7%	38.2%	42.5%	26.7%	32.2%

4.3 CONTINUOUS MEMBERS

Table 4-14 summarizes the curing conditions, applied loading and other relevant data for the 11 rectangular two-span members and 8 simply supported T-beams with cantilevers at one support investigated. Generally, the specimens were wet cured and the applied loading was typically uniformly distributed loads or point loads at midspan. The

specimens cover a wide range of reinforcement ratios, $0.50\% \leq \rho \leq 3.20\%$, and wide range of span-to-depth ratios, $8 \leq L/h \leq 70$. For the single-element idealization, $I_{e(avg)}$ is more influenced by I_e^+ (CSA 2014). Therefore, members were categorized based on the tensile reinforcing steel in the positive moment region, ρ^+. The last two studies shown, denoted with *, are presented in detail in Appendix F.

Table 4-14: Summary of Continuous Beam Studies

Study	Comment	Curing	Applied Loading	No. of Specimens	ρ^+ at Mid-Span (ρ')	ρ^- at Support (ρ')	L/h
Washa & Fluck (1956)	Long term "Plastic Flow" study. Equation based on test results and full f_r	Cured under wet canvas 7d, then concrete was exposed to air on all surfaces except the bottom.	UDL	3	1.59% - 1.65% (0%)	2.83% - 3.20% (2.48% - 3.54%)	30, 50 & 70
Branson (1965)	Equation based on test results and full f_r	No info given	UDL	2	0.69% or 2.07% (0%)	0.69% or 2.07% (0%)	22
El Mogy (2011)	FRP Study - Steel Control Specimen	Concrete surface was kept wet for 7d	Point Loads at Mid-Span	1	1.48% (0%)	1.11% (0%)	9
Habeeb (2008)	FRP Study - Steel Control Specimen	Wet cured, and covered until the date of testing	Point Loads at Mid-Span	1	0.84% (0%)	0.84% (0%)	9
Mahroug (2014a, 2014b)	FRP Study - Steel Control Specimen	Wet cured, and covered until the date of testing	Point Loads at Mid-Span	2	0.50% or 0.75% (0%)	0.50% or 0.75% (0%)	13
Guaralnick & Winter (1957, 1958)	T-Beams	Waterproof membrane stretched over each specimen. Forms removed after 3d and beams placed in moist room for 18d. Specimens dried in lab at 21d until testing at ~28d	UDL	8	0.72%-1.35% (0%)	0.72%-1.35% (0%)	11
*Bakoss et al. (1982)	Higher ρ, $I_e \rightarrow I_{cr}$ irrespective of the f_r	Moist cured 14d, kept in climate-controlled lab	Point Loads at Mid-Span, No Self Weight	1	1.74% (0%)	1.74% (0%)	23
*Mattock (1959)	Redistribution of design bending moments	No info given	Single Point Load + Self Weight	1	1.97% (0%)	0.98% (0%)	8

4.3.1 Single-Element Idealization – $I_{e(avg)}$ Investigation

For two-span members, the analysis procedure outlined in Section 3.3.2 was followed. In the single-element idealization, the average effective moment of inertia, $I_{e(avg)}$, according to Equation 9.4 of A23.3 (CSA 2014), is a weighted average of the effective moments of inertia at midspan and at the interior support, I_e^+ and I_e^-, respectively, computed as:

[4.1] $$I_{e(avg)} = (1 - \kappa)I_e^+ + \kappa I_e^-$$

where the weighting coefficient, κ, is equal to 0.15. The ACI Committee 318 Building Code (2014) permits $I_{e(avg)}$ to be computed as the average of I_e^+ and I_e^-, implying κ is equal to 0.50. ACI Committee 435 (1995) cites the ACI 318 procedures but suggest that, "improved results for continuous prismatic members can, however, be obtained using a weighted average" with κ equal to 0.15, consistent with A23.3-14. The basis for using a weighted average of I_e^+ and I_e^- is the report for computing deflections of continuous members by ACI Committee 435, Subcommittee 7 (1973) and Branson (1977) first suggested setting κ equal to 0.15 for beams with one end continuous. Based on these design codes the weighting coefficient, κ, is bounded between 0.15 and 0.50.

Typically, deflections computed using the single-element idealization for two-span members, like those tested by Washa and Fluck (1956) and Habeeb and Ashour (2008), are more conservative than those computed using the discretized-element idealization. A sensitivity analysis was therefore performed to determine the optimal value of κ within the bounds of 0.15 and 0.50. The beams investigated have computed deflections using the single-element idealization that exceed those computed using the discretized-element

idealization. Such differences are greatest when using the Branson Equation with the full modulus of rupture used to compute the cracking moment, so the sensitivity analysis focused on this case.

Table 4-15 and Figure 4-7 shows the deflection test-to-predicted ratios computed for various values of κ, and the ratio of I_e^+/I_e^-. For members with $I_e^+/I_e^- \approx 1$, the deflection test-to-predicted ratios are insensitive to κ. For member SSc-8d/2p, with $I_e^+/I_e^- = 1.24$, the deflection test-to-predicted ratio decreases when κ increases and causes $I_{e(avg)}$ to decrease, giving conservative results. Members with $I_e^+/I_e^- < 1$ have higher reinforcement ratios in the negative moment region and so are more realistic. For these members, the deflection test-to-predicted ratios increase when κ increases, because $I_{e(avg)}$ increases so smaller deflections are calculated. These members perhaps seem more sensitive to the value of κ in part because I_e^+/I_e^- is typically much less than 1. For the cases where $I_{e(avg)}$ is sensitive to κ, using the ACI 318 (2014) value of 0.50 gives the best results. Appendix G presents the sensitivity analysis performed using the Bischoff Equation with the full or reduced moduli to compute M_{cr} and the Branson Equation using $0.5f_r$ to compute M_{cr}. The findings are consistent with the obtained results.

Table 4-15: Test-to-Predicted Ratios

Study		Washa & Fluck (1956)			Mattock (1959)	Habeeb & Ashour (2008)	Mahroug et al. (2014)	Bakoss et al. (1982)	El-Mogy (2011)	Mean	Std. Dev.
Specimen		Y3,Y6	Z3,Z6	X3,X6	1-1	SScUU	C-S2-UU	2B1, 2B2	SSc-8d/2p		
I_e^+/I_e^-		0.61	0.70	0.71	0.78	1.03	1.07	1.07	1.24		
κ	0.15	0.85	0.84	0.86	0.90	0.86	1.15	0.98	0.90	0.92	10.4%
	0.20	0.87	0.86	0.88	0.91	0.86	1.15	0.97	0.89	0.92	9.8%
	0.25	0.90	0.88	0.90	0.92	0.86	1.15	0.97	0.88	0.93	9.3%
	0.30	0.92	0.89	0.91	0.93	0.86	1.14	0.97	0.87	0.94	9.0%
	0.35	0.95	0.91	0.93	0.94	0.86	1.14	0.96	0.86	0.94	8.8%
	0.40	0.97	0.93	0.95	0.96	0.85	1.13	0.96	0.85	0.95	8.8%
	0.45	1.00	0.94	0.96	0.97	0.85	1.13	0.96	0.84	0.96	8.9%
	0.50	1.02	0.96	0.98	0.98	0.85	1.13	0.96	0.84	0.96	9.2%

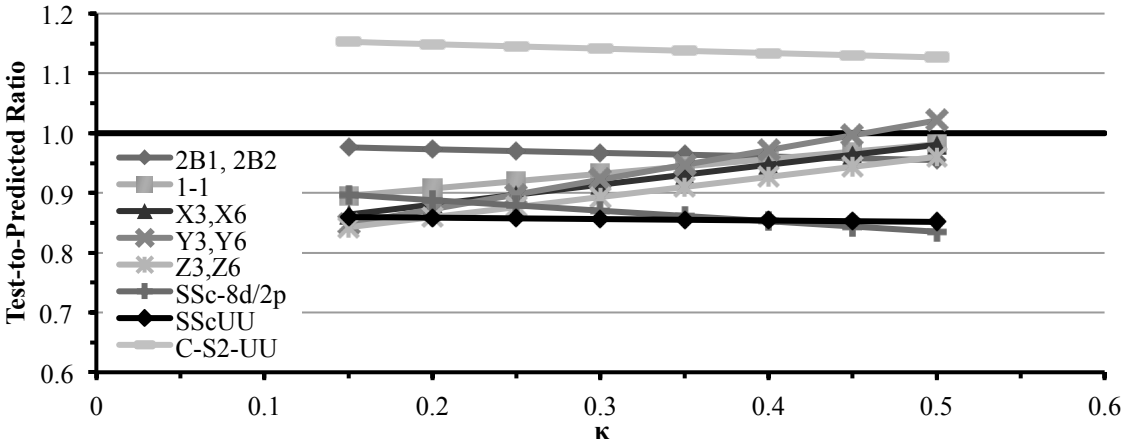

Figure 4-7: Sensitivity of Test-to-Predicted Ratios to κ

4.3.2 Study by Washa & Fluck (1956)

The study performed by Washa and Fluck (1956) investigated creep of reinforced concrete continuous beams by loading of two-span beams that were continuous over the interior support for 2½ years. Their primary focus was on the effect of compressive reinforcement on creep deflections. For the current investigation, only the recorded immediate deflections and the beam cross-sections that did not include compressive reinforcing steel in the positive moment region are relevant. Specimens X3,X6, Y3,Y6, and Z3,Z6 contained from 2.48% to 3.54% compressive reinforcing steel, ρ', in the negative moment region over the interior support, so the cracked moment of inertia was computed for the transformed section. The tensile reinforcing steel ratio ranged from 2.83% to 3.20% in the negative moment region, ρ^-, and from 1.59% to 1.65% in the positive moment region, ρ^+. The computed section properties, including I_{cr}^+, and I_{cr}^-, for the regions resisting positive and negative moments, respectively, are shown in Table 4-16.

Table 4-16: Two-Span Continuous Beam Section Properties – Washa & Fluck (1956)

Specimen	ρ^- (ρ')	ρ^+	I_{cr}^- (mm^4)	I_{cr}^+ (mm^4)
X3,X6	2.84% (2.48%)	1.65%	73.9×10^6	48.7×10^6
Y3,Y6	3.20% (3.20%)	1.64%	44.8×10^6	25.8×10^6
Z3,Z6	2.83% (3.54%)	1.59%	7.64×10^6	4.85×10^6

The specimens had very large reinforcement ratios, large span-to-depth ratios and were heavily loaded. They were therefore cracked over most of the member length, as shown in Figure 4-8(a). The cracking moments computed using the reduced moduli for use in the Branson and Bischoff Equations are shown on the left and right sides of Figure 4-8(a), respectively. The length of the cracked region and the ratio of M_{cr}/M_a are relatively insensitive to use of the full or reduced moduli of rupture to compute M_{cr}. The data shown are for Specimen X3,X6 but the other specimens are similar. The effective moment of inertia computed using the Branson and Bischoff Equations are shown on the left and right sides of Figure 4-8(b), respectively. The effective moment of inertia is insensitive to the moment of inertia equation or assumed modulus of rupture: I_e approaches I_{cr} for the majority of the member length.

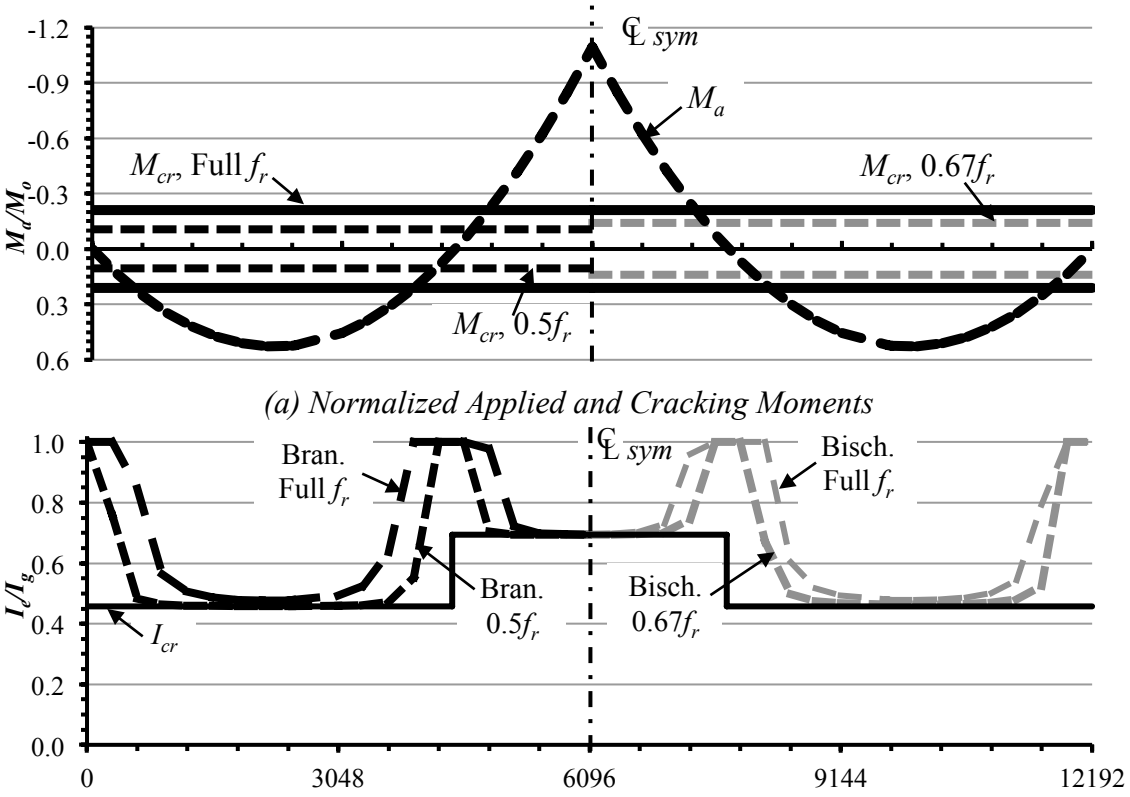

(a) Normalized Applied and Cracking Moments

(b) Normalized Effective and Cracked Moments of Inertia

Figure 4-8: Two-Span Beam X3,X6 – Washa & Fluck (1956)

Table 4-17 shows the test-to-predicted ratios for the various deflection calculation procedures. All methods are conservative and, because the extent of cracking is so large, accurately predicting M_{cr} is not necessary. In the single-element idealization, the average effective moment of inertia, $I_{e(avg)}$, is computed using Eq. [4.1] with κ equal to 0.15. Because I_{cr}^{+} is markedly less than I_{cr}^{-}, as shown in Table 4-16, and the member is severely cracked at midspan and over the interior support, $I_{e(avg)}$ approaches I_{cr}^{+} irrespective of the effective moment of inertia equation used or the modulus of rupture assumed. Thus, there is little difference in computed deflections when any of the single-element idealizations are adopted. Using the full modulus of rupture to compute the cracking moment gives conservative results despite the presence of tensile stresses due to

restraint of shrinkage because the ratio of M_{cr}/M_a is very low for the most of the positive region, thus the member is severely cracked and I_e approaches I_{cr}^+.

Table 4-17: Results of Washa & Fluck Two-Span Beams (1956)

Specimen	ρ^+ (%)	Test Δ_{MID} (mm)	Test-to-Predicted From Different Methods							
			$0.5f_r$		$0.67f_r$		Full f_r			
			Branson		Bischoff		Branson		Bischoff	
			m=3	m=4	m=2	m=3	m=3	m=4	m=2	m=3
X3,X6	1.65%	15.7	0.82	0.89	0.84	0.91	0.86	0.95	0.88	0.95
Y3,Y6	1.64%	25.4	0.81	0.92	0.83	0.93	0.85	0.96	0.86	0.96
Z3,Z6	1.59%	30.5	0.78	0.86	0.81	0.88	0.84	0.93	0.85	0.93
	Mean		0.80	0.89	0.83	0.90	0.85	0.95	0.86	0.95
	Std. Dev.		0.02	0.03	0.02	0.03	0.01	0.01	0.01	0.02
	CoV.		2.5%	3.1%	2.1%	2.8%	1.3%	1.3%	1.5%	1.7%

As the sensitivity analysis involving κ has shown, typically deflections computed using the single-element idealization are greater than those computed using the discretized-element idealization. Figure 4-9 shows the discretized two-span member, where dx_1 and dx_2 are variable-length elements that are selected to satisfy boundary conditions and locate the point of zero rotation, as described previously in Chapter 3. Figure 4-9 also shows the normalized cracked moment of inertia and normalized effective moments of inertia calculated for: the discretized-element idealization, $I_{e,d}$, on the ride side; the single-element idealization at midspan, I_e^+ and at the interior support, I_e^-, on the left side; and, the overall single-element average with κ equal to 0.15 or 0.50, $I_{e(avg)}$. The member is cracked at midspan and the interior support, so I_e^+ and I_e^- approach I_{cr}^+ and I_{cr}^-, respectively. When κ is equal to 0.15, $I_{e(avg)}$ is more influenced by I_e^+ and approaches I_{cr}^+, giving conservative results. When κ is equal to 0.50, $I_{e(avg)}$ is slightly closer to I_{cr}^- than I_{cr}^+ and gives smaller deflections.

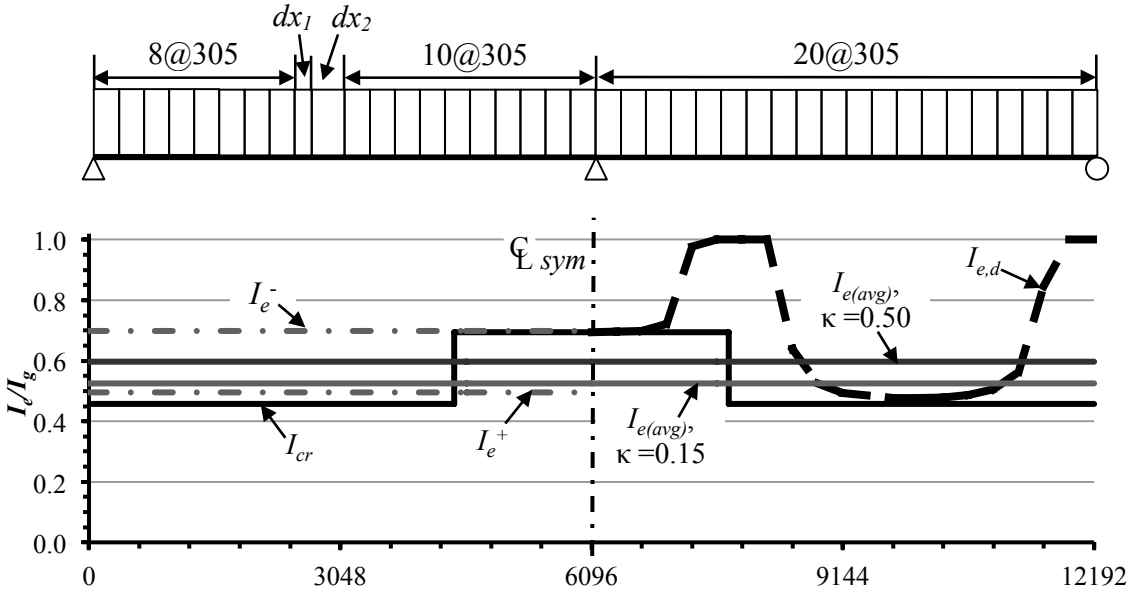

Figure 4-9: Normalized Effective and Cracked Moments of Inertia - Beam X3,X6 (Washa & Fluck 1956)

The conservatism of the single-element idealization results may also be attributed to post-cracking moment redistribution that it neglects. The greater cracked stiffness at the interior support increases the negative moment by 17% and reduces the midspan positive moment by 8.5% according to results obtained using the discretized-element idealization. The deflection computed for the discretized-element idealization is therefore less. When the I_e equations used with the single-element idealization are applied using the post-cracking redistributed moments, smaller deflections, that underestimate the observed deflection for κ equal to 0.15 or 0.50 by up to 12% or 24%, respectively, are obtained.

4.3.3 Study by Branson (1965) – Two-Span

Branson's study (1965) also included two continuous beams, LB-1 and LB-3, that were reinforced with one (ρ = 0.7%) and three (ρ = 2.1%) #3 bars, respectively, both at mid-span and over the interior support. Each span was 9ft (2.74m), so the total beam length

was 18ft (5.49m) and the cross section was 4×5in. (102×127mm). Uniform loading was applied using the same procedure as for the simply supported beams. The SDL-to-DL ratios were 2.0 and 5.5 for the beams reinforced with the one bar and three bars, respectively.

The normalized applied and cracking moments for Beams LB-1 and LB-3 are shown on the left and right sides of Figure 4-10(a), respectively. For the lightly loaded Beam LB-1, computing the cracking moment using the full modulus of rupture causes $M_{cr}/M_a > 1$ for the entire member length so the beam is uncracked. Alternatively, if M_{cr} is computed using the reduced moduli of rupture, the cracking moment is exceeded only at the location of the maximum positive moment near midspan or at the location of the maximum negative moment at the interior support. For the heavily loaded beam, LB-3, the length of cracking in the positive moment region varies greatly depending on the modulus of rupture assumed.

The left and right sides of Figure 4-10(b) show the normalized effective and cracked moments of inertia for Beams LB-1 and LB-3, respectively. For Beam LB-1, I_e equals I_g for most of the member length irrespective of the modulus of rupture used to compute M_{cr}. When M_{cr} is computed using the reduced moduli of rupture, I_e is less than I_g only at the locations of the minimum ratio of M_{cr}/M_a. For Beam LB-3, when the full f_r is used to compute the cracking moment I_e equals I_g for the most of the positive moment region. When the reduced moduli of rupture are used to compute M_{cr}, I_e approaches I_{cr} and the

length of the cracked region increases from 23% of the span length when using the full f_r, to 46% and 55% of the span length when using $0.67f_r$ and $0.5f_r$, respectively.

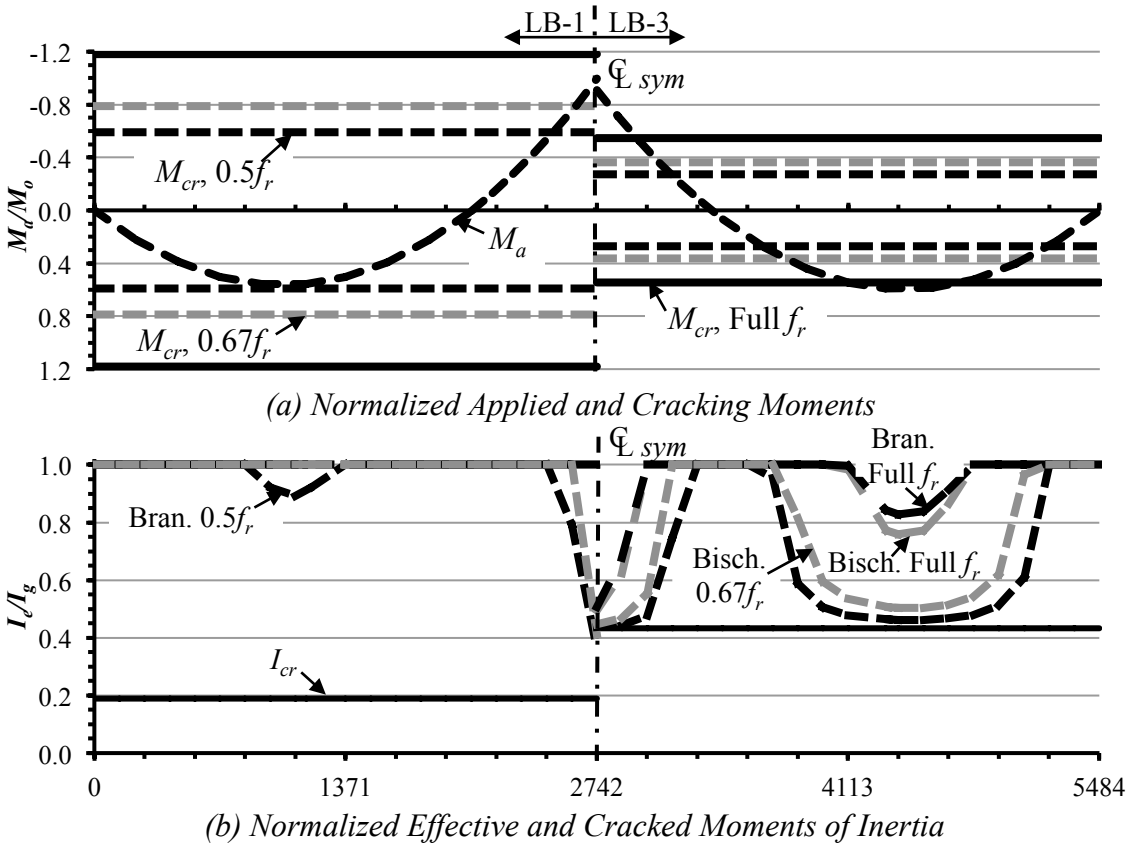

Figure 4-10: Two-Span Beams LB-1 (left side) & LB-3 (right side) – Branson (1965)

Table 4-18 shows the test-to-predicted ratios for the various deflection calculation procedures. There is little variability in the results for Beam LB-1 and, as for the Branson simple-span beams, the deflections computed using the reduced moduli of rupture are slightly conservative, and those computed using the full modulus of rupture are slightly unconservative. If the cracking moments are computed using the full modulus of rupture I_e equals I_g for both the single- and discretized-element idealizations so any difference in results between either idealization or either effective moment of inertia equation is

insignificant. The most conservative deflection is computed using the Branson Equation in a discretized-element idealization because, when $0.5f_r$ is assumed, $M_{cr}/M_a < 1$ near midspan implying the member is cracked in this region.

The variability in deflection results in Table 4-18 for Beam LB-3 again highlights the importance of accurately predicting the cracking moment, and so the length of the cracked region. When the full f_r is assumed the ratio of $M_{cr}/M_a \approx 1$ near midspan, and $I_{e(avg)}$ for the single-element idealization approaches I_g when using either the Branson or Bischoff Equations. Thus, the associated computed deflections are unconservative. When the reduced moduli are used to compute M_{cr} in the single-element idealization, M_{cr}/M_a is small near midspan and very small at the interior support. Because the cracked moments of inertia are the same in the positive and negative moment regions, $I_{e(avg)}$ approaches I_{cr} when using either the Branson or Bischoff Equation. Thus, the deflections computed using the single-element idealization with the reduced moduli are conservative for and, because M_{cr}/M_a is smaller when $0.5f_r$ is assumed, the Branson Equation is the most conservative. The differences in the deflections computed using the discretized-element idealization with the full or reduced f_r are due to the associated changes of cracked length as shown in Figure 4-10(b).

Table 4-18: Results of Branson's Two-Span Beams (1965)

Specimen	ρ^+ (%)	Test Δ_{MID} (mm)	Test-to-Predicted From Different Methods							
			$0.5f_r$		$0.67f_r$		Full f_r			
			Branson		Bischoff		Branson		Bischoff	
			m=3	m=4	m=2	m=3	m=3	m=4	m=2	m=3
LB-1	0.69%	0.5	0.94	0.87	0.95	0.94	1.04	1.05	1.04	1.05
LB-3	2.07%	1.4	0.63	0.63	0.71	0.70	1.15	1.08	1.12	1.04
	Mean		0.79	0.75	0.83	0.82	1.10	1.07	1.08	1.05
	Std. Dev.		0.22	0.17	0.17	0.16	0.07	0.02	0.06	0.01
	CoV.		28.2%	21.8%	20.1%	19.2%	6.5%	1.4%	5.1%	1.5%

4.3.4 Studies by El-Mogy (2011), Habeeb & Ashour (2008) and Mahroug et al. (2014a, 2014b)

El-Mogy (2011), Habeeb and Ashour (2008) and Mahroug et al. (2014a, 2014b) all investigated concrete slabs reinforced with Fibre-Reinforced Polymer (FRP) bars. In each study, one steel-reinforced control specimen continuous over two spans was tested. These results are relevant to the present investigation. The specifics of the studies and the specimens considered are summarized in Table 4-19. All specimens were wet cured, were loaded by point loads at midspan, and had reinforcement ratios ranging from 0.50% to 1.48%.

Table 4-19: Summary of FRP Studies

Study	Curing	Cross-Section (mm)	*L/h*	28 day f'_c (MPa)	Loading	Specimen	ρ^+	ρ^-
El-Mogy (2011)	Beams were cast and covered with a plastic sheet. The curing process started the next day and the concrete surface was kept wet for 7d. After 28d, all beams were prepared for testing.	200×300	9	28	Point Loads at Midspan	SSc-8d/2p	1.48%	1.11%
Habeeb & Ashour (2008)	All test specimens were demoulded after 24h, wet cured, and covered with polyethylene sheets until the date of testing.	200×300	9	26	Point Loads at Midspan	SScUU	0.84%	0.84%
Mahroug et al. (2014a, 2014b)	All specimens were covered with polyethylene sheets to reduced moisture loss during curing and stored in the lab under the same condition until testing.	150×500	13	43	Point Loads at Midspan	C-S-UU	0.50%	0.50%
						C-S2-UU	0.75%	0.75%

Table 4-20 summarizes the deflection test-to-predicted ratios for the various deflection calculation procedures for these steel-reinforced control specimens. As observed from the simply supported studies, the Branson Equation with the cracking moment computed

using the full modulus of rupture is unconservative for Beams C-S-UU and C-S2-UU, which have lower reinforcement ratios, and in particular the test-to-predicted ratios for specimen C-S-UU are markedly worse. This is attributed to the lack of conservatism of the Branson Equation at low reinforcement ratios (Scanlon & Bischoff 2008), and the underestimation of the length of the cracked region when the full modulus of rupture is assumed. When $0.5f_r$ is assumed the cracked length increases from 34% to 53% of the span length, markedly increasing the computed deflection. Like the results of Washa and Fluck (1956), deflections computed using the single-element idealization are more conservative than those computed using the discretized-element idealization. For these specimens, I_{cr}^{+}/I_{cr}^{-} ranges from 1.03 to 1.07 and the members are severely cracked at midspan and over the interior support, so $I_{e(avg)}$ approaches I_{cr}^{+} irrespective of the effective moment of inertia equation used or the assumed modulus of rupture.

Table 4-20: Results of Two-Span Steel Control Specimens

Specimen	ρ^{+} (%)	Test Δ_{MID} (mm)	Test-to-Predicted From Different Methods							
			$0.5f_r$		$0.67f_r$		Full f_r			
			Branson		Bischoff		Branson		Bischoff	
			m=3	m=4	m=2	m=3	m=3	m=4	m=2	m=3
SSc-8d/2p	1.48%	1.9	0.87	0.89	0.89	0.90	0.90	0.94	0.92	0.94
SScUU	0.84%	2.5	0.82	0.87	0.84	0.88	0.86	0.95	0.87	0.94
C-S-UU	0.50%	4.9	0.94	1.05	0.96	1.07	1.57	1.94	1.14	1.42
C-S2-UU	0.75%	4.0	1.02	1.08	1.05	1.10	1.15	1.29	1.11	1.21
	Mean		0.91	0.97	0.93	0.99	1.12	1.28	1.01	1.13
	Std. Dev.		0.09	0.11	0.09	0.11	0.33	0.47	0.14	0.23
	CoV.		9.5%	11.2%	9.7%	11.4%	29.2%	36.5%	13.5%	20.4%

Unlike the beams tested by Washa & Fluck, $I_e^{+}/I_e^{-} \approx 1$ and the cracked stiffnesses are similar, therefore, moment redistribution attributed to cracking is slight. Figure 4-11 shows the incremental deflection of the positive moment region of Beam SScUU tested by Habeeb and Ashour (2008) computed using the full modulus of rupture and the

Branson Equation to compute: the unique effective moment of inertia for each element of a discretized-element idealization, $I_{e,d}$, and the average effective moment of inertia for the single-element idealization, $I_{e,(avg)}$. The single-element idealization typically yields larger deflection increments and so a larger cumulative midspan deflection.

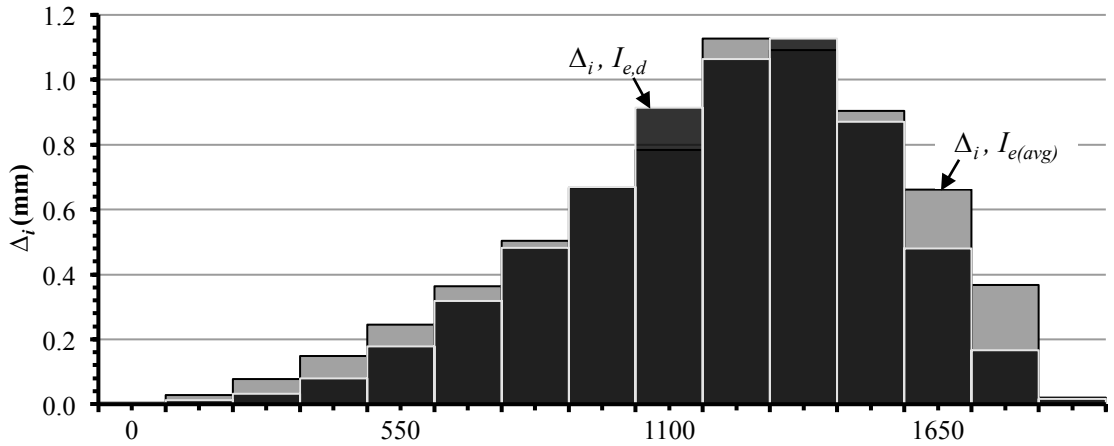

Figure 4-11: Incremental Deflection of Left Span of Beam SScUU – Habeeb & Ashour (2008)

4.3.5 Study by Guralnick & Winter (1957, 1958) – T-Beam Member

Guralnick and Winter (1957, 1958) performed a two-part study of high-strength, deformed steel bars for concrete reinforcement. Part I of the study included testing to destruction twenty-four simply supported T-beams cantilevered at one support to generate a negative bending moment over the support. In Part II, ten additional T-beams were tested to destruction. The specimens considered in the present investigation include the four T-beams that were loaded with a uniformly distributed load from each Part: Beams IIIA-1, IIIB-1, IIIC-1, IIID-1 from Part I (1957) and Beams IIIA-1m, IIIB-1m, IIIC-1m, IIID-1m from Part II (1958).

Table 4-21 shows the section properties of the members investigated. All specimens had identical overall dimensions with an overall length of 6.1m, consisting of a cantilever at one end of 1.7m and a simple span between supports of 4.1m. For the applied loading adopted, this geometry produces a negative bending moment over the support equal to the midspan moment, allowing the tensile reinforcement ratio to be the same in the positive and negative moment regions. Two design concrete compressive strengths were used, 21MPa and 34MPa, and all longitudinal reinforcement was an alloy steel having a nominal yield strength of 552MPa. The specimens from Part II, with the suffix "m" meaning "modified", were practically identical to those from the original study; however, the negative reinforcement was rearranged and distributed across the flange of the T-section and Beams IIIA-1m, and IIIC-1m had no stirrups. The ultimate flexural resisting moment, M_{f6}, was calculated assuming a steel yield stress of 60,000psi (414MPa) and a maximum concrete stress of $0.85f'_c$ in accordance with the ultimate strength criteria presented in the Appendix to ACI 318-56 (ACI 1956). The deflections were measured at service moments, M_s, computed as M_{f6}/1.8. The specimens were cured by stretching a waterproof paper membrane over the top of each form two hours after concrete placement, thus sealing all surfaces of the beam. The forms were removed three days later and the beams were placed in a constant-humidity moist room for 18 days. The specimens were stored approximately seven days in the open laboratory and tested at an age of approximately 28 days.

Table 4-21: T-Beam Section Properties – Guralnick & Winter (1957, 1958)

Specimen	ρ	I_{cr}^- (mm^4)	I_{cr}^+ (mm^4)	M_s (kN.m)	f'_c (MPa)	E_c (MPa)
IIIA-1	0.77%	643×10^6	838×10^6	83.4	21.6	16700
IIIB-1	0.44%	494×10^6	550×10^6	50.4	21.6	16700
IIIC-1	1.35%	570×10^6	706×10^6	147.6	36.5	36500
IIID-1	0.77%	391×10^6	458×10^6	86.9	36.5	36500
IIIA-1m	0.72%	606×10^6	834×10^6	94.3	27.7	20100
IIIB-1m	0.42%	519×10^6	579×10^6	55.7	22.3	19200
IIIC-1m	1.28%	686×10^6	979×10^6	115.6	33.5	27900
IIID-1m	0.72%	564×10^6	643×10^6	91.9	31.0	28100

Figure 4-12(a) shows the normalized applied and cracking moments for Beam IIIB-1 from Part I (1957): the cantilever is at the right end of the beam. At service moments, the beam is severely cracked for most of the positive moment region and in the negative moment region over the support. This specimen, and IIIB-1m, have the lowest reinforcement ratios and the other beams with higher reinforcement ratios are cracked over an even longer length. Figure 4-12(b) shows the normalized effective and cracked moments of inertia for Beam IIIB-1. Even when the full modulus of rupture is assumed, the applied moment exceeds the cracking moment for 70% of the member between supports, and I_e equals I_{cr} for the majority of the simply supported span.

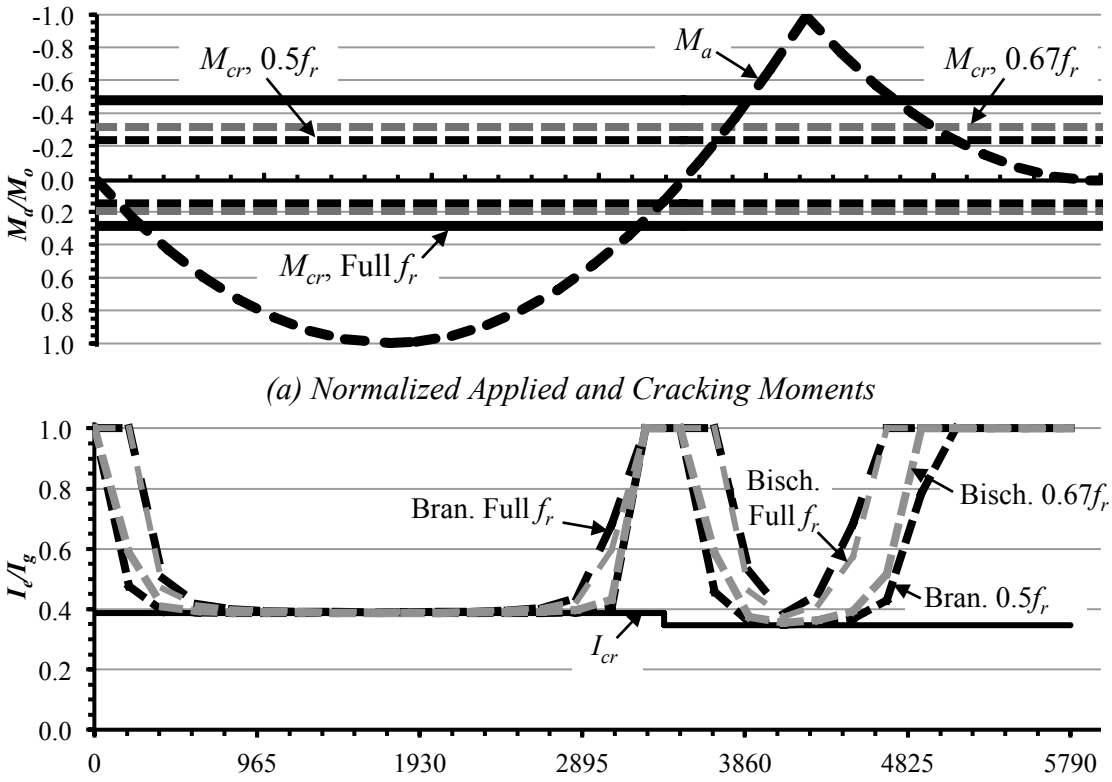

(a) Normalized Applied and Cracking Moments

(b) Normalized Effective and Cracked Moments of Inertia

Figure 4-12: T-Beam IIIB-1 – Guralnick & Winter (1957)

Table 4-22 shows the deflection test-to-predicted ratios computed using the various deflection calculation procedures for the specimens from both Part I and Part II of the investigation. The differences between the deflection calculations from various procedures are slight, because the members are sufficiently cracked that accurate prediction of M_{cr} is relatively unimportant. Thus I_e approaches I_{cr} irrespective of the modulus of rupture, the effective moment of inertia equation or idealization used to compute deflections.

Table 4-22: Results Guralnick & Winter (1957, 1958) – T-Beam Members

Specimen	ρ^+ (%)	Test Δ_{MID} (mm)	Test-to-Predicted From Different Methods							
			$0.5f_r$		$0.67f_r$		Full f_r			
			Branson		Bischoff		Branson		Bischoff	
			m=3	m=4	m=2	m=3	m=3	m=4	m=2	m=3
IIIA-1	0.77%	9.9	1.08	1.09	1.09	1.10	1.08	1.10	1.09	1.10
IIIB-1	0.44%	8.6	1.05	1.04	1.07	1.04	1.10	1.06	1.11	1.06
IIIC-1	1.35%	8.4	0.96	0.96	0.96	0.96	0.96	0.96	0.97	0.97
IIID-1	0.77%	9.4	1.19	1.19	1.21	1.20	1.25	1.21	1.25	1.21
IIIA-1m	0.72%	9.4	1.08	1.11	1.09	1.11	1.09	1.11	1.10	1.11
IIIB-1m	0.42%	6.9	0.91	0.90	0.93	0.91	0.94	0.92	0.96	0.92
IIIC-1m	1.28%	6.1	0.93	0.95	0.93	0.95	0.93	0.95	0.94	0.96
IIID-1m	0.72%	6.9	0.89	0.89	0.90	0.89	0.90	0.89	0.92	0.90
	Mean		1.01	1.02	1.02	1.02	1.03	1.03	1.04	1.03
	Std. Dev.		0.11	0.11	0.11	0.11	0.12	0.11	0.12	0.11
	CoV.		10.5%	10.6%	10.7%	10.6%	11.4%	10.8%	11.2%	10.8%

4.3.6 Overall Findings for Continuous Members

The investigation of two-span continuous members and simply supported T-beams with cantilevers at one support confirms the previous findings from the simply supported members. Accurate quantification of the cracking moment is essential when the applied moments at service are relatively small, such as Beam LB-3 tested by Branson (1965). In these cases the ratio of M_{cr}/M_a may vary greatly along the member length so accurate prediction of M_{cr} is necessary to delineate the cracked and uncracked regions. When the applied moment greatly exceeds the cracking moment, as is typical for members with higher reinforcement ratios, I_e approaches I_{cr} over most of the member length. In this case, demonstrated particularly by the T-beams tested by Guralnick and Winter (1957, 1958), the computed deflections are insensitive to the value of f_r assumed to compute M_{cr}.

Deflections computed using the single-element idealization are, typically, greater and so more conservative than those computed using the discretized-element idealization.

Factors such as the weighting coefficient, κ, the ratio of I_e^+/I_e^-, and moment redistribution attributed to cracking influence $I_{e(avg)}$ and so the conservatism of results obtained using the single-element idealization.

Figure 4-13(a) shows the variation of the test-to-predicted ratios for the various deflection calculation procedures using the reduced moduli of rupture with the positive moment reinforcement ratio. Using the reduced f_r gives conservative results for all reinforcement ratios, and this conservatism increases as ρ increases, because these members, typically, have larger applied moments, and I_e approaches I_{cr} over most of the member length. Typically the ratios corresponding to a particular test are superimposed on each other indicating the results from the various deflection calculation procedures using the recommended reduced moduli of rupture are consistent.

Figure 4-13(b) shows the test-to-predicted ratios for the various deflection calculation procedures when using the full modulus of rupture to compute the cracking moment. Using the full f_r to compute M_{cr} is more likely to give unconservative results, particularly when using the Branson Equation if the reinforcement ratio is less than 1%. This finding is consistent with that for simply supported members. There is also more variability of the test-to-predicted ratios when the reinforcement ratio is less than 1%. The greatest variability is for specimen C-S-UU tested by Mahroug (2014a) as previously discussed. For reinforcement ratios greater than 1%, the test-to-predicted ratios approach 1, because the member is more severely cracked and I_e approaches I_{cr} irrespective the effective moment of inertia equation or idealization used.

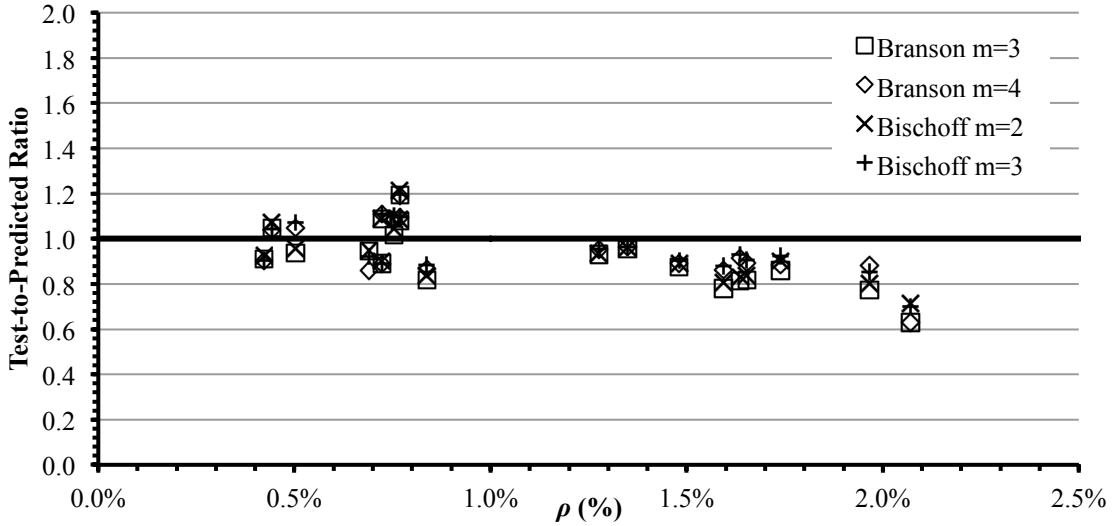

(a) Reduced Modulus of Rupture

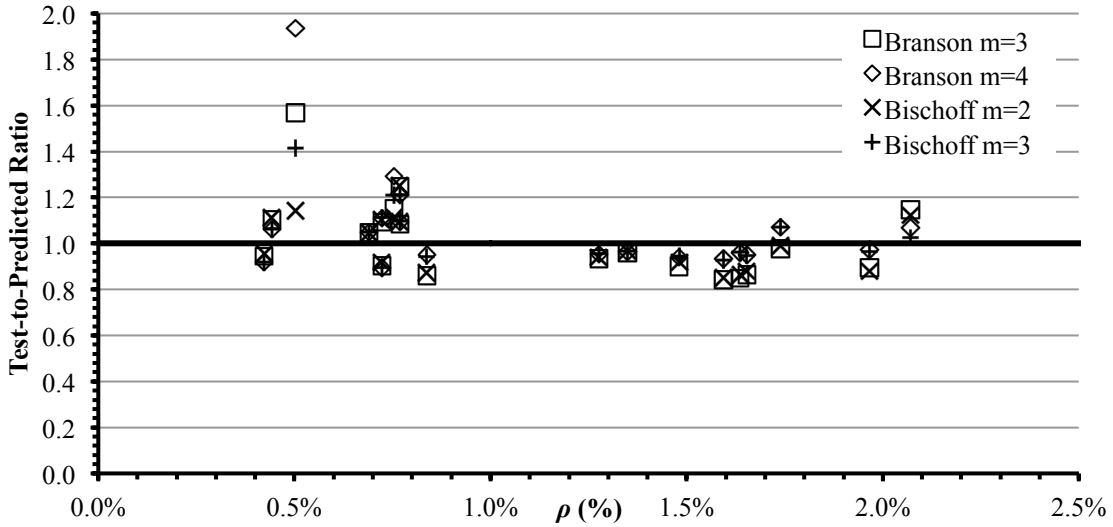

(b) Full Modulus of Rupture

Figure 4-13: Test-to-Predicted Ratio for Various Reinforcement Ratios – Continuous Members

Table 4-23 shows the mean, standard deviation and coefficient of variation for all continuous beam specimens investigated. When the cracking moment is computed using the reduced moduli in a single- or discretized-element idealization with either the Branson or Bischoff Equations, the mean values are conservative and consistent, with coefficients of variation less than 15%. When the cracking moment is computed using the

full modulus of rupture, either the Branson or Bischoff Equations in the single-element or discretized-element idealizations closely approximate the observed deflections. The Branson Equation, as expected, gives unconservative results, but the unconservativism is slight for the single-element idealization, as indicated by a mean value slightly greater than one. The Bischoff Equation in either a single-element or discretized-element idealization gives an excellent agreement to the observed deflections and the coefficients of variation are lower than those for the Branson Equation and are comparable to those when the cracking moment is computed using the reduced modulus of rupture.

Table 4-23: Overall Findings For Continuous Members

	Test-to-Predicted From Different Methods							
	$0.5f_r$		$0.67f_r$		Full f_r			
	Branson		Bischoff		Branson		Bischoff	
	m=3	m=4	m=2	m=3	m=3	m=4	m=2	m=3
Mean	0.91	0.94	0.93	0.96	1.02	1.07	1.00	1.04
Std. Dev.	0.13	0.13	0.12	0.12	0.18	0.23	0.12	0.13
CoV.	14.6%	13.4%	13.2%	12.2%	17.6%	21.9%	11.9%	12.6%

Table 4-24 shows the overall mean, standard deviation and coefficient of variation for all simply supported beams and continuous beams investigated. When the results are combined, the findings are consistent with the previous findings and the results are bounded between those of the simply supported and continuous members. Using the reduced modulus of rupture to compute the cracking moment yields consistent and conservative results for either idealization or effective moment of inertia equation assumed. The Branson Equation in either idealization with the full f_r to compute M_{cr}, as expected, gives unconservative results with high coefficients of variation. The Bischoff Equation in either idealization gives a close, but slightly unconservative, agreement to the observed deflections and the coefficients of variation are lower than those for the

Branson Equation and are comparable to those when the cracking moment is computed using the reduced modulus of rupture.

Table 4-24: Overall Findings for All Members

	Test-to-Predicted From Different Methods							
	$0.5f_r$		$0.67f_r$		Full f_r			
	Branson		Bischoff		Branson		Bischoff	
	m=3	m=4	m=2	m=3	m=3	m=4	m=2	m=3
Mean	0.82	0.82	0.84	0.84	1.16	1.19	1.04	1.07
Std. Dev.	0.18	0.19	0.18	0.18	0.38	0.43	0.26	0.30
CoV.	22.0%	22.8%	21.1%	21.2%	33.2%	35.8%	24.9%	28.2%

4.4 STATISTICAL ANALYSIS OF TEST-TO-PREDICTED RATIOS FOR ALTERNATIVE DEFLECTION CALCULATION PROCEDURES

ACI 435 (1995) states that "the magnitude of actual deflections in concrete structural elements…can only be estimated within a range of 20-40 percent accuracy." To explore the findings of the present investigation in the context of this statement, the probability that the test-to-predicted ratio falls within this range was computed, assuming these ratios are normally distributed. Checks were also performed to confirm the normality of the test-to-predicted ratios. For example, Figure 4-14 shows the variation of Z, the unit value of the standard normal distribution, with test-to-predicted ratios for deflections computed for the 46 simply supported members using the Bischoff Equation for the single-element idealization (m=2) assuming the cracking moment is computed using the reduced modulus of rupture. For virtually the full range of test-to-predicted values, the variation is linear and so can be described accurately using a normal distribution.

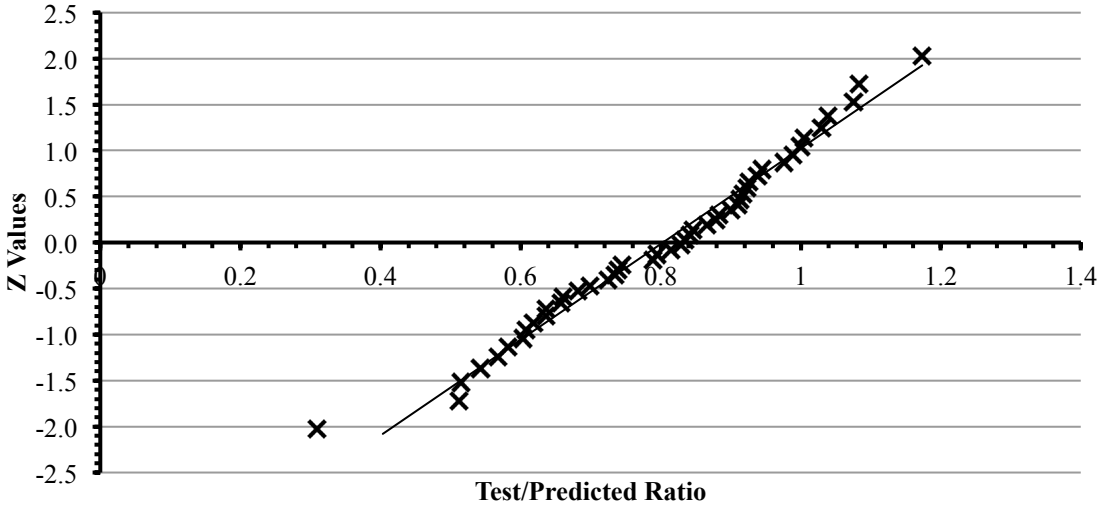

Figure 4-14: Z values for the Bischoff Equation, m=2, 0.67f_r

Figure 4-15 shows the test-to-predicted ratios for deflections computed for the 46 simply supported members using the Bischoff Equation for the single-element idealization (m=2) assuming the cracking moment is computed using the reduced modulus of rupture. The mean value is 0.80 with a standard deviation of 0.18, as shown in Table 4-12. These values have been rounded to two significant figures from more precise results obtained in a MS Excel spreadsheet. The shaded region corresponds to test-to-predicted ratios varying between 0.6 and 1.4, i.e. within 40% of the nominal value of 1. The shaded area, $A_{40\%}$, is the probability that a test-to-predicted ratio falls within this range. The lower limit of 0.6 is 1.10 sample standard deviations, s, below the mean, so the probability of a test-to-predicted ratio falling below this limit, P_L, is 13.51%. Similarly the upper limit of 1.4 is 3.26 standard deviations above the mean, so that probability of a test-to-predicted ratio exceeding this limit, P_U, is 0.06%. Thus the probability of a test-to-predicted ratio falling between these limits is (1 – 0.1351 – 0.0006 =) 0.8643.

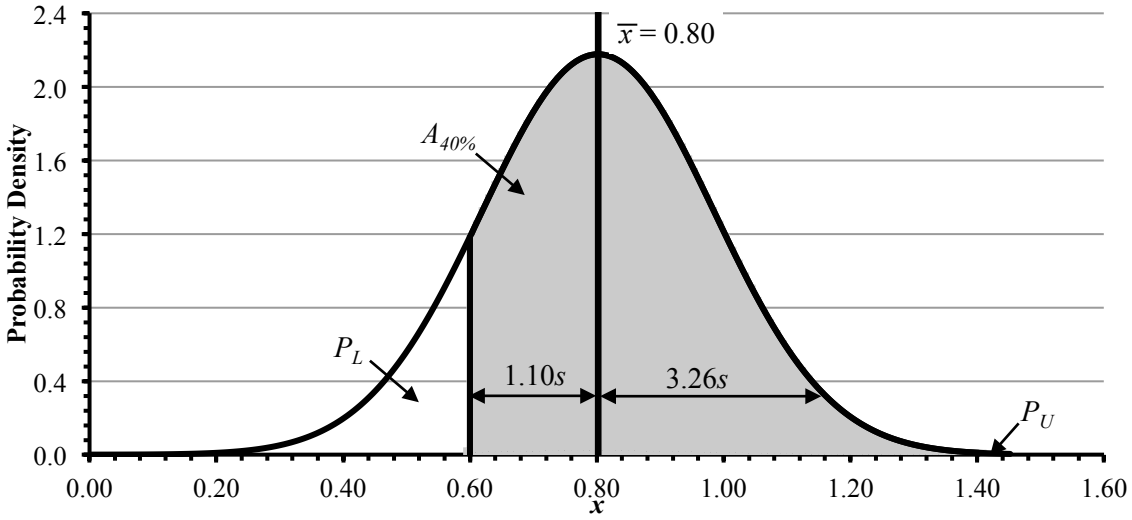

Figure 4-15: Normal Distribution for the Bischoff Equation, m =2, 0.67f_r

Table 4-25 shows the results of similar calculations for the various alternative deflection calculation procedures for simply supported members. The greatest probability that the test-to-predicted ratio will be between 0.6 and 1.4 is 86%, corresponding to deflections calculated with the Bischoff Equation for either the single- or discretized-element idealization with M_{cr} computed using the reduced modulus of rupture. In either case, the mean value of 0.80 also ensures that the computed deflection is conservative: there is a 13.5% chance that the actual deflection will be less than 0.6 times the computed value and only a 0.05% chance that it will be greater than 1.4 times the predicted value. In contrast, for deflections computed using the Branson Equation with the full modulus of rupture, there is roughly a one-in-three chance that the actual deflection exceeds 1.4 times the predicted value, the probability that the actual deflection is between 0.6 to 1.4 times the predicted value is only 54.4% to 58.8%. It might be expected that, if the 40% accuracy claim in ACI 435 (1995) was accurate, 95% of the observed deflections would

lie between 0.6 and 1.4 of the predicted value. This is not the case, suggesting that the "20-40 percent accuracy" suggested in ACI 435 (1995) underestimates the true uncertainty for these data.

Table 4-25: Accuracy of Deflection Calculation Procedures – Simply Supported Members

	Normal Distribution – Area ±40% Actual Deflection							
	$0.5f_r$		$0.67f_r$		Full f_r			
	Branson		Bischoff		Branson		Bischoff	
	m=3	m=4	m=2	m=3	m=3	m=4	m=2	m=3
Mean	0.78	0.77	0.80	0.80	1.22	1.24	1.05	1.08
Std. Dev.	0.18	0.18	0.18	0.18	0.43	0.48	0.30	0.35
P_L	16.7%	18.1%	13.5%	13.6%	7.6%	9.1%	6.3%	8.5%
P_U	0.03%	0.03%	0.06%	0.04%	33.6%	36.6%	12.2%	17.6%
$A_{40\%}$	83.3%	81.9%	86.4%	86.3%	58.8%	54.4%	81.5%	73.9%

Table 4-26 shows the results recomputed using the test-to-predicted ratios observed for continuous members. With the exception of deflections computed using the Branson Equation with the full f_r, all alternative deflection calculation procedures have at least a 99% probability that the actual deflections will lie within 40% of the predicted value. Table 4-26 also shows the probabilities that the actual deflection will be within 20% of the predicted value, $A_{20\%}$. In this case, deflections computed using the Bischoff Equation in a single-element idealization with the full f_r to compute M_{cr} is the most accurate approach, with the probability that the actual deflection lies within 20% of the predicted value reaching 90.8%. Again deflections computed assuming the reduced moment of inertia, whether using the Branson or Bischoff Equation, have a moderate chance of being conservative and only a slight chance of being unconservative. For the continuous members, the ACI 435 (1995) statement of "20-40 percent accuracy" is much more realistic.

Table 4-26: Accuracy of Deflection Calculation Procedures – Continuous Members

	Normal Distribution – Area ±40% Actual Deflection							
	$0.5f_r$		$0.67f_r$		Full f_r			
	Branson		Bischoff		Branson		Bischoff	
	m=3	m=4	m=2	m=3	m=3	m=4	m=2	m=3
Mean	0.91	0.94	0.93	0.96	1.02	1.07	1.00	1.04
Std. Dev.	0.13	0.13	0.12	0.12	0.18	0.23	0.12	0.13
P_L	0.92%	0.32%	0.34%	0.10%	0.97%	2.24%	0.04%	0.04%
P_U	0.01%	0.02%	0.01%	0.01%	1.68%	7.95%	0.04%	0.27%
$A_{40\%}$	99.1%	99.7%	99.6%	99.9%	97.4%	89.8%	99.9%	99.7%
P_L	19.7%	12.6%	13.9%	8.53%	11.1%	12.4%	4.56%	3.59%
P_U	1.56%	2.17%	1.59%	1.98%	15.6%	29.0%	4.64%	10.5%
$A_{20\%}$	78.8%	85.3%	84.5%	89.5%	73.3%	58.6%	90.8%	85.9%

Table 4-27 shows the results recomputed using the test-to-predicted ratios observed for all 65 members investigated. When the full database is considered the probability that the actual deflection is between 0.6 to 1.4 times the predicted value is greater than when only considering the simply supported members. The Bischoff Equation for either the single- or discretized-element idealization with M_{cr} computed using the reduced modulus of rupture has the most accurate approach, with the probability that the actual deflection lies within 40% of the predicted value reaching 91%. When M_{cr} is computed using the reduced moduli, there is less than a 12.0% chance that the actual deflection will be less than 0.6 times the computed value and less than a 0.10% chance that it will be greater than 1.4 times the predicted value. These findings suggest that the "20-40 percent accuracy" claim in ACI 435 (1995) is slightly optimistic: it underestimates the true uncertainty.

Table 4-27: Accuracy of Deflection Calculation Procedures – All Members

	Normal Distribution – Area ±40% Actual Deflection							
	$0.5f_r$		$0.67f_r$		Full f_r			
	Branson		Bischoff		Branson		Bischoff	
	m=3	m=4	m=2	m=3	m=3	m=4	m=2	m=3
Mean	0.82	0.82	0.84	0.84	1.16	1.19	1.04	1.07
Std. Dev.	0.18	0.19	0.18	0.18	0.38	0.43	0.26	0.30
P_L	11.4%	12.0%	8.78%	8.62%	7.27%	8.33%	4.47%	6.06%
P_U	0.06%	0.10%	0.08%	0.09%	26.6%	30.9%	8.06%	13.2%
$A_{40\%}$	88.5%	87.9%	91.1%	91.3%	66.1%	60.8%	87.5%	80.7%

4.5 CONCLUSIONS & RECOMMENDATIONS

Deflections of 46 simply supported members, 11 two-span continuous members and 8 simply supported T-beams cantilevered at one support were computed using the Branson and Bischoff Equations for the single- and discretized-element idealizations, and cracking moments computed using the full and reduced moduli of rupture. These calculations were based on the reported material properties, section geometries and other relevant data and compared to the observed deflections to quantify the accuracy of these various deflection calculation procedures. Factors necessary to compute deflections accurately were also identified.

The conclusions from this investigation are as follows:

1. Calculated deflections are particularly sensitive to the assumed cracking moment when the applied moment is low or, for lightly reinforced members, where the ratio of M_{cr}/M_a and associated length of the cracked region may differ markedly based on the modulus of rupture assumed.
2. When the ratio of M_{cr}/M_a is low, typical for beams with higher reinforcement ratios, the extent of cracking may cause I_e to approach I_{cr} over the full beam length. In this

case, the various deflection calculation procedures provide a reasonable estimate of the deflection and the effect of the assumed modulus of rupture on the prediction of M_{cr} is not significant.

3. Using the Branson or Bischoff Equations with the recommended reduced modulus of rupture to compute the cracking moment gives consistent and conservative results.
4. The Branson Equation with the full modulus of rupture to compute the cracking moment is unconservative for lightly reinforced members, particularly for simply supported beams, and has the greatest variability in results.
5. The Bischoff Equation with the cracking moment computed using the full modulus of rupture gives the best, but slightly unconservative, results and the standard deviation is lower than that for the Branson Equation.
6. For a two-span continuous member, the single-element idealization tends to give greater computed deflections than those obtained using the discretized-element idealization:
    a. For realistic members with higher reinforcement ratios in the negative moment region $I_e^+ < I_e^-$ and the average effective moment of inertia, $I_{e(avg)}$, tends to approach I_{cr}^+ so the computed deflections using the single-element idealization are conservative.
    b. For members with $I_e^+/I_e^- <1$, using an average of the effective moments of inertia at midspan and at the interior support, consistent with ACI 318 (2014), gives the best results.

7. For a two-span continuous member, the single-element idealization may not account sufficiently for moment redistribution caused by cracking and so is not preferred when the cracked stiffnesses of the positive and moment regions differ significantly.
8. When considering both simply supported and continuous members, the most accurate alternative deflection calculation procedure is the Bischoff Equation for either the single- or discretized-element idealization with M_{cr} computed using the reduced modulus of rupture, with the probability that the actual deflection lies within 40% of the predicted value reaching 91%. This level of probability is less than expected, suggesting that the "range of 20-40 percent accuracy" cautioned in ACI 435 (1995) is slightly optimistic: it underestimates the true uncertainty.

CHAPTER 5: SUMMARY, CONCLUSIONS & RECOMMENDATIONS FOR FUTURE RESEARCH

5.1 SUMMARY

Excessive deflection of concrete floor slabs is a recurring serviceability problem (Gilbert 2012, Stivaros 2012). Others have investigated contributing factors including: construction methods and associated loading (Kaminetzky & Stivaros 1994), cracking due to restrained shrinkage, creep and flexure (Bischoff 2007, Scanlon & Bischoff 2008), and early-age concrete properties (ACI 435 1995, Khan 1995). Provisions in current building codes, CSA A23.3-14 in Canada (CSA 2014) and ACI 318-14 in the United States (ACI 2014), account for some but not all of these effects. The effect of loading concrete members at very young ages (three days is not uncommon given current construction practices) on the associated deflections remains uncertain. Construction loads may subject young concrete to large bending moments causing flexural cracking. Accurate predictions of the modulus of rupture, the elastic modulus, and the cracked moment of inertia are necessary because computed deflections are sensitive to these properties.

Chapter 2 presented an investigation into the early-age material properties of concrete that impact computed instantaneous deflections. Concrete compression stress-strain data reported by others (Khan 1995, Jin et al. 2005) for concrete ages from 9.7 hours to 28 days were compared to the Todeschini (1964) and Modified Hognestad (1951) stress-strain relationships. Empirical equations presented in CSA A23.3-14 (CSA 2014) for

tensile strength and stiffness parameters were compared to experimentally determined values at young ages. Moment-curvature analyses derived using the reported concrete stress-strain data were compared to analyses based on conventional simplifying approximations and the Todeschini and Modified Hognestad relationships to quantify the accuracy of these methods for young-age concretes. The accuracy of early-age flexural rigidities obtained from moment-curvature analysis for rectangular cross sections with varying reinforcement ratios was also explored.

Chapter 3 presented the Branson and Bischoff Equations for the effective moment of inertia and typical single-element and discretized-element idealizations for deflection calculations. Test cases of flexural members with various end fixities, reinforcement ratios, and live-to-dead load ratios were explored. A mesh sensitivity analysis was performed to determine the largest practical mesh size for design office use. The value of the exponent *m* applied to the cracking-to-applied moment ratio term was verified for the Branson Equation used with a discretized-element idealization. A suitable modification to *m* was determined for the Bischoff Equation used with a discretized-element idealization. The effect of using ASTM A1035/A1035M Grade 100 (690) reinforcing steel, with higher yield strength than typical Grade 60 (400) reinforcing steel, on deflections was investigated. Discrepancies in results between the single- and discretized-element idealization, particularly for lightly reinforced three-span continuous members, were further explored.

Chapter 4 presented an investigation of the accuracy of deflections computed using the Branson or Bischoff Equations, the single- or discretized-element idealizations, and the full or reduced moduli of rupture to compute the cracking moment. Comparisons were made to the observed deflections of 46 simply supported and 19 continuous test beams investigated by others (e.g., Gilbert & Nejadi 2004a, 2004b, Washa & Fluck 1952). Deflections were computed based on the material properties, section geometries and other relevant data reported. The accuracy of these alternative deflection calculation procedures was quantified and factors that impact the accuracy were investigated. The members investigated covered a wide range of reinforcement and span-to-depth ratios, and were subjected to various curing conditions and applied loading. A sensitivity analysis for the weighting coefficient in the equation for the average effective moment of inertia for use in the single-element idealization was performed to determine the optimal value between the bounds set in A23.3-14 (CSA 2014) and ACI 318 (2014). A statistical analysis of test-to-predicted ratios for the alternative deflection calculation procedures to explore the accuracy of these methods in the context of the "20-40 percent accuracy" claim in ACI 435 (1995).

5.2 CONCLUSIONS

The major conclusions of this study are as follows:

1. The stress-strain response of young concrete in compression differs markedly from that of mature concrete (e.g., Khan 1995): young concretes do not exhibit strain softening and so do not have a clear strain corresponding to the maximum stress. The relationships that were derived based on mature concrete, like the

Todeschini and Modified Hognestad relationships, depend heavily on the value of strain corresponding to maximum stress and so are unable to accurately predict the response for concrete ages less than one day.

2. When the concrete age is at least one day, the CSA A23.3 (2014) empirical equations for the elastic modulus and the modulus of rupture accurately quantify values observed by Khan (1995).
3. Conventional simplifying approximations adopted for flexural analysis do not apply to concrete that is less than one day old. Using an elastic-cracked analysis to compute the yield moment may be inaccurate because the assumption of a linear-elastic response in compression is wrong. For the associated low compressive strength of concretes that are less than one day old, it is prudent for the practitioner to check the maximum *c/d* limit in A23.3 (CSA 2014) is satisfied.
4. Use of the Todeschini and Modified Hognestad relationships overestimates the initial rigidity in the ascending portion of the moment-curvature response at very young ages. When the concrete age exceeds 14.5 hours, this difference becomes negligible. The moment-curvature response is best predicted by the Modified Hognestad relationship because it predicts less strain softening than the Todeschini relationship.
5. Calculated deflections are particularly sensitive to the assumed cracking moment when the applied moment is low or, for lightly reinforced members, where the ratio of the cracking-to-applied moment and associated length of the cracked region is sensitive to the modulus of rupture assumed. When the applied moment

exceeds the cracking moment for most of the member length, typical for beams with higher reinforcement ratios, the effective moment of inertia approaches the cracked moment of inertia, irrespective of the modulus of rupture assumed, and the various deflection calculation procedures provide a reasonable estimate of the deflection. When using the recommended reduced moduli of rupture, the computed results are consistent and conservative. Using the full modulus of rupture with the Branson Equation gives the least conservative and least accurate results.

6. For continuous members, the single-element idealization tends to give greater computed deflections than those computed using the discretized-element idealization. When the effective moment of inertia at midspan is much less than that at the interior support, typical for members with higher reinforcement ratios in the negative moment regions, the average effective moment of inertia computed using Equation 9.4 from A23.3 (CSA 2014) approaches the cracked moment of inertia of the cross section in the positive moment region at midspan, and so is conservative.
7. When considering both simply supported and continuous members, the most accurate alternative deflection calculation procedure is the Bischoff Equation for either the single- or discretized-element idealization with M_{cr} computed using the reduced modulus of rupture, $0.67f_r$. The probability that the actual deflection lies within 40% of the predicted value in this case is 91%. This probability suggests

that the "range of 20-40 percent accuracy" cautioned in ACI 435 (1995) is slightly optimistic: it may underestimate the true uncertainty.

5.3 RECOMMENDATIONS FOR FUTURE RESEARCH

Recommendations for future work are as follows:

1. The current research has only focused on instantaneous flexural deflections. There still remains a knowledge gap concerning the effect of early-age loading on time-dependent deflections caused by creep and shrinkage. Current provisions in CSA A23.3-14 (2014) and ACI 318 (2014) apply a long-term multiplier to the instantaneous deflection to predict the time-dependent deflection. This method may not accurately account for the construction load history and the duration of loading, which also may be uncertain at the time of design. There is therefore a need to quantify the accuracy of the current approaches for predicting long-term deflections. It is envisaged that this will follow a similar procedure to that used in the current research to investigate short-term deflections and making comparisons to observed deflections reported by others.
2. Two-way slab deflections are typically computed using an equivalent frame method (CAC 2016) or in a discretized analysis using proprietary FEA software (i.e., SAFE 2014). The procedures and equation derived for one-way members can be applied to two-way members by idealizing them as column strips and middle strips. The findings of the current investigation regarding the Bischoff Equation for the effective moment of inertia can, therefore, be verified for the computation of two-way slab deflections. For non-uniform loading and irregular

geometries and layouts, FEA software may be preferred to simplified method. It is essential to confirm that the software appropriately accounts for the effect of cracking, accurately identifying the regions where the applied moment exceeds cracking moment, and computing the effective moment of inertia using the suitable value of *m* for a discretized-element idealization, and correctly redistributes the total static moment to account for the effect of cracking (CAC 2016). The findings of the current investigation should be verified for use in the computation of two-way slab deflections in FEA analysis software. Observed deflections of two-way slabs in the field can be used to quantify the accuracy of the simplified equivalent frame method and computer-based procedures.

3. The existing database of experimental results for deflections of reinforced concrete members lacks data from recent experimental programs. There is a need for current data on both instantaneous and time-dependent deflections, for members that are: lightly reinforced, using either Grade 60 (400) or ASTM A1035/A1035M Grade 100 (690) reinforcing steel; continuous spans, including three-span members; and, subjected to varying applied loading, such as uniform loading, concentrated point loads and pattern loading on continuous members.
4. The designer is faced with many uncertainties when trying to accurately predict deflections, such as concrete material properties and construction loading and load history. To account accurately for all of these effects, structural monitoring of a reinforced concrete slab starting from the time of construction should be performed. The ideal structure would be a parking garage with symmetric layout

as it is the simplest case more easily analyzed using the simplified methods in current code provisions.

REFERENCES

ACI Committee 318. 2014. *Building code requirements for structural concrete (ACI 318-14) and Commentary*, American Concrete Institute, Farmington Hills, MI, USA.

ACI Committee 318. 1956. *Building code requirements for structural concrete (ACI 318-56)*, American Concrete Institute, Detroit, MI, USA.

ACI Committee 318. 1947. *Building code requirements for structural concrete (ACI 318-47)*, American Concrete Institute, Detroit, MI, USA.

ACI Committee 347. 2005. *Guide for Shoring/Reshoring Concrete Multistory Buildings (ACI 347.2R-05),* American Concrete Institute, Farmington Hills, MI, USA.

ACI Committee 435. 1995. *Control of deflection in concrete structures (ACI 435R-95),* American Concrete Institute, Farmington Hills, MI, USA.

ACI Committee 435, Subcommittee 7. 1973. Deflection of Continuous Concrete Beams. *ACI Journal Proceedings,* 70 (12): 781-787.

ACI Innovation Task Group 6. 2010. *Design Guide for the Use of ASTM A1035/A1035M Grade 100 (690) Steel Bars for Structural Concrete (ACI ITG-6R-10)*, American Concrete Institute, Farmington Hills, MI, USA.

Bakoss, S.L., Gilbert, R.I., Faulkes, K.A., & Pulmano, V.A. 1982. Long-term deflections of reinforced concrete beams. *Magazine of Concrete Research*, 34 (121): 203-212.

Bischoff, P.H. 2005. Reevaluation of deflection prediction for concrete beams reinforced with steel and fiber reinforced polymer bars. *Journal of Structural Engineering, ASCE*, 131 (5): 752–767.

Bischoff, P.H. 2007. Rational model for calculating deflection of reinforced concrete beams and slabs. *Canadian Journal of Civil Engineering,* 34 (8): 992-1002.

Branson, D.E. 1965. *Instantaneous and time-dependent deflections of simple and continuous reinforced concrete beams,* HPR Rep. No. 7, Part 1, Alabama Highway Department, Bureau of Public Roads, Montgomery, AL, USA.

Branson, D.E. 1977. *Deformation of Concrete Structures,* 1st Edition, McGraw-Hill Companies, New York, NY, USA.

Canadian Standards Association (CSA). 2014. *Design of Concrete Structures*, CAN/CSA-A23.3-14, Mississauga, Ontario, Canada.

Cement Association of Canada (CAC). 2016. *CAC Concrete Design Handbook*, 4th Edition, Cement Association of Canada, Ottawa, Canada.

Computers & Structures, Inc. 2016. *SAFE 2014* (Version 14.2.0) [Computer Software].

Cook, R.D., Malkus, D.S., & Plesha, M.E. 2002. *Concepts and Applications of Finite Element Analysis*, 4th Edition, John Wiley & Sons Inc, Hoboken, NJ, USA.

Corley, W.G., & Sozen, M.A. 1966. Time-Dependent Deflections of Reinforced Concrete Beams. *ACI Journal Proceedings,* 63 (3): 373-386.

El-Mogy, M. 2011. *Behaviour of Continuous Concrete Beams Reinforced with FRP Bars,* Ph.D. Thesis, University of Manitoba, Winnipeg, MB, Canada.

El-Nemr, A. 2013. *Serviceability of Concrete Members Reinforced with FRP Bars*. Ph.D. Thesis, Université de Sherbrooke, Sherbrooke, QC, Canada.

Ellingwood, B.R., Galambos, T.V., MacGregor, J.G., & Cornell, C.A. 1980. *Development of a Probability Based Load Criterion for American National Standard A58,* NBS Special Publication No. 577*,* National Bureau of Standards, Washington, D.C., USA.

Espion, B. 1988. *Long-term sustained loading tests on reinforced concrete beams: A selected database,* Bulletin du Service Génie Civil, 88-1, Univ. Libre de Bruxelles, de Bruxelles, Brussels, Belgium.

Gilbert, R.I. & Nejadi, S. 2004a. *An experimental study of flexural cracking in reinforced concrete members under short term loads*, UNICIV report R; no. R-434. University of New South Wales, Sydney, Australia.

Gilbert, R.I. & Nejadi, S. 2004b. *An experimental study of flexural cracking in reinforced concrete members under sustained loads,* UNICIV report R; no. R-435. University of New South Wales, Sydney, Australia.

Gilbert, R.I. 2012. *Creep and Shrinkage Induced Deflections in RC Beams and Slabs,* ACI SP-284, Andy Scanlon Symposium on Serviceability and Safety of Concrete Structures: From Research to Practice, American Concrete Institute, Farmington Hills, MI, USA, pp. 13-1 to 13-15.

Grundy, P., & Kabaila, A. 1963. Construction Loads on Slabs with Shored Formwork in Multistory Buildings. *ACI Journal Proceedings,* 60 (12): 1729-1738.

Guralnick, S.A. & Winter, G. 1957. *An investigation of high-strength, deformed steel bars for concrete reinforcement,* Report No. TSR 4730-7146, Part I, Department of Structural Engineering, School of Civil Engineering, Cornell University, Ithaca, NY, USA.

Guralnick, S.A. & Winter, G. 1958. *An investigation of high-strength, deformed steel bars for concrete reinforcement,* Report No. TSR 4730-7146, Part II, Department of Structural Engineering, School of Civil Engineering, Cornell University, Ithaca, NY, USA.

Habeeb, M.N., & Ashour, A.F. 2008. Flexural behavior of continuous GFRP reinforced concrete beams. *Journal of Composites for Construction*, 12 (2): 115-124.

Hibbeler, R.C. 2012. *Structural Analysis,* 8th Edition, Pearson Prentice Hall, Upper Saddle River, NJ, USA.

Hognestad, E. 1951. *A Study of Combined Bending and Axial Load in Reinforced Concrete Members*, Bulletin 399, University of Illinois Engineering Experiment Station, Urbana, IL, USA.

Jin, X., Shen, Y. & Li, Z. 2005. Behaviour of high- and normal-strength concrete at early ages. *Magazine of Concrete Research,* 57 (1): 339-345.

Kaminetzky, D., & Stivaros, P.C. 1994. Early-Age Concrete: Construction Loads, Behavior, and Failure. *Concrete International,* 16 (1): 58-63.

Khan A. A. 1995. *Concrete Properties and Thermal Stress Analysis of Members at Early Ages,* Ph.D Thesis, McGill University, Montreal, Canada.

MacGregor, J.G & Bartlett, F.M. 2000. *Reinforced Concrete, Mechanics and Design*, 1st Canadian Edition, Prentice-Hall, Scarborough, Canada.

Mahroug, M.E.M., Ashour, A.F., & Lam, D. 2014a. Experimental response and code modelling of continuous concrete slabs reinforced with BFRP bars. *Composite Structures*, 107: 664-674.

Mahroug, M.E.M., Ashour, A.F., & Lam, D. 2014b. Tests of continuous concrete slabs reinforced with carbon fibre reinforced polymer bars. *Composites Part B: Engineering*, 66: 348-357.

Mattock, A.H. 1959. Redistribution of Design Bending Moments in Reinforced Concrete Continuous Beams, *Proceedings, Institution of Civil Engineers*, 13: 35-46.

Microsoft Excel for Mac 2011 (Version 14.5.8) [Computer Software].

Monette, L, & Gardner, N.J. 2015. Shored/Reshored Construction of Flat Plats. *Concrete International,* 37 (9): 25-32.

Park, H.G., Hwang, H.J., Hong, G.H., Kim, Y.N., & Kim, J.Y. 2012. Immediate and Long-Term Deflections of Reinforced Concrete Slabs Affected by Early-Age Loading and Low Temperature. *ACI Structural Journal*, 109 (3): 413-422.

Scanlon, A., & Bischoff, P.H. 2008. Shrinkage restraint and loading history effects on deflection of flexural members. *ACI Structural Journal,* 105 (4): 498–506.

Stivaros, P.C. 2012. *Control of Deflection in Concrete Slabs and Effects of Construction Loads,* ACI SP-284, Andy Scanlon Symposium on Serviceability and Safety of Concrete Structures: From Research to Practice, American Concrete Institute, Farmington Hills, MI, USA, pp. 17-1 to 17-13.

Todeschini, C.E, Bianchini, A.C., & Kesler, C.E. 1964. Behavior of Concrete Columns Reinforced with High Strength Steels. *ACI Journal Proceedings,* 61 (6): 701-716.

Washa, G.W. 1947. Plastic Flow of Thin Reinforced Concrete Slabs. *ACI Journal Proceedings,* 44 (3): 237-260.

Washa, G.W., & Fluck, P.G. 1952. Effect of Compressive Reinforcement on the Plastic Flow of Reinforced Concrete Beams. *ACI Journal Proceedings,* 49 (8): 89-108.

Washa, G.W., & Fluck, P.G. 1956. Plastic Flow (Creep) of Reinforced Concrete Continuous Beams. *ACI Journal, Proceedings*, 52 (5): 549-561.

Whitney, C.S. 1937. Reinforced Concrete Members Under Flexure or Combined Flexure and Direct Compression. *Journal ACI,* 33: 483-498.

Yu, W.W. 1960. *Instantaneous and Long-Time Deflections of Reinforced Concrete Beams,* Ph.D Thesis, Cornell University, Ithaca, NY, USA.

APPENDIX A: STEPS FOR MOMENT-CURVATURE ANALYSIS

The general steps in a moment-curvature analysis are shown in Figure 2-9. This appendix summarizes the specific steps to conduct the analysis, including computing the magnitude and line of action of the resultant concrete compressive force using the different material idealizations. A sample calculation is shown for a concrete beam with cross section 300×600mm, reinforced with Grade 400 steel at a depth, d, of 520mm, and reinforcement ratio of 0.5% (A_s = 780mm^2) at an age of 1 day using the Khan (1995) data to represent the concrete material, with concrete compressive strength, f_0, of 11.5MPa computed for a concrete compressive strain, ε_i, of 0.0020.

A.1. Concrete in Compression Idealized Using Stress-Strain Data

Integration based on piece-wise linearization of the concrete stress-strain relationship was used to compute the moment-curvature response. The resultant force magnitude and location were calculated so that the moment and associated curvature could be determined. Figure A-1 shows for ε_i=0.0020, σ_i=10.8MPa, ε_{i-1}=0.0018 and σ_{i-1}=11.1MPa from the reported data (Khan 1995) and $d\varepsilon$ =0.0002. Figure A-2 shows the effective cross sections, strain distributions and stress distributions assumed for the moment-curvature analysis derived using these stress-strain data.

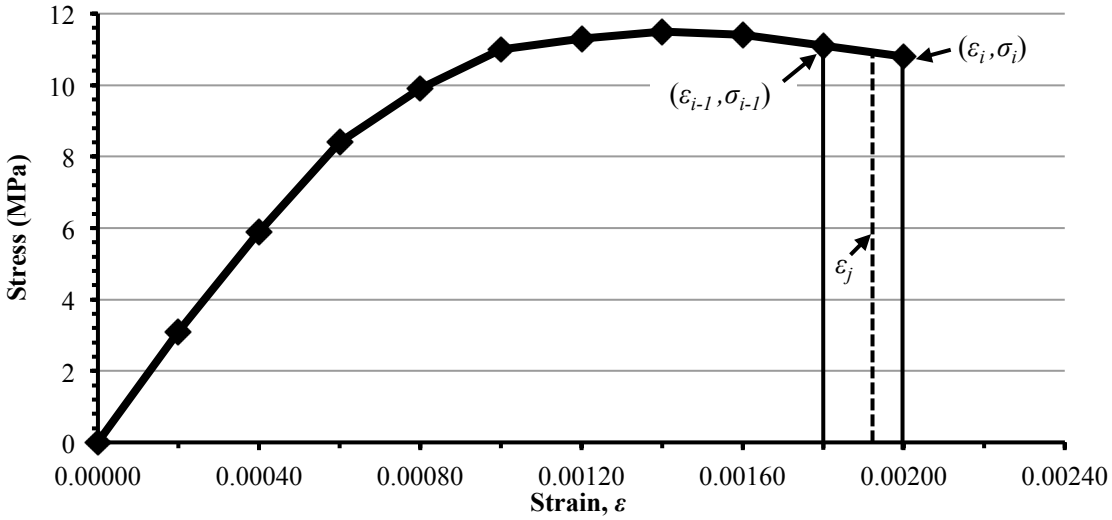

Figure A-1: Stress-Strain Curve from Khan (1995) at 1 day

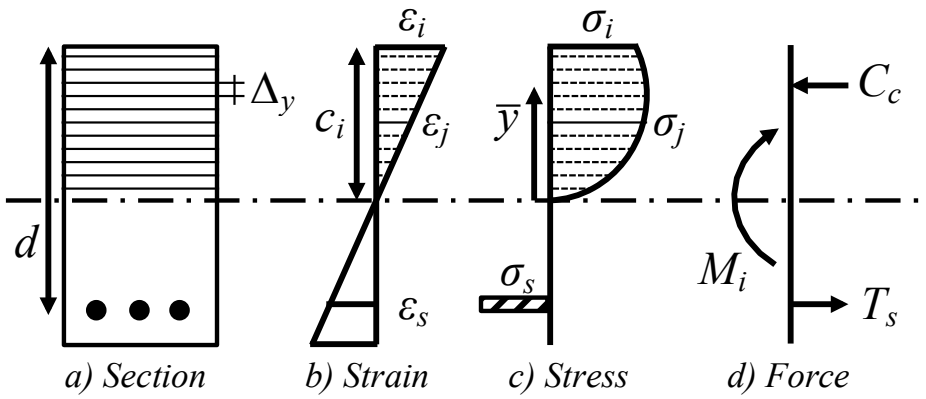

Figure A-2: Discretization of Compression Region for Moment-Curvature Analysis

The steps for analysis are as follows:

1. Increment the value of strain at the extreme compression fibre, ε_i, and assume a neutral axis depth, c_i.

3. Discretize the compression region, c_i, in to n elements. For this analysis n was chosen to be 12. The thickness of the each element, Δ_y, is:

[A.1] $$\Delta_y = \frac{c_i}{n}$$

4. Compute the distance from the neutral axis, c_i, to the top of each discrete element and the corresponding compressive strain for $j = 1 \ldots n$:

[A.2] $$y_j = (\Delta_y) j$$

[A.3] $$\varepsilon_j = y_j \left(\frac{\varepsilon_i}{c_i} \right)$$

5. Compute the corresponding compressive stress by linear interpolation of the stress-strain data:

[A.4] $$\sigma_j = \frac{(\sigma_i - \sigma_{i-1})}{(\varepsilon_i - \varepsilon_{i-1})} (\varepsilon_j - \varepsilon_{i-1}) + \sigma_{i-1}$$

where $(\varepsilon_{i-1}, \sigma_{i-1})$ and $(\varepsilon_i, \sigma_i)$ are the stress-strain data points that bound the value ε_j, as shown in Figure A-1.

6. Compute the resultant compression force, F_j, acting on each element as:

[A.5] $$F_j = \left[\sigma_{j-1} + \frac{(\sigma_j - \sigma_{j-1})}{2} \right] b \Delta_y$$

where b is the element width.

7. Determine the moment of the resultant compression force about the axis of zero strain:

[A.6] $$F_j y_j = \left[\sigma_{j-1} (y_j - \frac{\Delta_y}{2}) + \frac{(\sigma_j - \sigma_{j-1})}{2} (y_j - \frac{\Delta_y}{3}) \right] b \Delta_y$$

8. Determine the location of the resultant compression force:

[A.7] $$\bar{y} = \frac{\Sigma F_j y_j}{\Sigma F_j}$$

9. Calculate the compressive force magnitude as the summation of the forces acting on each discrete element:

[A.8] $$C_c = \Sigma F_j$$

10. Determine steel strain:

[A.9] $$\varepsilon_s = \varepsilon_i \left(\frac{d - c_i}{c_i} \right)$$

where d is the depth to the reinforcing steel.

11. Calculate the steel stress:

[A.10] $$\sigma_s = \begin{cases} \varepsilon_s E_s & \varepsilon_s \leq \varepsilon_y \\ f_y & \varepsilon_s > \varepsilon_y \end{cases}$$

where E_s is Young's Modulus of steel (200,000MPa) and the steel yield strain, ε_y, is f_y/E_s, or 0.002 for f_y = 400MPa.

12. From force equilibrium, $T_s + C_c = 0$, iterate c_i until $\sum F = 0$ using the MS Excel SOLVER function.

13. Calculate the moment:

[A.11] $$M_i = \sigma_s A_s (d - c_i + \bar{y})$$

where A_s is the area of steel.

14. Calculate the curvature:

[A.12] $$\phi_i = \frac{\varepsilon_i}{c_i}$$

15. Repeat steps for increments of strain until the moment is 90% of maximum in the descending branch of the moment-curvature response.

The following is an example calculation using the Khan (1995) one-day-old concrete stress-strain data for ε_i=0.0020, σ_i=10.8MPa, ε_{i-1}=0.0018 and σ_{i-1}=11.1MPa. For illustrative purposes, the correct value of c_i to achieve horizontal force equilibrium, as determined from the MS Excel SOLVER function, is shown.

$c_i = 117.1mm$

$\Delta_y = 117.1/12 = 9.8mm$

For j = 1

$y_1 = (9.8) \times 1 = 9.8mm$

$\varepsilon_1 = 9.8 \times (0.0020/117.1) = 0.00017$

From stress-strain data for $\varepsilon_1=0.00017$: $\sigma_i=3.1MPa$, $\sigma_{i-1}=0MPa$, $\varepsilon_i=0.00020$, $\varepsilon_{i-1}=0$

$\sigma_1 = (3.1 – 0)/(0.00020 – 0) \times (0.00017 – 0) + 0 = 2.58MPa$

$F_1 = [0 + (2.58 – 0)/2](300)(9.8) = 3,780N$

$F_1y_1 = [0(9.8 – 9.8/2) + ½(2.58 – 0) \times (9.8 – 9.8/3)](300)(9.8) = 34,400N.mm$

Repeat for j = 2… 11

For j = 12

$y_{12} = (9.8) \times 12 = 117.1mm$

$\varepsilon_{12} = 117.1 \times (0.0020/117.1) = 0.0020$

From stress-strain data for $\varepsilon_{12}=0.0020$: $\sigma_i=10.8MPa$, $\sigma_{i-1}=11.1MPa$, $\varepsilon_i=0.0020$, $\varepsilon_{i-1}=0.0018$

$\sigma_{12} = (10.8 – 11.1)/(0.0020 – 0.0018) \times (0.0020 – 0.0018) + 11.1 = 10.8MPa$

From discretized analysis: $\sigma_{11} = 11.1MPa$

$F_{12} = [11.1 + (10.8 – 11.1)/2](300)(9.8) = 32,000N$

$F_{12}y_{12} = [11.1(117.1 – 9.8/2) + ½(10.8– 11.1) \times (117.1 – 9.8/3)](300)(9.8)$
$= 3,590,000N.mm$

$\bar{y} = (34,400 + ... + 3,590,000)/(3,780 + ... + 32,000) = 69.2mm$

$C_c = 3,780 + ... + 32,000 = 312,000N$

$\varepsilon_s = 0.0020 \times [(520 – 117.0)/117.0] = 0.0069 > \varepsilon_y = 0.0020$

$\sigma_s = f_y = 400MPa$

$T_s = 400 \times 780 = 312,000N$

$\Sigma F = -312,000 + 312,000 = 0$

$M_i = 400 \times 780(520 – 117.1 + 69.2) = 147,300,000N.mm$

$\phi_i = 0.0020/117.0 = 17.1 \times 10^{-6}\ mm^{-1}$

A.2. Concrete Idealized Using Todeschini Model

Using the equation for strain at peak stress, Eq. [2.7], the Todeschini relationship was used to determine the moment-curvature response, as shown in Figure A-3.

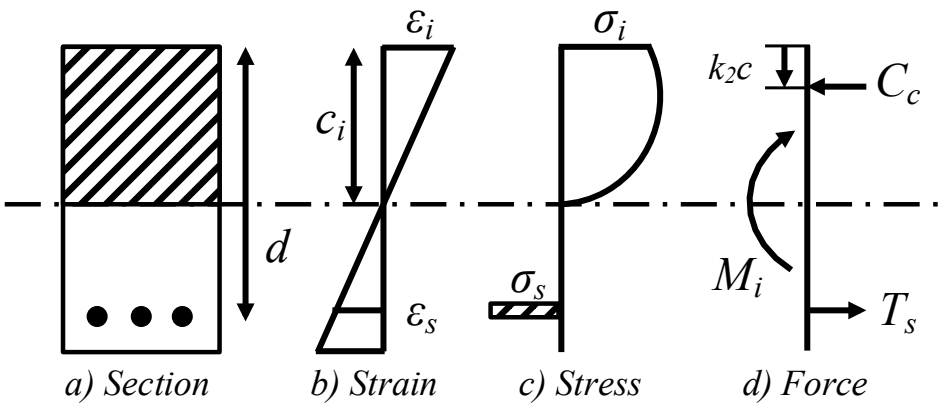

Figure A-3: Todeschini Model Moment-Curvature Analysis

This was achieved by replacing the previous steps 2 to 8 from the concrete idealized by stress-strain data analysis with the following procedure:

2. Calculate the strain at peak stress, ε_0, from Eq. [2.7].

3. Calculate the ratio, x, of the extreme compression fibre strain, ε_i, to the strain at peak stress, ε_0.

[A.13] $$x=\frac{\varepsilon_i}{\varepsilon_0}$$

4. Determine the extreme fibre concrete stress, σ_i, using Todeschini's equation:

[A.14] $$\sigma_i=\frac{2f_0x}{(1+x^2)}$$

5. Calculate the factor k_1 to find the average compressive stress, σ_{avg}, over the compression zone.

[A.15] $$k_1=\frac{ln(1+x^2)}{x}$$

[A.16] $$\sigma_{avg}=k_1\sigma_i$$

6. Compute the magnitude of compression force:

[A.17] $$C_c=\sigma_{avg}c_ib$$

7. Determine the neutral axis depth, c_i, iteratively to satisfy force equilibrium.

8. Determine the location of the resultant compressive force by calculating the factor k_2, measured from the extreme compression fibre.

[A.18] $$k_2 = 1 - 2\left(\frac{x - \tan^{-1}(x)}{x^2 k_1}\right)$$

where $\tan^{-1}(x)$ is in radians.

9. Determine the moment as:

[A.19] $$M_i = T_s(d - k_2 c_i)$$

and curvature from Eq. [A.12].

The following is an example calculation using the Todeschini model computed for concrete compressive strength, f_0, of 11.5MPa, elastic modulus, E_c, computed from Eq. [2.2] as 15,300MPa for a concrete compressive strain, ε_i, of 0.0020 using the Khan data (1995). For illustrative purposes, the correct value of c_i to achieve horizontal force equilibrium, as determined from the MS Excel SOLVER function, is shown.

$c_i = 144.5mm$
$\varepsilon_0 = 1.71 \times (11.5/15{,}300) = 0.0013$
$x = 0.0020/0.0013 = 1.55$
$\sigma_i = (2 \times 11.5 \times 1.55)/(1 + 1.55^2) = 10.5MPa$
$k_1 = ln(1 + 1.55^2)/1.55 = 0.79$
$\sigma_{avg} = 0.79 \times 10.5 = 9.1MPa$
$C_c = 9.1 \times 144.5 \times 300 = 312{,}000N$
$\varepsilon_s = 0.0020 \times [(520 - 144.5)/144.5] = 0.0071 > \varepsilon_y = 0.0020$
$\sigma_s = f_y = 400MPa$
$T_s = 400 \times 780 = 312{,}000N$
$\Sigma F = -312{,}000 + 312{,}000 = 0$
$\tan^{-1}(1.55) = 0.998rad$
$k_2 = 1 - 2\{[1.55 - 0.998]/[1.55^2(0.79)]\} = 0.42$
$M_i = 312{,}000[520 - 0.42(144.5)] = 147{,}300{,}000N.mm$
$\phi_i = 0.0020/144.5 = 17.5 \times 10^{-6}\ mm^{-1}$

A.3. Concrete Idealized Using Modified Hognestad Model

Using the equation for strain at peak stress, Eq. [2.9], the Modified Hognestad relationship can be used to determine the moment-curvature response, as shown in Figure A-4. The internal compressive force in the concrete is computed as two components, C_{c1} and C_{c2}, where C_{c1} represents the compression force generated by the ascending part of the stress-strain relationship, and C_{c2} represents the compression force generated by the descending part of the stress-strain relationship.

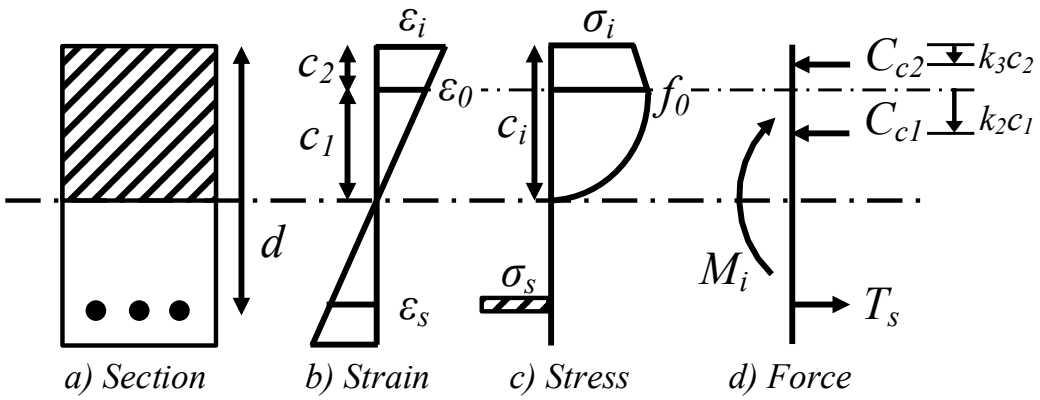

Figure A-4: Modified Hognestad Model Moment-Curvature Analysis

For $\varepsilon_i \leq \varepsilon_0$, the moment-curvature analysis was achieved by replacing steps 2 to 8 from the concrete idealized by stress-strain data analysis with the following procedure:

2. Calculate the strain at peak stress, ε_0, from Eq. [2.9].

3. Calculate the ratio, x, of the extreme compression fibre strain, ε_i, to the strain at peak stress, ε_0, from Eq. [A.13].

4. Determine the extreme fibre concrete stress using the Modified Hognestad equation:

[A.20] $$\sigma_i = f_0\left[2x - x^2\right]$$

5. Calculate the factor k_1 to find the average compressive stress, σ_{avg}, over the compression zone.

[A.21] $$k_1 = x\left(1 - \frac{x}{3}\right)$$

6. Compute the average compressive stress, σ_{avg}, from Eq. [A.16] and the magnitude of the compression force from Eq. [A.17].

[A.16] $$\sigma_{avg} = k_1 \sigma_i$$

[A.17] $$C_c = \sigma_{avg} c_i b$$

7. Determine the neutral axis depth, c_i, iteratively to satisfy force equilibrium.

8. Determine the location of the resultant compressive force by calculating the factor k_2, measured from the extreme compression fibre.

[A.22] $$k_2 = \frac{(4 - x)}{12\left(1 - \frac{x}{3}\right)}$$

9. Determine the moment from Eq. [A.19] and curvature from Eq. [A.12].

For $\varepsilon_i > \varepsilon_0$, the depth of the compression zone under the ascending branch of the stress-strain relationship, c_1, is the distance from the axis of zero strain to the point where $\varepsilon_i = \varepsilon_0$. To compute the compression force generated by the ascending part of the stress-strain relationship, C_{c1}, $x_1 = 1$ and therefore $k_1 = 0.67$ and $k_2 = 0.375$. Where k_2 is the distance from point where $\varepsilon_i = \varepsilon_0$ to the resultant compressive force. The moment-curvature analysis for strains greater than the strain at peak stress is achieved by replacing steps 3 to 9 above with the following:

3. Determine the depth of the compression zone, and resultant compression force attributed to the ascending branch of the stress-strain relationship as:

[A.23] $$c_1=\frac{\varepsilon_0}{\varepsilon_i}c_i$$

[A.24] $$C_{c1}=\sigma_{avg}c_1 b$$

[A.25] $$\sigma_{avg}=0.67f_0$$

4. Determine the concrete stress at the extreme compression fibre using the Modified Hognestad equation:

[A.26] $$\sigma_i=f_0\left[1-0.15\left(\frac{x-1}{\frac{\varepsilon_{ult}}{\varepsilon_0}-1}\right)\right]$$

5. Determine the resultant compressive force for the trapezoidal portion of the Modified Hognestad stress-strain curve, C_{c2}.

[A.27] $$C_{c2}=\sigma_{2,avg}c_2 b$$

[A.28] $$\sigma_{2,avg}=\frac{\sigma_i+f_0}{2}$$

[A.29] $$c_2=c_i-c_1$$

6. Determine the neutral axis depth, c_i, iteratively to satisfy force equilibrium.

[A.30] $$\sum F=T_s+C_{c1}+C_{c2}=0$$

7. Determine the location of the resultant compressive force C_{c2} by calculating the factor k_3 measured from the extreme compression fibre.

[A.27] $$k_3=\frac{1}{2}-\frac{(\sigma_i-f_0)}{6(\sigma_i+f_0)}$$

8. Knowing this determine the moment as:

[A.28] $$M_i=C_{c1}(d-c_2-k_2c_1)+C_{c2}\left(d-k_3c_2\right)$$

and curvature from Eq. [A.12].

The following is an example calculation using the Modified Hognestad model for concrete compressive strength, f_0, of 11.5MPa, elastic modulus, E_c, computed from Eq. [2.2] of 15,300MPa computed for a concrete compressive strain, ε_i, of 0.0020 using the Khan data (1995). For illustrative purposes, the correct value of c_i to achieve horizontal force equilibrium, as determined from the MS Excel SOLVER function, is shown.

$c_i = 117.8mm$

$\varepsilon_0 = 1.8 \times (11.5/15{,}300) = 0.0014 < \varepsilon_i = 0.0020$

Therefore, need to determine both C_{c1}, *where:* $k_1=0.67$ *and* $k_2=0.375$, *and* C_{c2}.

$c_1 = (0.0014/0.0020) \times 117.8 = 79.9mm$

$\sigma_{avg} = 0.67 \times 11.5 = 7.7MPa$

$C_{c1} = 7.7 \times 79.9 \times 300 = 183{,}800N$

$x = 0.0020/0.0014 = 1.47$

$\sigma_i = 11.5\{1 - 0.15[(1.47 - 1)/(0.0038/0.0014 - 1)]\} = 11.0MPa$

$\sigma_{avg,2} = (11.0 + 11.5)/2 = 11.3MPa$

$c_2 = 117.8 - 79.9 = 37.9mm$

$C_{c2} = 11.3 \times 37.9 \times 300 = 128{,}200N$

$\varepsilon_s = 0.0020 \times [(520 - 117.8)/117.8] = 0.0068 > \varepsilon_y = 0.0020$

$\sigma_s = f_y = 400MPa$

$T_s = 400 \times 780 = 312{,}000N$

$\Sigma F = -312{,}000 + 183{,}800 + 128{,}200 = 0$

$k_3 = ½ - (11.0 - 11.5)/[6(11.0 + 11.5)] = 0.50$

$M_i = 183{,}800[520 - 37.9 - 0.375(79.9)] + 128{,}200[520 - 0.50(37.9)] =$

$= 147{,}300{,}000N.mm$

$\phi_i = 0.0020/117.8 = 17.0 \times 10^{-6}\ mm^{-1}$

APPENDIX B: MS EXCEL SPREADSHEET CHECK USING $I_e=I_g$

To ensure a high level of confidence in the analysis performed and the MS Excel spreadsheet used a final check was performed by using I_e equal to I_g for the entire beam length. Using the gross moment of inertia in both the single-element and discretized-element idealizations removes one variable and allows for a more reliable comparison between the conventional analysis and the analysis performed in this study. Table B-1 shows the percent difference between the deflections calculated using conventional beam analysis (e.g. Hibbeler 2012) that lead to Equation [B.1] and the results of the discretized analysis.

[B.1] $$\Delta_{MID}=\frac{5w_aL^4}{384E_cI_e}+\frac{M_a^-L^2}{8E_cI_e}$$

Table B-1: Comparison of Computed Deflections for $I_e=I_g$

ρ	w_L/w_D	Eq. [B.1] Δ_{MID}	*Discretized* Δ_{MID}	% Diff
0.5%	0.5	2.2	2.2	0.25%
1.0%	1.0	5.6	5.6	0.18%
1.5%	1.5	9.1	9.1	0.15%

The computed deflections are the same to two significant figures, and more precise values obtained in the MS Exce spreadsheet were used to compute the relative differences. The differences between each method of analysis are minimal for various reinforcement ratios and live-to-dead load ratios. The methodology adopted for the discretized-element idealization is therefore accurate and the spreadsheet-based solutions presented in Chapter 3 are without any fundamental errors.

APPENDIX C: MESH SENSITIVITY ANALYSIS WITH POINT LOAD

For a three-span continuous beam, Figure C-1 shows the positive moment resulting from applying a concentrated dead load to all spans and a concentrated live load to the middle span only exceeds the negative moment at an interior support with adjacent spans loaded. Therefore, the positive moment reinforcement was set equal to 0.5%, 1.0% or 1.5% and the negative moment reinforcement was selected to provide the necessary resistance.

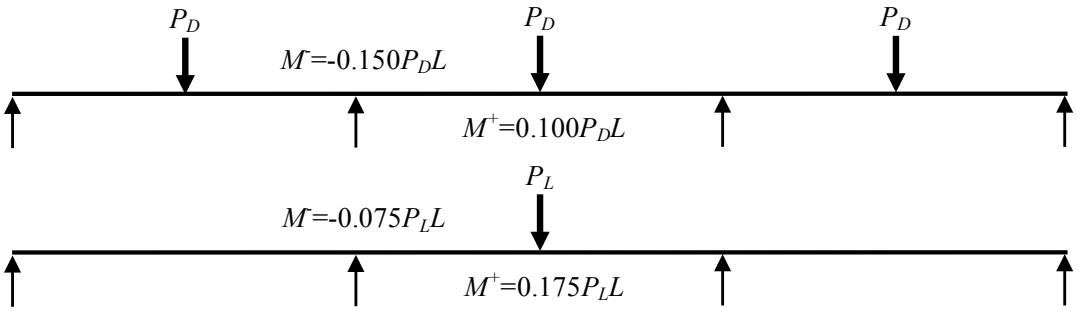

Figure C-1:Pattern Point Loading and CAC (2016) Moment Coefficients

Treating the finest mesh of 50-elements as the "gold standard", Table C-1 compares the maximum deflection computed using the larger meshes to that computed using the 50-element mesh. These results are consistent with those seen for a uniformly loaded member in Table 3-3: increasing the element size will decrease the level of accuracy, and the effect of the moment gradient near the supports is marginally important, as seen when comparing the constant-length 5-element mesh to the variable-length $2^+\_3^-$-element mesh.

Table C-1: Sensitivity of Maximum Deflection to Mesh Size – Concentrated Point Load

	% Difference with respect to the 50 Element Result								
	P_L/P_D=0.5			P_L/P_D=1.0			P_L/P_D=1.5		
# of Elements	**ρ=0.5%**	**ρ=1.0%**	**ρ=1.5%**	**ρ=0.5%**	**ρ=1.0%**	**ρ=1.5%**	**ρ=0.5%**	**ρ=1.0%**	**ρ=1.5%**
20	-0.2%	0.0%	0.0%	-0.1%	0.0%	0.0%	0.0%	0.0%	0.1%
10	-0.7%	0.0%	0.1%	-0.3%	0.0%	0.0%	-0.6%	-0.4%	0.4%
7	-0.7%	-0.2%	0.2%	-0.5%	1.3%	0.3%	-0.9%	-0.1%	-0.1%
5	-2.5%	0.5%	0.7%	-3.5%	1.7%	-1.1%	-2.7%	0.5%	-0.5%
$6^-\_12^+$	0.2%	0.4%	-0.1%	0.0%	0.1%	0.1%	0.0%	0.0%	0.1%
$6^-\_7^+$	0.1%	0.2%	-0.2%	-0.2%	-0.1%	0.1%	-0.2%	-0.2%	-3.3%
$4^-\_12^+$	0.7%	0.0%	1.0%	0.2%	0.0%	0.4%	0.2%	0.1%	0.1%
$2^-\_3^+$	-2.4%	3.1%	0.7%	-2.7%	1.1%	0.2%	-2.0%	0.3%	0.0%

Figure C-2(a) shows the applied and cracking moments normalized by total nominal moment, $M_0=PL/4$. Figure C-2(b) shows the variation I_e/I_g as computed using different meshes for ρ of 0.5% and w_L/w_D of 0.5, which typically shows the greatest mesh sensitivity. The I_e/I_g values for constant-length 50-, and 5-element meshes are compared on left side of Figure C-2(b). The 50-element mesh more effectively simulates the uncracked region of the member than the coarser 5-element mesh. Similarly, the comparison of I_e/I_g values for the variable-length element meshes, shown on the right side Figure C-2(b), indicate that the finer meshes are more efficient in simulating the stiffness in the uncracked region. These results are consistent with the findings of the mesh sensitivity analysis performed for a member under uniform loading. In practice, using a constant-length 10-element mesh per half-span yields results within 1% of the 50-element mesh and the effort required to locate the point of inflection likely outweighs any benefit attributable to the use of a finer mesh in the negative moment region.

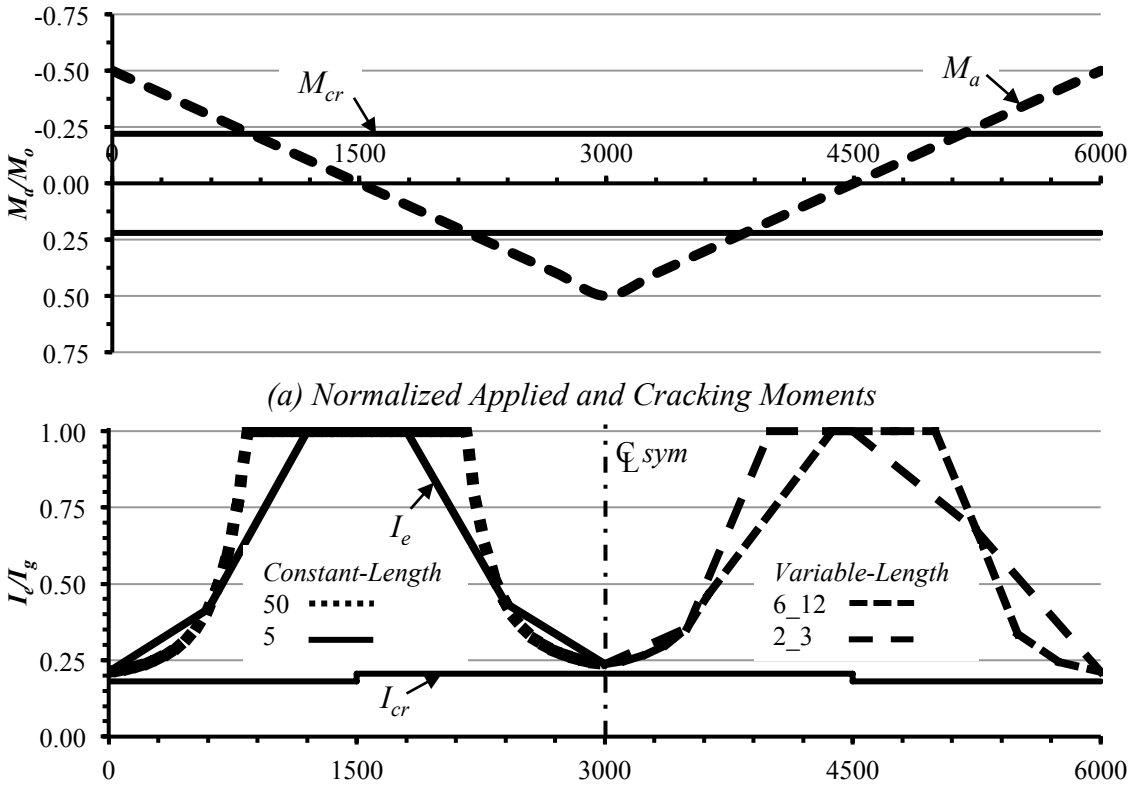

(a) Normalized Applied and Cracking Moments

(b) Normalized Effective and Cracked Moments of Inertia

Figure C-2: Analysis of Discretized Three-Span Continuous Beam with Different Meshes with a Concentrated Point Load, Branson

APPENDIX D: SIMPLY SUPPORTED MEMBER MESH SENSITIVITY ANALYSIS

The simply supported member was discretized using elements of uniform lengths of $L/40$, $L/20$, $L/10$, and $L/6$, where L is the span length. Treating the finest mesh of $L/40$ as the "gold standard", Table D-1 shows the percent differences between the maximum deflection computed using the 40-element mesh and that for the coarser meshes. The results in Table D-1 indicate that decreasing the number of elements will increase the error, as expected. A positive difference indicates that the maximum deflection computed using the 40-element mesh is greater than that for the larger meshes. It can be concluded that using an element length of $L/10$ is suitable for practical in-office use and gives deflections that, while unconservative, are within 1% of those computed using the 40-element mesh. In Chapter 3, the "gold standard" 40-element mesh was used to verify the exponent m in the Branson and Bischoff Equations in a discretized-element idealization. In Chapter 4, a uniform element length of $L/20$ was used, as the computed deflections gives results within 0.2% of those computed using the 40-element mesh and the extra computational demand, as compared to the 10-element mesh for practical design office use, was not a concern.

Table D-1: Sensitivity of Maximum Deflection to Mesh Size – Simply Supported Member

	% Difference with respect to the 40 Element Result								
	w_L/w_D = 0.5			**w_L/w_D = 1.0**			**w_L/w_D = 1.5**		
# of Elements	**ρ = 0.5%**	**ρ = 1.0%**	**ρ = 1.5%**	**ρ = 0.5%**	**ρ = 1.0%**	**ρ = 1.5%**	**ρ = 0.5%**	**ρ = 1.0%**	**ρ = 1.5%**
20	0.2%	0.2%	0.1%	0.2%	0.2%	0.1%	0.2%	0.2%	0.1%
10	0.9%	0.6%	0.7%	1.0%	0.6%	0.7%	1.0%	0.6%	0.7%
6	1.9%	1.9%	1.2%	2.0%	1.9%	2.1%	2.0%	1.9%	2.1%

APPENDIX E: DETERMINATION OF *m* FOR USE WITH THE BISCHOFF EQUATION IN A DISCRETIZED-ELEMENT IDEALIZATION USING SOLVER FUNCTION

Using the previously developed MS Excel spreadsheet, the SOLVER function was used to determine the value of *m* for the discretized-element idealization that would give a mid-span deflection equal to that computed in the single-element idealization using the Bischoff Equation. Iteration was needed for the two-span members because of the moment redistribution due to cracking. Table E-1 shows these *m* values; the results suggest that *m* equal to 2 would be suitable for a wide range of concrete members, with various fixities, reinforcement ratios and loading ratios. This was contrary to the initial assumption of *m=3* so the discretized-element idealization was again performed using *m* equal to 2. Table E-2, Table E-3, and Table E-4 show the results and those computed using *m* equal to 3 for the simply supported, two-span continuous and three-span continuous beams, respectively.

Table E-1: SOLVER values for *m* in discretized-element idealization

		SOLVER *m*		
ρ^-	**w_L/w_D**	**Simply Supported**	**Two-Span**	**Three-Span**
0.5%	0.5	2.68	2.58	10.72
	1	2.69	3.17	4.68
	1.5	2.71	3.49	3.72
1.0%	0.5	2.46	2.00	2.25
	1	2.46	2.14	1.98
	1.5	2.47	2.37	1.86
1.5%	0.5	2.45	1.84	1.59
	1	2.46	1.98	1.50
	1.5	2.46	2.13	1.44

Table E-2 shows that m of 2 in a discretized-element idealization gives slightly unconservative results for simply supported beams and yields larger relative differences than those computed using m of 3.

Table E-2: Summary of Simply Supported Beam Computed Deflections with m=2

	ρ=0.5%			M_r=46.5kN.m			w_f=18.4kN/m	
	Branson			**Bischoff**				
w_L/w_D	***Single Element m=3*** Δ_{MID}	***Discretized m=4*** Δ_{MID}	**% Diff**	***Single Element m=2*** Δ_{MID}	***Discretized m=2*** Δ_{MID}	**% Diff**	***Discretized m=3*** Δ_{MID}	**% Diff**
0.5	19.4	19.8	-2.1%	18.6	17.2	7.8%	19.1	-2.6%
1	18.6	19.0	-2.2%	17.9	16.4	8.2%	18.3	-2.5%
1.5	18.1	18.5	-2.3%	17.5	16.0	8.5%	17.9	-2.5%
	ρ=1.0%			M_r=87.6kN.m			w_f=34.6kN/m	
	Branson			**Bischoff**				
w_L/w_D	***Single Element m=3*** Δ_{MID}	***Discretized m=4*** Δ_{MID}	**% Diff**	***Single Element m=2*** Δ_{MID}	***Discretized m=2*** Δ_{MID}	**% Diff**	***Discretized m=3*** Δ_{MID}	**% Diff**
0.5	23.5	23.4	0.0%	22.9	22.4	2.1%	23.2	-1.3%
1	22.7	22.7	0.0%	22.2	21.7	2.2%	22.5	-1.3%
1.5	22.3	22.3	0.0%	21.7	21.2	2.2%	22.0	-1.4%
	ρ=1.5%			M_r=123.5kN.m			w_f=48.8kN/m	
	Branson			**Bischoff**				
w_L/w_D	***Single Element m=3*** Δ_{MID}	***Discretized m=4*** Δ_{MID}	**% Diff**	***Single Element m=2*** Δ_{MID}	***Discretized m=2*** Δ_{MID}	**% Diff**	***Discretized m=3*** Δ_{MID}	**% Diff**
0.5	24.7	24.7	0.2%	24.5	24.2	1.0%	24.6	-0.5%
1	24.0	24.0	0.2%	23.7	23.5	1.0%	23.8	-0.6%
1.5	23.6	23.5	0.2%	23.3	23.0	1.1%	23.4	-0.6%

Table E-3 shows for ρ of 0.5% and 1.0% m of 2 in a discretized-element idealization is unconservative as compared to all other methods for deflection calculation, and for ρ of 1.5% there is no significant difference between deflections computed using m of 2 or m of 3 in a discretized-element idealization.

Table E-3: Summary of Two-Span Continuous Beam Computed Deflections with m=2

	ρ-=0.50%		ρ+=0.40%	M^-_r=46.5kN.m		M^+_r=38.0kN.m		w_f=11.6kN/m
	Branson			**Bischoff**				
w_L/w_D	***Single Element m=3*** Δ_{MID}	***Discretized m=4*** Δ_{MID}	**% Diff**	***Single Element m=2*** Δ_{MID}	***Discretized m=2*** Δ_{MID}	**% Diff**	***Discretized m=3*** Δ_{MID}	**% Diff**
0.5	18.3	19.7	-7.5%	16.5	15.0	10.5%	18.8	-2.9%
1	19.6	19.9	-1.4%	17.8	15.0	18.6%	18.9	3.7%
1.5	20.3	20.0	1.7%	18.4	15.0	22.3%	19.0	6.8%
	ρ-=1.00%		ρ+=0.82%	M^-_r=87.6kN.m		M^+_r=73.7kN.m		w_f=21.9kN/m
	Branson			**Bischoff**				
w_L/w_D	***Single Element m=3*** Δ_{MID}	***Discretized m=4*** Δ_{MID}	**% Diff**	***Single Element m=2*** Δ_{MID}	***Discretized m=2*** Δ_{MID}	**% Diff**	***Discretized m=3*** Δ_{MID}	**% Diff**
0.5	26.1	26.5	-1.8%	25.1	25.0	0.1%	26.0	-3.8%
1	27.8	28.3	-1.6%	26.7	26.4	1.2%	27.6	-3.0%
1.5	28.8	28.9	-0.2%	9.8	26.8	3.2%	28.0	-1.2%
	ρ-=1.50%		ρ+=1.18 %	M^-_r=123.5kN.m		M^+_r=101.0kN.m		w_f=30.9kN/m
	Branson			**Bischoff**				
w_L/w_D	***Single Element m=3*** Δ_{MID}	***Discretized m=4*** Δ_{MID}	**% Diff**	***Single Element m=2*** Δ_{MID}	***Discretized m=2*** Δ_{MID}	**% Diff**	***Discretized m=3*** Δ_{MID}	**% Diff**
0.5	28.5	28.6	-0.6%	27.9	28.3	-1.5%	28.4	-1.9%
1	30.3	30.6	-0.8%	29.7	30.1	-1.3%	30.3	-2.0%
1.5	31.4	31.6	-0.5%	30.8	30.9	-0.4%	31.1	-1.3%

Table E-4 shows a similar trend to the simply supported and two-span continuous beams, for ρ of 0.5% using m of 2 in a discretized-element idealization gives unconservative results for three-span continuous beams. Using m of 2 in a discretized-element idealization for ρ of 1.5% gives results comparable to the single-element idealization, whereas, m of 3 in a discretized-element idealization gives results comparable to those computed using the Branson Equation in a discretized-element idealization.

Table E-4: Summary of Three-Span Continuous Beam Computed Deflections m=2

	ρ-=0.50%		ρ+=0.34%	M^-_r=46.5kN.m		M^+_r=32.0kN.m		w_f=14.2kN/m
	Branson			**Bischoff**				
w_L/w_D	***Single Element m=3*** Δ_{MID}	***Discretized m=4*** Δ_{MID}	**% Diff**	***Single Element m=2*** Δ_{MID}	***Discretized m=2*** Δ_{MID}	**% Diff**	***Discretized m=3*** Δ_{MID}	**% Diff**
0.50	5.9	4.6	23.0%	5.0	2.7	46.7%	3.0	40.8%
1.00	9.8	9.1	7.7%	9.9	6.7	32.5%	8.1	18.4%
1.50	12.1	12.0	1.0%	12.5	9.4	25.1%	11.4	9.2%
	ρ-=1.00%		ρ+=0.66%	M^-_r=87.6kN.m		M^+_r=60.2kN.m		w_f=26.8kN/m
	Branson			**Bischoff**				
w_L/w_D	***Single Element m=3*** Δ_{MID}	***Discretized m=4*** Δ_{MID}	**% Diff**	***Single Element m=2*** Δ_{MID}	***Discretized m=2*** Δ_{MID}	**% Diff**	***Discretized m=3*** Δ_{MID}	**% Diff**
0.50	13.1	14.5	-10.4%	12.5	12.0	3.8%	13.6	-8.9%
1.00	18.3	20.3	-10.8%	17.5	17.5	-0.3%	19.4	-10.9%
1.50	21.3	23.6	-11.0%	20.3	20.7	-2.0%	22.7	-11.7%
	ρ-=1.50%		ρ+=1.00 %	M^-_r=123.5kN.m		M^+_r=87.6kN.m		w_f=37.7kN/m
	Branson			**Bischoff**				
w_L/w_D	***Single Element m=3*** Δ_{MID}	***Discretized m=4*** Δ_{MID}	**% Diff**	***Single Element m=2*** Δ_{MID}	***Discretized m=2*** Δ_{MID}	**% Diff**	***Discretized m=3*** Δ_{MID}	**% Diff**
0.50	14.5	16.4	-13.5%	14.0	14.7	-5.7%	15.8	-13.4%
1.00	19.8	22.1	-11.8%	19.2	20.4	-6.3%	21.5	-12.4%
1.50	22.8	25.3	-11.2%	22.2	23.7	-6.8%	24.9	-12.2%

This investigation shows that 3 is an appropriate value for m in the Bischoff Equation for a discretized-element idealization for a wide range of concrete members, with various fixities, reinforcement ratios, and live-to-dead load ratios.

APPENDIX F: OTHER STUDIES CONSIDERED FOR VERIFICATION OF DEFLECTION CALCULATION PROCEDURES

The analyses of specimens from the studies in Table 4-1 and Table 4-14 that were not described in detail in Chapter 4 are presented. These studies confirmed the findings of those in Chapter 4 and support the conclusions made.

F.1. Study by Park et al. (2012) – Simply Supported

The study by Park, Hwang, Hong, Kim and Kim (2012) focused on the effects of early-age construction loading and the material properties of concrete cured at low temperatures on the immediate and long-term deflections of reinforced concrete slabs. A total of seven one-way slabs were tested and, for the purposes of the present investigation, the results from four are relevant. The specimens were simply supported members with a span of 4.5m, a cross section of 800×160mm, giving a span-to-depth ratio, L/h, of 28, and reinforcement ratio of either 0.5% or 1.0%. The members were loaded with two concentrated point loads near midspan and were tested at an age of 3 or 7 days.

For these young concretes, the associated compressive strengths are low and therefore the computed moduli of rupture are low. Thus the ratio of M_{cr}/M_a is low irrespective of the reduced or full moduli of rupture assumed and the applied loads greatly exceed M_{cr} for most of the member length. Table F-1 shows using either the reduced or full moduli of rupture to compute deflections, generally, gives conservative and relatively consistent

results using the Branson or Bischoff Equations in either a single-element or discrete-element idealization.

Table F-1: Results of Park et al. (2012)

Specimen	ρ (%)	Test Δ_{MID} (mm)	Test-to-Predicted From Different Methods							
			$0.5f_r$		$0.67f_r$		Full f_r			
			Branson		Bischoff		Branson		Bischoff	
			m=3	m=4	m=2	m=3	m=3	m=4	m=2	m=3
T3B	0.52%	39.0	0.85	0.85	0.87	0.86	0.89	0.90	0.89	0.89
T7B	0.50%	22.0	0.56	0.57	0.58	0.58	0.66	0.67	0.63	0.63
T3S	0.52%	26.8	0.89	0.90	0.92	0.92	1.04	1.06	1.00	1.01
TT3B	1.04%	20.6	0.73	0.74	0.74	0.74	0.75	0.76	0.76	0.76
	Mean		0.76	0.76	0.78	0.78	0.83	0.85	0.82	0.82
	Std. Dev.		0.15	0.15	0.15	0.15	0.17	0.17	0.16	0.16
	CoV.		19.3%	19.3%	19.4%	19.3%	20.0%	20.2%	19.6%	19.7%

F.2. Study by Bakoss et al. (1982) – Simply Supported

Bakoss, Gilbert, Faulkes, and Pulmano (1982) tested both continuous and simply supported concrete members under sustained loading. The recorded instantaneous deflections are relevant to the present investigation. The beams were cast in timber forms and moist-cured for 14 days after casting. Thereafter the beams were kept in a climate-controlled laboratory. This curing procedure was intended to minimize moisture loss and, therefore, minimize the tensile stresses due to restraint of shrinkage. The predicted deflections are therefore computed using cracking moments calculated using both the full and reduced moduli of rupture.

The simply supported beam tests began 28 days after casting. Two concentrated loads at the third-points of the span loaded the specimen 1B2, which had a reinforcement ratio of 1.74%, typical of a beam section. The resulting mid-span bending moment was 62% of the calculated moment capacity of the section, Figure F-1(a). Figure F-1(a) also shows

the ratio of M_{cr}/M_a varies depending on the modulus of rupture assumed, with the $0.5f_r$ and $0.67f_r$ shown on the left and right sides, respectively, and so the cracked length differs markedly. The left and right side of Figure F-1(b) shows the effective moments of inertia computed using the Branson or Bischoff Equations, respectively, with the full or reduced moduli of rupture and the cracked moments of inertia. For this loading arrangement and higher reinforcement ratio, I_e approaches I_{cr} irrespective of the modulus of rupture assumed. Table F-2 shows the discrepancies between the deflections computed using the Branson and Bischoff Equations are slight. Using the reduced modulus of rupture is overly conservative because the curing conditions reduced the tensile stresses due to restraint of shrinkage.

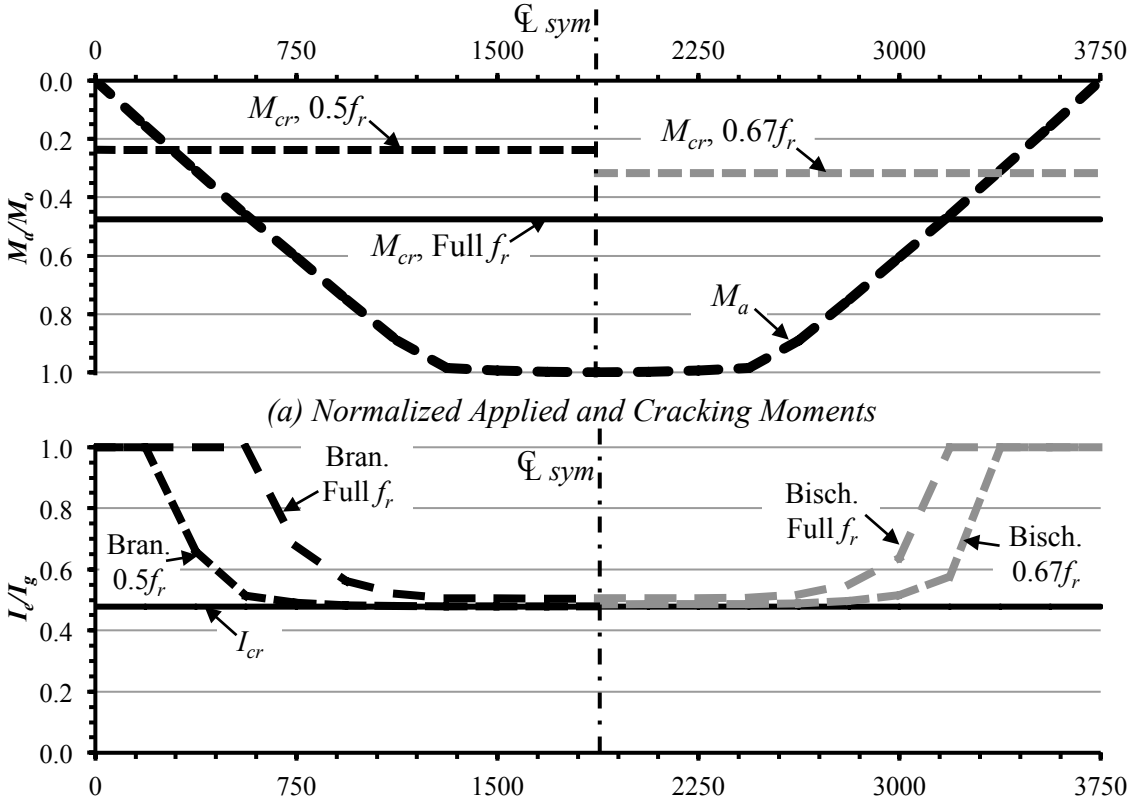

(a) Normalized Applied and Cracking Moments

(b) Normalized Effective and Cracked Moments of Inertia

Figure F-1: Simply Supported Beam 1B2 – Bakoss et al. (1982)

Table F-2: Results of Bakoss et al. (1982) – Simply Supported

Specimen	ρ (%)	Test Δ_{MID} (mm)	Test-to-Predicted From Different Methods							
			$0.5f_r$		$0.67f_r$		Full f_r			
			Branson		Bischoff		Branson		Bischoff	
			m=3	m=4	m=2	m=3	m=3	m=4	m=2	m=3
1B2	1.74%	8.9	0.66	0.66	0.68	0.68	0.72	0.73	0.73	0.72

F.3. Study by Bakoss et al. (1982) – Two-Span

The continuous beams, 2B1 and 2B2, tested by Bakoss et al. (1982) both had a cross section of 100×150mm, equal spans of 3.5m, and were singly reinforced sections with 2 S12 deformed bars, ρ = 1.7%. Tests on the two continuous beams began at 23 days after casting. The beams were loaded with two point loads applied to the center of each span, applied in the horizontal plane to eliminate the effects of self-weight from the observed values. Like the simply supported beams tested, the resulting maximum negative moment was 63% of the calculated moment capacity. The measured deflections reported by Bakoss et al. (1982) are the averages of three readings taken at the midpoints of three identical spans, as readings at one span were discarded because of instrument malfunction.

Figure F-2(a) shows the normalized applied and cracking moment computed with the full modulus of rupture and M_{cr} computed using $0.5f_r$ and $0.67f_r$ on the left and right sides, respectively. The applied moment exceeds the cracking moment both at mid-span and over the interior support for all cracking moments computed. The extent of the cracked region is larger when the reduced moduli of rupture are used, but the difference in the extent of crack using $0.5f_r$ or $0.67f_r$ is slight. Figure F-2(b) shows the normalized effective and cracked moments of inertia computed using the full and reduced moduli and

the Branson and Bischoff Equations on the left and right sides, respectively. There is very little difference in the effective moment of inertia computed using the full modulus of rupture with either the Branson or Bischoff Equations.

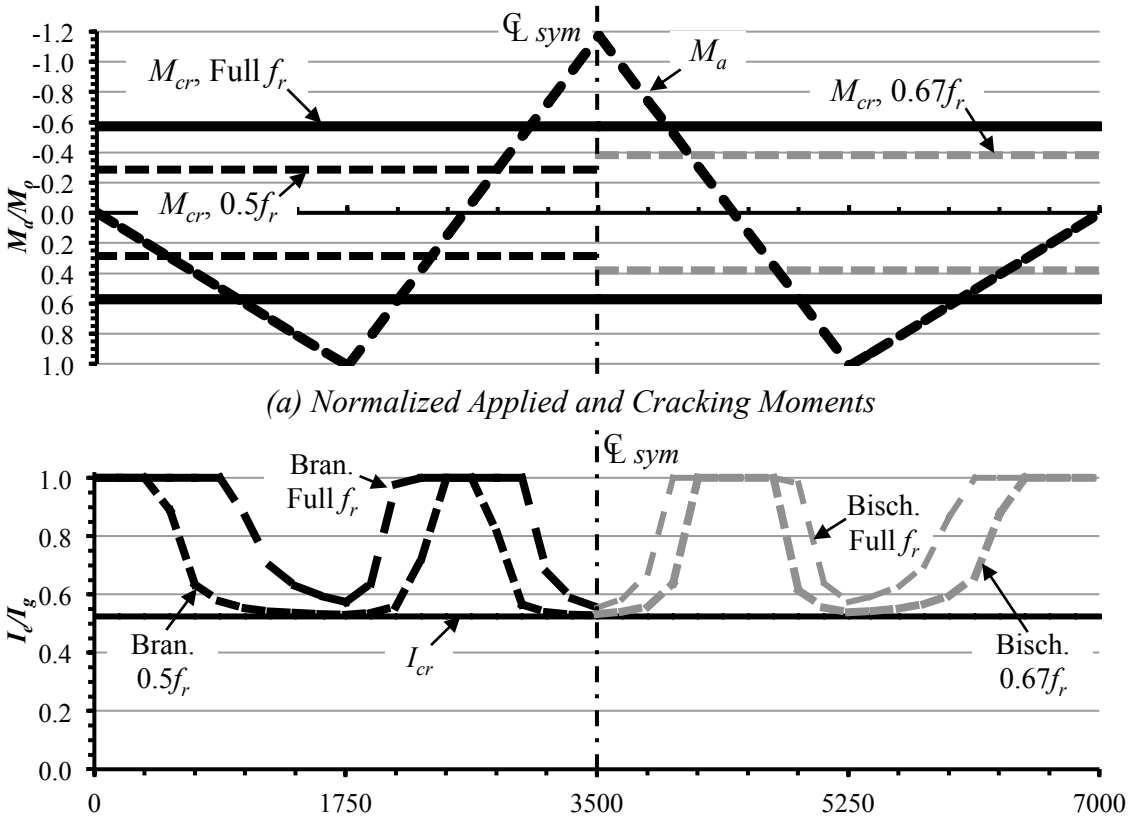

(a) Normalized Applied and Cracking Moments

(b) Normalized Effective and Cracked Moments of Inertia

Figure F-2: Two-Span Beam 2B1/2B2 – Bakoss et al. (1982)

Table F-3 shows the deflection test-to-predicted ratios computed from the alternative deflection calculation procedures. The results reflect the observations of Figure F-2; the differences in results are slight and using the reduced moduli of rupture again yields conservative results. The discretized-element idealizations performed with the full modulus of rupture gives slightly unconservative results as it underestimates the extent of the cracked regions. The single-element idealizations tend to predict more conservative

results than those computed in a discretized-element idealization for the reasons previously explained in Chapter 4: $I_{e(avg)}$ approaches I_{cr}^{+}.

Table F-3: Results of Bakoss et al. (1982) – Two-Span

Specimen	ρ^{+} (%)	Test Δ_{MID} (mm)	Test-to-Predicted From Different Methods							
			$0.5f_r$		$0.67f_r$		Full f_r			
			Branson		Bischoff		Branson		Bischoff	
			m=3	m=4	m=2	m=3	m=3	m=4	m=2	m=3
2B1/2B2	1.7%	4.9	0.86	0.88	0.90	0.93	0.98	1.07	0.99	1.07

F.4. Study by Mattock (1959) – Two-Span

Mattock (1959) performed two series of tests that investigated the redistribution of bending moments in two-span continuous beams. Series 1 included two-span continuous rectangular members designed for the same working load, but using various distribution of design bending moments. Beam 1-1 was designed without moment redistribution and was relevant for the present investigation. Loading was a single point load of 2.25 tons (22.1kN) applied to the left span plus self-weight.

Figure F-3(a) shows the normalized applied and cracking moments computed from the full and reduced moduli of rupture. The point load is applied to the left span and the applied moment exceeds all cracking moments for most of the span length. The extent of the cracked region on the right span depends on the modulus of rupture used to compute the cracking moment, the cracked length increases from 26% of the span length when using the full f_r to 39% and 51% when using $0.67f_r$ and $0.5f_r$, respectively. Figure F-3(b) shows the normalized effective and cracked moments of inertia computed using the both

idealizations and effect moment of inertia equations. Depending on the modulus of rupture assumed I_e equals I_g to a different extent, especially for the right span.

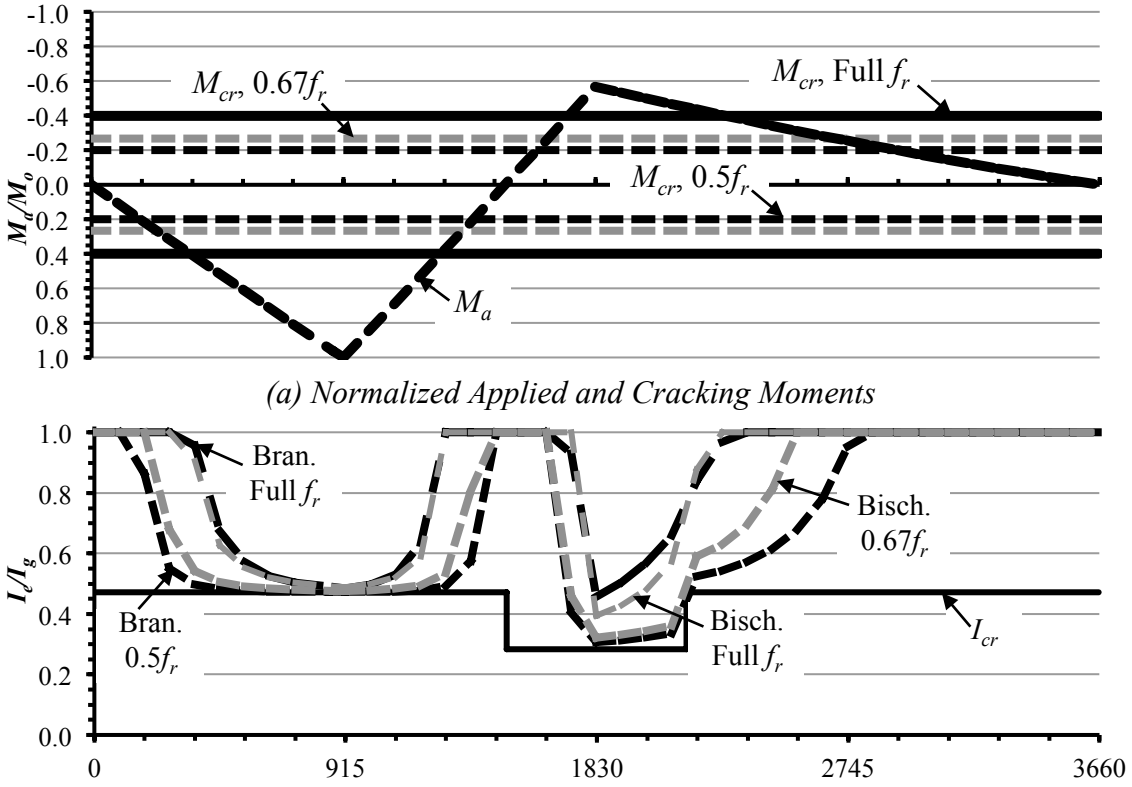

(a) Normalized Applied and Cracking Moments

(b) Normalized Effective and Cracked Moments of Inertia

Figure F-3: Two-Span Beam 1-1 – Mattock (1959)

Table F-4 shows the deflection test-to-predicted ratios computed using the alternative deflection calculation procedures. For this type of applied loading and higher reinforcement ratio, most of the left span, which contributes the most to the computed deflection, is cracked, thus the computed deflections are conservative irrespective of the f_r assumed. The extent of the cracked region is less when using the full modulus of rupture, and smaller deflections are therefore computed. The single-element idealization, again, gives more conservative results than those computed using the discretized-element idealization for the reasons previously explained in Chapter 4: $I_{e(avg)}$ approaches I_{cr}^{+}.

While the loading arrangements differ, the importance of accurately predicting M_{cr} seen in the test performed by Mattock (1959) is consistent with Bakoss et al. (1982).

Table F-4: Results of Mattock (1959)

Specimen	ρ^+ (%)	Test Δ_{MID} (mm)	Test-to-Predicted From Different Methods							
			$0.5f_r$		$0.67f_r$		Full f_r			
			Branson		Bischoff		Branson		Bischoff	
			m=3	m=4	m=2	m=3	m=3	m=4	m=2	m=3
1-1	2.0%	1.1	0.78	0.88	0.80	0.85	0.90	0.97	0.88	0.97

APPENDIX G: SENSITIVITY OF TEST-TO-PREDICTED RATIOS TO THE VALUE OF κ

Tables G-1, G-2 and G-3 show the deflection test-to-predicted ratios computed for various values of κ, and the ratio of I_e^+/I_e^- computed for the Bischoff Equation with the full f_r, the Bischoff Equation with $0.67f_r$, and the Branson Equation with the $0.5f_r$, respectively. The results are similar to the sensitivity analysis using the Branson Equation with the full f_r, as seen in Table 4-15. For Beam 1-1, tested by Mattock (1959), the ratio of I_e^+/I_e^- varies markedly depending on the effective moment of inertia equation used and the modulus of rupture assumed to compute the cracking moment. Irrespective of the f_r adopted I_e^+ approaches I_{cr}^+. However, as f_r is reduced I_e^- approaches I_{cr}^-, which is markedly less than I_{cr}^+. Cases where I_{cr}^- is less than I_{cr}^+ are not common in practice. This case shows the relationship between κ and the ratio of I_e^+/I_e^- is inversely proportional: for $I_e^+/I_e^- > 1$, which is not common in practice, using κ = 0.15 gives the best test-to-predicted ratios; for $I_e^+/I_e^- < 1$, using κ = 0.50 gives the best test-to-predicted ratios; and, for $I_e^+/I_e^- \approx 1$, the deflection test-to-predicted ratios are insensitive to κ.

Table G-1: Test-to-Predicted Ratios – Bischoff Equation, Full f_r

Study		Washa & Fluck (1956)			Mattock (1959)	Habeeb & Ashour (2008)	Mahroug et al. (2014)	Bakoss et al. (1982)	El-Mogy (2011)	Mean	Std. Dev.
Specimen		Y3,Y6	Z3,Z6	X3,X6	1-1	SScUU	C-S2-UU	2B1, 2B2	SSc-8d/2p		
I_e^+/I_e^-		0.62	0.70	0.71	0.98	1.03	1.04	1.06	1.24		
κ	0.15	0.86	0.72	0.88	0.88	0.87	1.11	0.99	0.92	0.90	11.3%
	0.20	0.89	0.73	0.89	0.88	0.87	1.11	0.99	0.91	0.91	10.7%
	0.25	0.91	0.75	0.91	0.88	0.87	1.11	0.98	0.90	0.91	10.3%
	0.30	0.94	0.76	0.93	0.88	0.87	1.10	0.98	0.89	0.92	9.9%
	0.35	0.96	0.77	0.94	0.88	0.87	1.10	0.98	0.88	0.92	9.7%
	0.40	0.98	0.79	0.96	0.88	0.87	1.10	0.98	0.87	0.93	9.6%
	0.45	1.01	0.80	0.98	0.88	0.86	1.10	0.97	0.86	0.93	9.7%
	0.50	1.03	0.82	0.99	0.88	0.86	1.10	0.97	0.85	0.94	9.9%

Table G-2: Test-to-Predicted Ratios – Bischoff Equation, $0.67f_r$

Study		Washa & Fluck (1956)			Mattock (1959)	Habeeb & Ashour (2008)	Mahroug et al. (2014)	Bakoss et al. (1982)	El-Mogy (2011)	Mean	Std. Dev.
Specimen		Y3,Y6	Z3,Z6	X3,X6	1-1	SScUU	C-S2-UU	2B1, 2B2	SSc-8d/2p		
I_e^+/I_e^-		0.59	0.66	0.68	1.38	1.01	1.02	1.02	1.23		
κ	0.15	0.83	0.81	0.84	0.80	0.84	1.05	0.90	0.89	0.87	8.0%
	0.20	0.86	0.82	0.86	0.79	0.84	1.04	0.90	0.88	0.87	7.7%
	0.25	0.88	0.84	0.88	0.78	0.84	1.04	0.90	0.87	0.88	7.7%
	0.30	0.91	0.86	0.89	0.77	0.84	1.04	0.90	0.86	0.88	7.9%
	0.35	0.94	0.88	0.91	0.76	0.83	1.04	0.90	0.85	0.89	8.3%
	0.40	0.96	0.90	0.93	0.74	0.83	1.04	0.90	0.85	0.89	8.9%
	0.45	0.99	0.92	0.95	0.73	0.83	1.04	0.90	0.84	0.90	9.7%
	0.50	1.01	0.94	0.97	0.72	0.83	1.04	0.89	0.83	0.90	10.7%

Table G-3: Test-to-Predicted Ratios – Branson Equation, $0.5f_r$

Study		Washa & Fluck (1956)			Mattock (1959)	Habeeb & Ashour (2008)	Mahroug et al. (2014)	Bakoss et al. (1982)	El-Mogy (2011)	Mean	Std. Dev.
Specimen		Y3,Y6	Z3,Z6	X3,X6	1-1	SScUU	C-S2-UU	2B1, 2B2	SSc-8d/2p		
I_e^+/I_e^-		0.58	0.64	0.66	1.45	1.00	1.01	1.01	1.23		
κ	0.15	0.81	0.78	0.82	0.78	0.82	1.02	0.86	0.87	0.84	7.8%
	0.20	0.84	0.80	0.84	0.76	0.82	1.02	0.86	0.86	0.85	7.5%
	0.25	0.87	0.82	0.85	0.75	0.82	1.02	0.86	0.86	0.86	7.6%
	0.30	0.89	0.84	0.87	0.74	0.82	1.02	0.86	0.85	0.86	7.9%
	0.35	0.92	0.86	0.89	0.72	0.82	1.02	0.86	0.84	0.87	8.4%
	0.40	0.95	0.88	0.91	0.71	0.82	1.02	0.86	0.83	0.87	9.1%
	0.45	0.97	0.90	0.93	0.70	0.82	1.02	0.86	0.82	0.88	10.0%
	0.50	1.00	0.92	0.95	0.69	0.82	1.01	0.86	0.81	0.88	11.1%

CURRICULUM VITAE

Name: Caitlin Mancuso

Post-secondary Education and Degrees:

Master of Engineering Science, M.E.Sc.
The University of Western Ontario
London, Ontario, Canada
2014-2016

Bachelor of Engineering Science, B.E.Sc
The University of Western Ontario
London, Ontario, Canada
2010-2014

Honours and Awards:

Alexander Graham Bell Canada Graduate Scholarship (CGSM) A provided by Natural Sciences and Engineering Research Council of Canada (NSERC)
2015-2016

Queen Elizabeth II Graduate Scholarship in Science and Technology (QEII-GSST) provided by the Province of Ontario
2014-2015

Related Work Experience:

Teaching Assistant
The University of Western Ontario
2014-2016

Publications:

Mancuso, C., and Bartlett, F.M. 2016. *Instantaneous Deflections of Concrete Slabs Computed Using Discretized Analysis*, Proceedings of the 5th International Structural Specialty Conference, STR 855, London, ON, Canada, pp. 10.

Mancuso, C., and Bartlett, F.M. 2014. *Built-up Wrought-iron Compression Member with Missing Stitch Rivets*, Electronic Proceedings, 37th IABSE Symposium Report. 37th International Association for Bridge and Structural Engineering Symposium, Madrid, Spain, pp. 304-305.